DOKUZ EYLÜL UNIVERSITY

GRADUATE SCHOOL OF NATURAL AND APPLIED SCIENCES

ASSESSMENT OF THE THERMAL INSULATION PERFORMANCE OF 3D PRINTED CONCRETE WALLS

by

Kunda CHAMATETE

June, 2024

İZMİR

ASSESSMENT OF THE THERMAL INSULATION PERFORMANCE OF 3D PRINTED CONCRETE WALLS

A Thesis Submitted to the
Graduate School of Natural and Applied Sciences of Dokuz Eylül University
In Partial Fulfillment of the Requirements for the Degree of Master of Science in Civil Engineering, Structural Program

by

Kunda CHAMATETE

June, 2024

İZMİR

M.Sc. THESIS EXAMINATION RESULT FORM

We have read the thesis entitled **"ASSESSMENT OF THE THERMAL INSULATION PERFORMANCE OF 3D PRINTED CONCRETE WALLS"** completed by **KUNDA CHAMATETE** under the supervision of **ASSOC. PROF. DR. ÇAĞLAR YALÇINKAYA**, and we certify that in our opinion it is fully adequate, in scope and quality, as a thesis for the degree of Master of Science.

.....

Assoc. Prof. Dr. Çağlar YALÇINKAYA

Supervisor

.....

Assoc. Prof. Dr. Gökhan ŞAKAR

Jury Member

.....

Asst. Prof. Dr. Mehmet Alper ÇANKAYA

Jury Member

Prof. Dr. Okan FISTIKOĞLU

Director

Graduate School of Natural and Applied Sciences

ACKNOWLEDGEMENT

Firstly, I wish to thank God, who has been faithful throughout the days of my life. I also wish to thank my friends and family, who have been supportive throughout this journey. I wish to especially thank Sharon Luchembe for making me a father. Fatherhood has been a life-changing journey for me, and my son has been my biggest motivation throughout this thesis journey—to finish and go and meet him. I also wish to thank Mulewa Sinkala and Mwape Chamatete, who have always been there to talk with me when I needed to be heard. I further wish to thank my housemates, Michael Kingsley Afful and Ayodele Akin-Adamu, who have become family since moving to Türkiye. I also want to acknowledge the Türkiye Scholarship Board for granting me an opportunity to study at Türkiye. But most importantly, I would like to express my heartfelt gratitude to my project supervisor, Assoc. Prof. Dr. Çağlar YALÇINKAYA, who has tremendously groomed me into research work and guided me throughout this project thesis.

Kunda CHAMATETE

ASSESSMENT OF THE THERMAL INSULATION PERFORMANCE OF 3D PRINTED CONCRETE WALLS

ABSTRACT

The construction industry is very dependent on manual labor. It faces challenges such as material waste and a shortage of skilled labor. However, three-dimensional concrete printing (3DCP) technology is a potential answer. It particularly allows for formwork-free and fast construction, unlimited design freedom, and savings on labor, among many other benefits. This technology could disrupt the construction industry in the future. However, there is little focus on the thermal performance of three-dimensional printed concrete walls as the sector undergoes digital transformation. This thesis study numerically examines the thermal performance of three-dimensional printed concrete (3DPC) walls, focusing on the effects of the infill structure, cavity insulation, and thermal bridging. A series of numerical studies were conducted on large-scale, commercially applied 3DPC walls using infill structures having sufficient structural integrity. A constitutive model was developed, validated against published literature, and then applied to lattice structures. The effects of filament width, web length, and web configuration, as well as the contact area of webs with the interior face shell and granular filling materials, were studied. The thermal efficiency of the insulation was also determined. It was established that for the same thickness, contour lengths, and void percentages, void area affects the thermal performance of 3DPC walls under stagnant air conditions. In contrast, web length, filament width, and contact (intersection) area between the webs and face shells affect the thermal behavior due to thermal bridging when cavities are filled with insulating materials. Furthermore, the absence or lack of direct connection between the exterior and interior faces by the webs exhibits superior thermal performance. The application of foam concrete in 3DCP, as well as combined double-row walls, significantly improves the thermal efficiency of insulation.

Keywords: Thermal performance; 3D printed concrete; Energy-efficient buildings; Thermal bridging; Finite element modeling; Insulation performance.

3B YAZDIRILMIŞ BETON DUVARLARIN ISI YALITIM PERFORMANSININ DEĞERLENDIRILMESI

ÖZ

İnşaat endüstrisi el emeğine çok bağımlıdır. Malzeme atıkları ve nitelikli işçi eksikliği gibi zorluklarla karşı karşıyadır. Ancak üç boyutlu beton yazdırma (3BBY) teknolojisi potansiyel bir çözümdür. Diğer birçok faydaları arasında özellikle kalıpsız ve hızlı imalat, sınırsız tasarım özgürlüğü ve iş gücü tasarrufu sağlar. Bu teknoloji gelecekte yapı endüstrisini altüst edebilir. Sektör dijital dönüşüm geçirmesine rağmen üç boyutlu yazdırılmış beton (3BYB) duvarların termal performansına çok az odaklanılmıştır. Bu tez çalışması, 3BYB duvarların termal performansını incelerken, dolgu yapısının, boşluk yalıtımının ve ısı köprüsünün etkileri üzerinde durmaktadır. Büyük ölçekli, ticari olarak uygulanmış 3BYB duvarlar üzerinde yeterli yapısal bütünlüğe sahip olan dolgu yapıları kullanılarak bir dizi sayısal çalışma gerçekleştirilmiştir. Bir bünye modeli geliştirilmiş, yayınlanmış literatürle doğrulanmış ve daha sonra kafes (iç örgü) yapısına uygulanmıştır. Filament genişliği, ağ uzunluğu ve ağ konfigürasyonunun yanı sıra ağların iç yüz kabuğu ve granüler dolgu malzemeleriyle temas alanının da etkileri incelenmiştir. Yalıtımın ısıl verimliliği de belirlenmiştir. Aynı kalınlık, kontur uzunlukları ve boşluk yüzdeleri için boşluk alanının, durgun hava koşulları altında 3BYB duvarların termal performansını etkilediği tespit edilmiştir. Buna karşılık ağ uzunluğu, filament genişliği ve ağlar ile yüz kabukları arasındaki temas (kesişme) alanı, boşluklar yalıtım malzemeleriyle doldurulduğunda termal köprüleme nedeniyle termal davranışı etkilemektedir. Ayrıca, ağların dış ve iç yüzleri arasında doğrudan bağlantının noksanlığı veya bulunmaması, üstün termal performans sergilemektedir. 3BBY'de köpük betonun yanı sıra birleşik çift sıralı duvarların uygulanması, yalıtımın ısıl verimliliğini önemli ölçüde artırmaktadır.

Anahtar Kelimeler: Termal performans; 3D basılmış Beton; Enerji verimli binalar; Termal köprü; Sınırlı element modelleme; Yalıtım performansı.

CONTENTS

Page

M.Sc. THESIS EXAMINATION RESULT FORM……..……..…ii
ACKNOWLEDGEMENT iii
ABSTRACT…..... iv
ÖZ……. v
LIST OF FIGURES ix
LIST OF TABLES xii

CHAPTER ONE - INTRODUCTION 1

1.1 Background of the study 1
1.2 Aim and objective of this research 6

CHAPTER TWO - LITERATURE REVIEW 7

2.1 Automation of the Construction Industry 7
2.2 The Technology of Additive Manufacturing 8
2.2.1 Extrusion-Based 3D-Printing 9
2.2.2 Selective Binding Powder/Particle-Bed-Based Method 11
2.2.3 Shotcrete-Based Method 14
2.3 Properties of 3D printed concrete 16
2.4 Materials for 3D-Printed Concrete 16
2.5 Structural Properties of 3D-Printed Concrete 17
2.6 Thermal Properties of 3D Printed Concrete 17
2.7 Insulation materials in construction 18
2.8 Insulation Techniques in Buildings 19
2.9 Heat Transfer Mechanisms 20
2.9.1 Conduction 20
2.9.2 Convection 21
2.9.3 Radiation 22
2.10 Heat transfer in 3DPC walls 23
2.11 Analytical Methods of Heat Transfer 23
2.11.1 Multilayer plane walls 24

2.11.2 Parallel Path Method 26
2.11.3 Isothermal Planes (Series–Parallel Path) Method 28
2.12 Numerical Methods of Heat Transfer 30
2.13 Finite Element Method (FEM) 31
2.13.1 Discretization of the Domain 32
2.13.2 Formulation of Governing Equations 33
2.13.3 Assignment of Material Properties and Boundary Conditions 33
2.13.4 Assembly of System Equations 34
2.13.5 Application of Solver 35
2.13.6 Convergence and Solution Accuracy 35
2.13.7 Post-Processing and Visualization 36
2.14 Two-dimensional (2D) numerical models 37
2.14.1 Test Case 1 38
2.14.2 Test Case 2 39
2.15 Three-dimensional (3D) numerical models 41
2.15.1 Test Cases 1 and 2 41
2.15.2 Test Case 3 42
2.15.3 Test Case 4 44

CHAPTER THREE - NUMERICAL STUDIES 46

3.1 Overview of Thesis 46
3.2 Development of the Finite Element Model 48
3.2.1 Heat Transfer Analysis 48
3.2.2 Mesh Sensitivity Analysis 52
3.2.3 Validation of Finite Element Model 54

CHAPTER FOUR - EFFECTS OF THE INFILL-GEOMETRY 57

4.1 Introduction 57
4.2 Parametric Study 59
4.3 Results and Discussion 60
4.4 Conclusions 64

CHAPTER FIVE - EFFECTS OF LATTICE TYPE, FILAMENT WIDTH, AND GRANULAR FILLING MATERIAL 66

5.1 Introduction 66
5.2 Methodology and Analysis 69
5.2.1 Parametric Study 70
5.2.2 Thermal Insulation of Efficiency 74
5.3. Results and Discussion 75
5.3.1. Effect of Area of Stagnant Air 75
5.3.2. Effect of Cavity Insulation 78
5.3.3. Effect of Geometric Properties of Insulated Lattice Structures 82
5.3.4. Thermal Efficiency of Insulation 83
5.4 Conclusions 86

CHAPTER SIX - THERMAL BRIDGING EFFECTS IN 3D PRINTED FOAM CONCRETE.. 88

6.1 Introduction 88
6.2 Methodology and Analysis 91
6.2.1 Parametric Study 92
6.2.2 Thermal Efficiency of Insulation 96
6.3 Results and Discussion 96
6.3.1. Effect of Contact Area 97
6.3.2. Effect of Webs 100
6.3.3. Thermal Efficiency of Insulation 101
6.4 Conclusions 103

CHAPTER SEVEN - SUMMARY AND CONCLUSIONS 105

REFERENCES 109

LIST OF FIGURES

Page

Figure 1. 1 Illustration of an extruded 3DCP element via robotic gantry system (Black Buffalo, 2023) 3

Figure 1. 2 Commercial (large-scale) printing of house (a) On-site printing (Black Buffalo, 2023) (b) View of a finished product (Apis Cor, 2023) 4

Figure 2. 1 3DCP by Extrusion (ICON, 2023) 10

Figure 2. 2 (a) CC Multiple nozzle assembly (b) first large-scale walls printed by CC (Khoshnevis et al., 2006) 11

Figure 2. 3 Printing procedures of Binder Jetting (a) layering powder on printing bed (b) Application of binding agent (c) Removal of loose particles and cleaning (d) Final product ((Shakor et al., 2021)..... 12

Figure 2. 4 (a) Selective paste intrusion (SPI) printer (b) SPI-manufactured tube with internal double bracing (Weger & Gehlen, 2021) 13

Figure 2. 5 (a) Prototype particle bed printer for selective cement activation (Lowke et al., 2018) (b) Example of a free-form geometry, manufactured by Selective Cement Activation (Design: K. Henke, manufacturing: B. Saile, D. Talke)(Talke et al., 2023)..... 14

Figure 2. 6 SC3DP (a) Setup (b) Free-formed SC3DP (Heidarnezhad & Zhang, 2022) 15

Figure 2. 7 Four main phenomena of heat transfer through 3DPC wall panels: conductive heat transfer through the gas (blue) and solid (red), convective (pink) heat transfer within the cells, and radiative (green) (Inspired by Briels et al., 2023) 23

Figure 2. 8 The thermal resistance network for heat transfer through a two-layer plane wall subjected to convection on both sides (Çengel & Ghajar, 2015). 26

Figure 2. 9 The thermal resistance network for heat transfer through a plane wall subjected to convection on both sides and the electrical analogy (Çengel & Ghajar, 2015). 26

Figure 2. 10 Calculation schematic for the parallel path method (Kośny & Yarbrough, 2022). 27

Figure 2. 11 Typical two-core concrete block (Perlite Institute, 2013) 29
Figure 2. 12 A schematic presentation of thermal resistance for a two-core concrete block (Perlite Institute, 2013) 29
Figure 2. 13 Element Types (Frunză & Luca, 2010) (b) The default free tetrahedral mesh feature in Ansys is applied to the entire model (Walter Frei, 2015). 32
Figure 2. 14 Assembly of a 3x3 matrix system in the form K·Ø = F (Rehman et al., 2017) 34
Figure 2. 15 Surface heat flux contour map of the W2-wall panel 37
Figure 2. 16 The analytical solution of heat transfer through half a square column at 28 points of an equidistant grid (ISO 10211) 38
Figure 2. 17 Test case 1 performed in THERM (ISO 10211) 39
Figure 2. 18 Test case 2 for 2D heat transfer (ISO 10211) 39
Figure 2. 19 Modelling of Test Case 2 in THERM by Martins (2020) 40
Figure 2. 20 Test case 1 results in Ansys by Martins (2020) 41
Figure 2. 21 Test case 2 results in Ansys by Martins (2020) 42
Figure 2. 22 Test Case 3 for 3D heat transfer (ISO 10211) 42
Figure 2. 23 Modelling of Test Case 3 in Ansys by Martins (2020) 43
Figure 2. 24 Test case 4 for three-dimensional heat transfer (ISO 10211) 44
Figure 2. 25 Modelling of Test Case 4 in Ansys by Martins, C. M. D. O. (2020) 44
Figure 3. 1 Flowchart for the organization of the thesis work. 48
Figure 3. 2 The application of boundary conditions to the FE models (dimensions in mm). 52
Figure 3. 3 Hollow concrete block layouts studied. Source: Henrique dos Santos, G., Fogiatto, M. A., and Mendes, N, numerical analysis of thermal transmittance of hollow concrete blocks. Journal of Building Physics, 41(1), 7–24, copyright © 2017 by SAGE Journals. Reprinted by Permission of SAGE Publications. 53
Figure 3. 4 Mesh sensitivity analysis. 53
Figure 3. 5 U-value results were obtained from the FE models developed by the author and those determined by Henrique dos Santos et al. (2017). 55
Figure 3. 6 Plan view of Structure 1 (dimensions in mm). Source: redrawn based on data from Tamini et al. (2023). 55

Figure 4. 1 Wall configurations chosen for the study Only exterior (EO) (No infill structure); Square Zigzag (SQ); Wavy Zigzag (WV) 60
Figure 4. 2 Reductions in U-values due to cavity insulation 62
Figure 4. 3 Percentage reductions due to cavity insulation..... 63
Figure 4. 4 Void-concrete ratios 63
Figure 4. 5 Surface heat fluxes of the half models of the 3DPC wall panels 64
Figure 5. 1 Wall types (35 mm filament width) for the parametric analysis (dimensions in mm). 71
Figure 5. 2 Surface heat flux contour maps with stagnant air in cavities. 77
Figure 5. 3 Thermal transmittance variations with void area. 78
Figure 5. 4 Surface heat flux contour maps of loose fill perlite insulated walls..... 79
Figure 5. 5 Surface heat flux contour maps of EPS insulated walls. 80
Figure 5. 6 Reductions in U-values due to cavity insulation. 81
Figure 5. 7 Thermal transmittance variations with area of insulation. 82
Figure 5. 8 Thermal Efficiency (T_{Eff}) of Insulation of Perlite and EPS..... 84
Figure 6. 1 Wall types (35 mm filament width) for the parametric analysis (dimensions in mm). 93
Figure 6. 2 Surface heat flux contour maps of EPS cavity-filled walls. 98
Figure 6. 3 Thermal transmittance variations with area of insulation. 99
Figure 6. 4 Thermal Efficiency (T_{Eff}) of EPS Insulation. 102

LIST OF TABLES

Page

Table 2. 1 Test Case 1 surface temperature results obtained by THERM (ISO 10211) 39
Table 2. 2 Geometric and thermal properties and boundary conditions of Test Case 2 for 2D heat transfer (ISO 10211) 40
Table 2. 3 Test Case 2 surface temperature results stipulated by ISO 10211 40
Table 2. 4 Test case 2 surface temperature results obtained by Martins (2020) 41
Table 2. 5 Boundary conditions of Test Case 2 for two-dimensional heat transfer (ISO 10211) 43
Table 2. 6 Comparison between the values defined in ISO 10211 and software Ansys, for Test Case 3. 43
Table 2. 7 Comparison between the values defined in ISO 10211 and software Ansys, for test case 4. 45
Table 4. 1 Standard thermal transmittance values as per national regulations for climatic zones of the Koppen-Geiger climate classification (M. Kottek, 2006) 58
Table 4. 2 Detailed description of the parametric study 60
Table 4. 3 Thermal transmittance values of all models in the parametric study 61
Table 5. 1 Thermal properties of materials. 70
Table 5. 2 Detailed description of the parametric study. 72
Table 5. 3 Thermal transmittance values of all models in the parametric study 75
Table 5. 4 Thermal efficiency of insulation of perlite and EPS. 84
Table 6. 1 Thermal properties of materials. 92
Table 6. 2 Detailed description of the parametric study. 95
Table 6. 3 Thermal transmittance values of all models in the parametric study 97

CHAPTER ONE
INTRODUCTION

1.1 Background of the study

Due to the lack of innovation in construction processes, which for decades have remained almost entirely based on manual labor, the construction industry is considered a low-tech industry (Harty, 2008). This is because, as Tidd et al. (2005) point out, the primary focus of innovation strategy in the construction sector is on using technology from elsewhere to reinforce other competitive advantages.

The construction industry continues to rely heavily on manual labor. It generates a substantial amount of material waste, confronts a skills shortage, and accounts for 30% of workplace injuries (Marchment & Sanjayan, 2021). In recent years, it has been widely criticized for its delayed adoption of digital advances compared to other industry sectors such as manufacturing and agriculture (Pessoa et al., 2021).

Productivity in these industries has been rising due to automation and digitization but it has stagnated in the building industry (Wangler et al., 2017). In comparing worker productivity across 20 nations, Nasir et al. (2014) discovered that the US performed the lowest, with an annual compound rate of -0.84%. Hong Kong, Singapore, and the United Kingdom are among the developed nations that have also experienced low productivity (Harty, 2008; Lim & Alum, 1995; Lo et al., 2006).

Building construction is considered a resource-intensive sector that places a great deal of stress on the environment. Buildings are the primary energy consumers in Europe, contributing 40% of energy consumption and 36% of CO_2 emissions in the EU (Gerasina et al., 2020), buildings are the primary energy consumers in Europe, contributing 40% of energy consumption and 36% of CO_2 emissions in the EU. Besides, 36% of the energy utilized, 30% of the raw materials used, and 12% of the potable water consumed in the US were attributed to buildings (Klotz et al., 2007). According to Deeming (2021), there is a possibility that the world's population will

surpass 10.9 billion by the year 2100, which will unavoidably stimulate the need for housing.

Currently, there is a growing consumption of non-renewable resources and a high demand for urbanization. However, given the negative impact of the construction industry on climate change, it is critical to improve the industry's efficiency and sustainability. Research into the integration of specialized digital and automated technologies is underway. This will bridge the gap between present construction methods and an optimum automation-oriented approach. It will also as well as address the challenges of slow integration.

Building Information Modeling (BIM) opened the way for improved information management in the construction industry by simplifying and encouraging the use of digital technology and solutions (Pessoa et al., 2021; Wangler et al., 2017). In recent years, there has been a surge in demand for prefabricated building components, as well as investment in the automation of these operations. Autonomous and robotically controlled site-based jobs involving earth-moving machines are gradually being used, with success in the mining sector (Melenbrink et al., 2020).

However, the use of large-scale additive manufacturing (AM) is increasing, necessitating further research. This technology has a disruptive potential to alter the construction sector (Kazemian et al., 2022). When compared to traditional construction methods, three-dimensional concrete printing (3DCP) has demonstrated technical, social, economic, and environmental benefits. It allows for the production of more complex shapes at lower costs. It also allows for the future combined use of 3DCP, Building Information Modeling (BIM), and artificial intelligence (Salet & Wolfs, 2016; Tan, 2018).

3DCP technology employs robotic devices and specifically developed concrete mixtures to quickly construct custom-tailored buildings (Kazemian et al., 2017; Nematollahi et al., 2017). This robotic construction technology may help improve the environmental impact of construction by minimizing waste and emissions, cutting

energy consumption, and optimizing structural design (De Schutter et al., 2018; Vantyghem et al., 2020). By removing the need for formwork and enabling the creation of structurally optimal buildings, 3DCP reduces material consumption and allows for a waste-free construction procedure. Another issue is the regular injuries and fatalities on construction sites, which are addressed. Finally, it is possible to use sustainable cementitious materials in three-dimensional printed concrete (3DPC). Recent studies have explored the use of sustainable cementitious materials in 3DCP, including partial replacement of ordinary Portland cement with supplementary materials, partial substitution of natural aggregate with recycled aggregate, or industrial wastes (Chen et al., 2022). Figure 1.1 shows an illustration of 3DCP by robotic extrusion.



Figure 1. 1 Illustration of an extruded 3DCP element via robotic gantry system (Black Buffalo, 2023)

Various researchers have examined the feasibility of implementing 3DCP. Wu et al. (2016) reviewed the application of 3D printing in construction, Khoshnevis et al. (2006) studied mega-scale fabrication by contour crafting, Timchuk & Evloeva, (2020) focused on the transformation of the construction industry into a digital economy, and De Schutter et al. (2018) emphasized the need for active rheology and stiffening control.

However, the digital transformation of the building industry is just getting started. This is in contrast to other sectors like the automobile and medical industries, which have fully embraced digital technologies (Pessoa et al., 2021). Despite materials, robotics, and structural stability receiving most of the attention from researchers, there are still numerous aspects of building performance that require more study. The absence of suitable solutions for thermal insulation has received less attention than issues with buildability and extrudability, difficulties installing reinforcements, anisotropic behavior, and low bond strength (H. Zhang & Xiao, 2021). Furthermore, the thermal performance of 3D-printed building envelopes and thermal bridging effects have received less attention from researchers. Figure 1.2 shows large-scale applications of 3DCP.



(a)



(b)

Figure 1. 2 Commercial (large-scale) printing of house (a) On-site printing (Black Buffalo, 2023) (b) View of a finished product (Apis Cor, 2023)

Thermal performance in 3DPC building envelopes is affected by various factors. These factors include infill geometry, cavity size, and insulation. Several researchers have studied the thermal behavior of 3DPC envelopes. Nemova et al. (2022) developed an energy-efficient envelope that adheres to climatic zones. Mansouri et al. (2022) showed that subdividing big cavities into smaller ones can greatly lower heat flux. Alkhalidi & Hatuqay (2020) designed affordable, energy-efficient housing units by balancing voids and printed material. Suntharalingam et al. (2021) showed that intricate designs such as lattice structures or double-rowed honeycombs are capable of trapping air thereby improving insulation. AlZahrani et al., 2022) studied the energy efficiency of infill structures with the same void-to-concrete ratios.

The lack of technical design standards in 3DCP leads to thermal performance studies that overlook structural aspects. In most of the studies on the thermal performance of 3DPC envelopes, the selection of infill structure is not clearly addressed. Furthermore, in all the previous studies, the potential of foam concrete (FC) in enhancing the energy efficiency of 3DPC envelopes has still not been studied. All the studies solely concentrate on normal concrete. Meanwhile, FC has tremendous potential as an innovative, cost-effective, and ecologically sound construction material. Besides, the cavity-filling material used in previous studies (Alkhalidi & Hatuqay, 2020; Suntharalingam et al., 2021), expanded polylactic acid (E-PLA), a bio-based foam material, still has limited applications. While E-PLA has a niche market due to its green characteristics when compared to traditional materials, it still has a higher cost, lower thermal resistance (R-value), high sensitivity to moisture, relatively poor fire resistance, limited availability in some regions, and lack of extensive long-term performance data (Faruk et al., 2012; Parker et al., 2011; Stark & Matuana, 2007).

Therefore, this thesis work aims to examine the impact of the infill geometry on the energy performance of large-scale, commercially applied 3DPC walls using infill structures of sufficient structural integrity. The effects of infill structure, cavity insulation, and thermal bridging were studied. The effects of void area, filament width, and insulation percentage are examined. Foam concrete is also incorporated,

and thermal bridging effects are also investigated. Furthermore, because of wide availability, granular materials i.e. expanded polystyrene (EPS) and loose-fill perlite are used in this work. Numerous additional considerations, including affordability, sustainability, recyclability, conformity to irregular shapes, and ease and variety of application, all played a role in the decision to choose this material. Lastly, this work also aims to determine the extent to which thermal bridges affect the effective usage of granular insulating materials.

1.2 Aim and objective of this research

The aims and objectives of this research work include the following:

1. To determine the effect of infill geometry on the thermal performance.
2. To determine the effect of the void area on the thermal performance.
3. To determine the effect of granular cavity-fill materials on the thermal performance.
4. To determine the effect of the area of insulation on cavity-filled 3DPC envelopes.
5. To determine the effect of filament width, and web length on thermal performance.
6. To determine the thermal bridging effects of web configuration and the contact (intersection) area of webs with the interior face shells.
7. To determine the thermal efficiency of insulation due to infill geometry.
8. To determine the effect of the application of foam concrete on the thermal efficiency of insulation.
9. To identify lattice structures with optimal thermal performance.

CHAPTER TWO
LITERATURE REVIEW

In this section, the automation and digital transformation of the construction industry, and the technology of additive manufacturing technology are discussed. Furthermore, the mechanisms and the methods of analysis of heat transfer, as well as properties of 3DPC and insulation techniques commonly applied in the construction are reviewed.

2.1 Automation of the Construction Industry

Currently, the world is heading toward Industry 4.0. The Internet of Things (IoT) and digitization is making this shift possible for most industries. However, the construction industry is still lagging. It still has not enjoyed broad automation nor the advantages of the third industrial revolution. Using automation can boost quality assurance and productivity. Industry 3.0 requires a more forward-thinking strategy that takes cues from automated sectors that have found success, such as manufacturing. The construction industry is poised to embrace additive manufacturing, also known as 3D printing, as a means of bridging the gap between industries 3.0 and 4.0 (Marchment & Sanjayan, 2021).

Due to the high cost and complexity of automating huge construction processes, materials, and components, the construction industry is now lagging manufacturing (Khoshnevis et al., 2006). But automation has begun to creep into other areas of construction as well, like integrated robotic systems and prefabricated building components. Although these developments have led to costly procedures with little financial gain over conventional techniques, they have increased productivity, safety, and quality (Buswell et al., 2007; Pegna, 1997; Tibaut et al., 2016). With its inherent complexity and quality requirements, onsite robotic production or assembly of the superstructure is the main focus of construction automation as it is now. If successful, this will completely disrupt the construction sector and change it (Caffrey et al. 2016).

Concrete is the principal building material; hence, automation of structural concrete construction appears to be inevitable or essential. To ensure success, the sector must adapt to automation's inherent complexities and quality needs. Concrete is the second most extensively used construction material after water, with an estimated 10 km^3 utilized globally each year. Despite the construction material being environmentally friendly, its raw processing produces 5–8% of world greenhouse gas emissions (Flatt et al., 2012; Wangler et al., 2017). Concrete has been utilized since the Roman era. However, its construction methods frequently use formwork or molds. As architecture grows more free-form, more curved shapes are required, resulting in higher cost and waste (Kim et al., 2015; Wangler et al., 2017, 2019).

William Urschel and Thomas Edison were forerunners in advancing concrete construction technology; Urschel filed patents for a wall-building machine and Edison for a single-poured house (Marchment & Sanjayan, 2021). Prefabrication is now used in modern concrete construction processes to avoid onsite formwork, but onsite concrete construction is still frequently required. Slip forming is one method of onsite formwork minimization that uses a dynamic moving formwork to reduce formwork labor but has geometric restrictions.

Digital concrete, which incorporates robotics and automation, promises to reduce concrete waste and labor costs and improve design freedom without the use of traditional formwork. Technological advancements in digital concrete include 3D-printing of formworks and concrete, automated installation of reinforcing steel molds, and dynamic and flexible formworks (Flatt & Wangler, 2018; Wangler et al., 2017, 2019).

2.2 The Technology of Additive Manufacturing

Additive Manufacturing (AM), often known as 3D printing, is a fast-developing technology that allows for the direct creation of 3D objects in successive layers from digital models (ASTM F42, 2015). AM was first created in the 1980s and has since been effectively implemented in a variety of industries, including aerospace, automotive manufacturing, biomedical, consumer, and food (Gao et al.,

2015). Today, AM methods have become an essential component of modern product development. There are even affordable desktop versions available for home usage (Pearce et al. 2010). The process involves slicing an object's computer-based representation, such as 3D CAD drawings, into cross-sectional layers and converting them into material placement and location commands.

The printing process is then controlled by stepper motors using a three-axis system once these instructions are sent to them. Precise 2D layers of the chosen material are stacked on top of one another to create 3D objects (Pegna, 1997; Tibaut et al., 2016). In additive manufacturing, material extrusion, powder bed fusion, vat photopolymerization, material jetting, binder jetting, sheet lamination, and directed energy deposition are the most commonly employed layering procedures and techniques (Marchment & Sanjayan, 2021). However, only the methods applicable to 3DCP are discussed here.

2.2.1 Extrusion-Based 3D-Printing

Extrusion 3DCP is a popular technology because of its simplicity and scalability; it evolved from fused deposition modeling (FDM) in polymer 3D printers. The technique involves pumping a stiff cementitious mix into a print head, where the material is squeezed out of a nozzle to produce a layer; thereby building up a structure layer by layer. This method is one of the most widely used of all in 3DCP. Its variations include continuous extrusion, layer-by-layer extrusion, and robotic arm extrusion (Alkhalidi & Hatuqay, 2020). The material properties of the concrete mix are critical. It must be pumpable through hoses to maintain its shape, adhere properly to the layer behind, and avoid distortion due to the weight of the layers to be printed on top (Buswell et al., 2018).

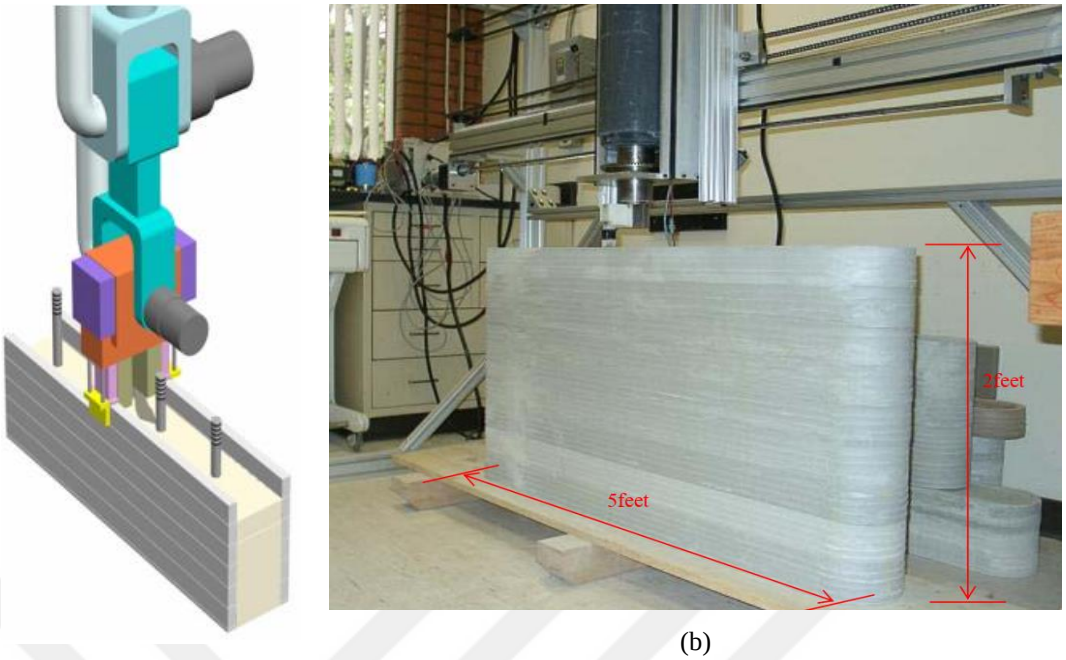
The infrastructure normally includes a pump that pushes the print material along a hose to the print head, which can be articulated with robotic machinery. Extrusion-based processes include advantages such as rapid printing speed, ease of material handling, and adaptability for larger-scale construction applications. Prof. Behrokh Khoshnevis first proposed the approach in 1997 at the Southern University of

California in the United States. In 2008, a second research group at Loughborough University investigated 3DCP, which has since grown into the foundation of extrusion 3DCP (Lim et al., 2011). Figure 2.1 is an appropriate illustration of extrusion 3DCP printing.



Figure 2. 1 3DCP by Extrusion (ICON, 2023)

Prof. Behrokh Khoshnevis invented Contour Crafting (CC) technology to automate whole-house construction (Khoshnevis, 2004). Initially employing clay as the print material, CC's main feature is the employment of two robotic, moveable trowels on the outside of the nozzle. These trowels enable the smooth production of planar surfaces at any angle, avoiding the layered pattern typical of 3D printing. The method expanded to include cement as the print material, with a stiff paste extrusion originating from a square nozzle in a rectilinear pattern. CC was used to construct the exterior shell, while the inside shell was filled with filler or a concrete mixture. The first large-scale wall was printed and presented in 2004 (Khoshnevis, 2004; Hwang & Khoshnevis, 2004). Figure 2.2 shows the multiple nozzle assembly and the first large-scale walls printed by CC.



(a) (b)

Figure 2. 2 (a) CC Multiple nozzle assembly (b) first large-scale walls printed by CC (Khoshnevis et al., 2006)

2.2.2 Selective Binding Powder/Particle-Bed-Based Method

Selective binding of powder or particle bed is a 3DCP technique in which pozzolanic powders or sand or aggregate particles are laid, deposed, or leveled in a bed layer. A print head then applies a binding or activating agent, usually a liquid or paste, to create a printed item. This method necessitates the use of a self-contained bed and the movement of either the bed platform or the side-form supports. The printer's size and additional cleaning post-processing make it unsuitable for large-scale on-site applications.

It is better suited to off-site construction as it uses prefabricated components with high degrees of precision and dimensional accuracy. There are three primary binding mechanisms: binder jetting, selective paste intrusion (SPI), and selective cement activation (SCA) (Buswell et al., 2020; Lowke et al., 2018; Weger et al., 2016).

Binder jetting involves the deposition of a liquid binding agent onto a powder bed. This is done in a layer-by-layer fashion, hence creating a solid object. The unbound

material, mostly sand, is then vacuumed out of the printing bed and recycled for other printing tasks. In construction, binder jetting has gained attention for its potential to print large-scale structures. Rael & San Fratello (2018) discuss the application of binder jetting for the fabrication of architectural components using sandstone. They showcased its viability for construction.

Due to the nature of binder jetting is an off-site process. When compared to extrusion-based approaches, this technology enables the creation of complex shapes with greater resolution (Alkhalidi & Hatuqay, 2020). According to Kumar & Sathiya (2021), the application of a powder bed presents the possibility of producing lightweight constructions with optimum geometries. However, problems such as acquiring sufficient strength and bonding in the printed structure must be solved, which makes process and material optimization crucial for powder-based methods.

Companies such as Voxteljet® have commercialized this approach, with printers measuring up to 4 x 2 x 1 m (Bester et al., 2021). The amount of detail and printing can range from 300 to 600 dpi. This technology brings up the possibility of manufacturing intricate formwork for concrete casting, with claims that fabrication costs and time are lower than alternative methods (Lowke et al., 2018). Figure 2.3 shows the printing procedure by binder jetting.

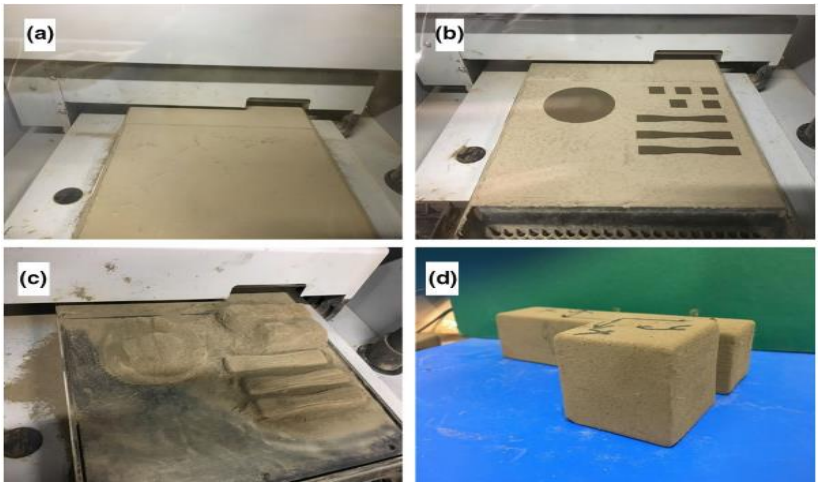


Figure 2. 3 Printing procedures of Binder Jetting (a) layering powder on printing bed (b) Application of binding agent (c) Removal of loose particles and cleaning (d) Final product (Shakor et al., 2021)

Selective Paste Intrusion (SPI) is a printing technique that employs large aggregates (usually 5mm or smaller) in the absence of binder powder. The procedure involves depositing a paste-like activated binder solution, similar to cement paste, onto dry aggregates, which allows for faster layer build height rates. Instead of being jetted, the paste is extruded or poured with a high viscosity (Buswell et al., 2020; Lowke et al., 2018).

However, the main problem is the ability of the paste to completely permeate the aggregates and prevent void formation (Pierre et al., 2018). SPI lowers the total amount of ordinary Portland cement (OPC) used, resulting in lower costs and CO_2 emissions. Furthermore, the surface finish is determined by the size of the stones utilized and has a rough, jagged appearance. Figure 2.4 shows a printer used for SPI and a finished product.



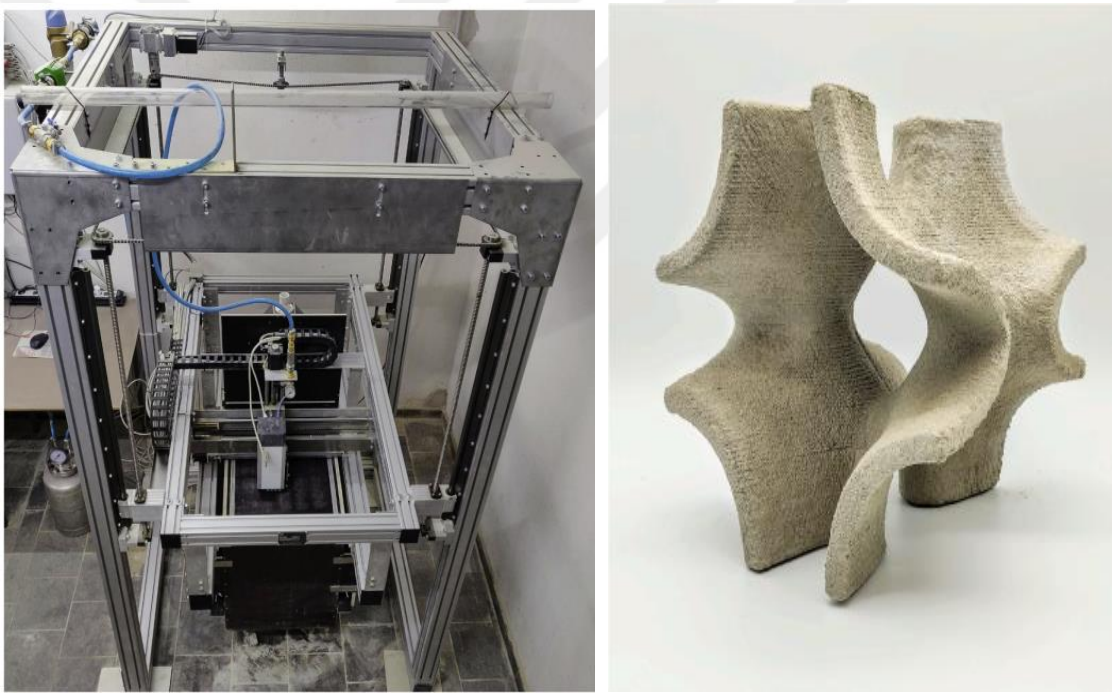
(a) (b)

Figure 2. 4 (a) Selective paste intrusion (SPI) printer (b) SPI-manufactured tube with internal double bracing (Weger & Gehlen, 2021)

Selective Cement Activation (SCA) is a technique that involves the mixing of a dry aggregate particle. This is usually sand, with a dry binder powder, typically cement. Fine layers of a dry cement-sand mixture are solidified locally by applying water. This technology is appropriate for plaster bed powder-style 3D printers. It has been used effectively with other cementitious materials such as geopolymer (Shakor et al., 2020; Xia et al., 2018). However, difficulties with adopting this

technology in large-scale applications include the size of the printing infrastructure required to store loose material as well as the subsequent removal of loose material.

The powder bed materials are sensitive to moisture in the air, demanding factory production and transportation to the site. Enrico Dini's 'D-Shape' technology, introduced in 2007, was a large-scale pioneer of this method. These days, machines that measure up to 12 m by 12 m by 10 m can be employed on-site to create objects. Practical uses for D-Shape technology include footbridges, one-shot printed homes, and artificial reefs for restoring marine biodiversity (Marchment & Sanjayan, 2021). Figure 2.5 is a suitable illustration of SCA.



(a) (b)

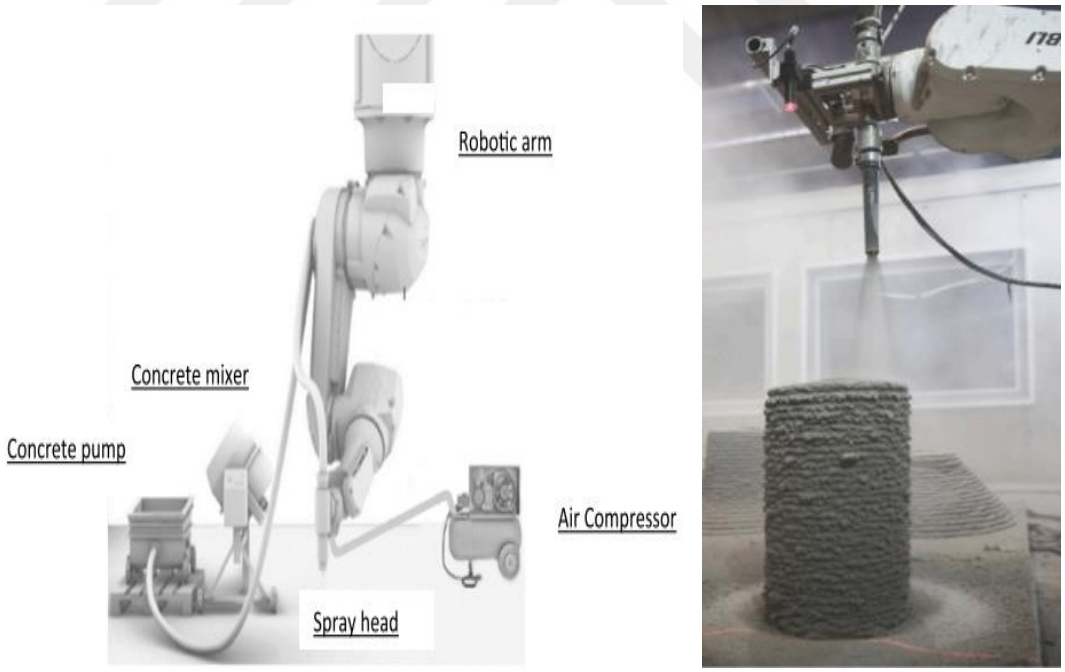
Figure 2. 5 (a) Prototype particle bed printer for selective cement activation (Lowke et al., 2018) (b) Example of a free-form geometry, manufactured by Selective Cement Activation (Talke et al., 2023).

2.2.3 Shotcrete-Based Method

Since the 1920s, shortcrete—also referred to as sprayed concrete—has been utilized for tunnel, mining, and maintenance projects. It compacts a concrete mixture in a hose, spraying it and pressurizing it onto a surface using pneumatic force. There are two types: wet shotcrete, which uses pre-mixed wet concrete that is sprayed, and

dry shotcrete, which is pumped through the hose dry and concurrently sprayed from the nozzle with water. Wet shotcrete offers advantages like thin layers on horizontal and vertical surfaces, reinforcements, and a high cement content. However, the application is frequently manual and labor-intensive (Marchment & Sanjayan, 2021).

Automated tasks in large spaces and tunnels can now be completed by robotic machinery (Benvenuto & Bäcklin, 2019; Lindemann et al., 2019; Liu et al., 2020; Lu et al., 2019; Schuler & Sawodny, 2019). The concept of shotcrete 3D printing (SC3DP) is an application of shotcrete technology that has been investigated by researchers at the University of Braunschweig, Claustral, and Hannover in collaboration. SC3DP supports thin layers in a variety of geometries, incorporated or preinstalled reinforcement, and has the ability to print overhanging structures when combined with accelerator admixture (Liu et al., 2020; Lu et al., 2020; Neudecker et al., 2016). Figure 2.6 shows a schematic setup of SC3DP and a printing example.



(a) (b)

Figure 2. 6 SC3DP (a) Setup (b) Free-formed SC3DP (Heidarnezhad & Zhang, 2022)

2.3 Properties of 3D printed concrete

Achieving a successful application of 3DPC in construction requires careful consideration of the material choices, comprehension of structural characteristics, and optimization of thermal and acoustic behavior. Enhancing the properties of 3DPC to satisfy structural requirements has been one of the most common subjects of recent research. This involves refining mix designs, including fibers, using recycled or sustainable aggregates, and so on (Rahul et al., 2022; C. Zhang et al., 2021).

Furthermore, advances in automation, real-time monitoring, and optimization algorithms are helping to increase the scalability and efficiency of 3D printing in construction. These developments are crucial for solving structural integrity, material uniformity, and overall efficiency difficulties in 3DPC constructions (Sepasgozar et al., 2020). The next sections discuss 3DPC materials, structural qualities, and thermal properties.

2.4 Materials for 3D-Printed Concrete

When it comes to 3D-printed concrete, the generally traditional materials adopted are mainly cement and fine sand in most cases. However, the nature of the free formwork technology has attracted research into the use of novel materials to improve its fresh state properties such are early strength, rheology, and extrudability (Zhang et al., 2021).

Recent developments in AM have prompted researchers to investigate the use of supplement cementitious materials (SCMs), phase change materials (PCM), admixtures, fibers, and special aggregates. There is also research on the application of alternative binders, including alkali-activated compounds and geopolymers (Hou et al., 2020; Khoshnevis, 2004; Le et al., 2012). The choice of constituting materials greatly affects the printability, durability, and strength of 3DPC structures.

2.5 Structural Properties of 3D-Printed Concrete

It is essential to understand the structural characteristics of 3DPC before using it in construction. When compared to traditionally cast concrete, the layer-by-layer deposition technology results in anisotropic behavior and diminished mechanical properties (Adams et al., 2022). The mechanical properties and structural integrity of 3DPC are influenced by variables such as layer height, printing speed, infill density, and curing techniques (Ahmed et al., 2022). Dey et al. (2023) reported that 3D-printed concrete elements demonstrate adequate structural integrity and load-bearing capacity. This indicates the potential of this technology for innovative applications in construction.

Nodehi et al. (2022) studied the long-lasting qualities of concrete structures exposed to environmental stresses like moisture seeping in, freeze-thaw cycles, and exposure to chemicals. The study showed the importance of material choice and printing methods. It also demonstrated the importance of implementing the right post-processing methods to make 3D-printed concrete structures that last a long time and work well structurally.

2.6 Thermal Properties of 3D Printed Concrete

The thermal performance of 3DPC largely depends on the thermal properties of the constituted materials of the mix design. Some of the important properties influencing the thermal behavior of 3DPC are thermal conductivity, specific heat, and density (Alkhalidi & Hatuqay, 2020). The desired thermal characteristics of a 3DPC envelope can be attained by altering the mix design (Le et al., 2012). With calls for environmental responsibility, it is necessary to optimize the thermal characteristics of 3DPC. In doing so, energy-efficient buildings can be a norm.

Phase change materials (PCMs) possess superior thermoregulatory and thermal storage capacities. They have the potential to enhance the insulative properties of concrete thus enhancing its energy efficiency. Cui et al. (2022) successfully microencapsulated paraffin into a 3D printable material. They lead to the

development of a 3D-printed phase-change concrete that exhibits favorable printability and buildability. Favorable thermal comfort can be achieved in 3D-printed facilities with the use of PCMs. Cuevas et al. (2021) examined the physical characteristics of 3D printable lightweight concrete mixtures. They incorporated recycled glass particles and expanded microspheres. They found that by changing the mixture and adding materials with poor thermal conductivity, the weight and thermal insulation of the concrete can be improved.

2.7 Insulation materials in construction

Thermal insulation is an essential component of conventional building methods, impacting energy efficiency, occupant comfort, and environmental sustainability. Due to their low cost and simplicity of installation, materials such as mineral rock wool and expanded polystyrene (EPS) have historically been used extensively in insulating buildings (Muhieldeen et al., 2021; Ijjada & Nayaka, 2022).

Depending on availability, rock wool can be used for a variety of applications because of its high density and low thermal conductivity. Rock wool enhances the thermal resistance of building envelopes (Yildiz, 2008). Furthermore, Yucel et al. (2003) remark on the excellent thermal properties of expanded polystyrene (EPS) as an insulation material, promoting its adoption in the building sector.

Novel approaches to improve insulation in masonry construction are being investigated. Jelle et al. (2015) research explores the application of revolutionary insulating materials in masonry walls, namely aerogels, and emphasizes how they can minimize thickness while offering outstanding thermal resistance. Aerogels have the potential to offer better insulation in a thin form due to their extremely low thermal conductivity (Cuce et al., 2014). According to (Ismaiel et al., 2022), normal-density closed-cell polyurethane foam efficiently insulates by retaining air inside its cells.

In addition, foam glass aggregate (FGA) has remarkably low thermal conductivity. This is because of trapped air spaces in its closed-cell structure (Bradette et al., 2019).

Similarly, Airium, a cellular lightweight concrete insulation material, has similar potential thermal insulating capabilities. This is because of its low thermal conductivity and thermal mass (Anber, 2024). The possibility of using phase change materials (PCMs) cannot be overemphasized. They absorb and release heat during phase transitions. As a result, they are able to regulate the internal climate of a structure and lower the HVAC costs (Cui et al., 2022).

There is also a discernible trend in conventional constructions toward the use of sustainable and natural insulating materials. Hempcrete is one such material that has gained traction as a viable alternative. It is a composite made of hemp fibers, lime, and water. It has thermal characteristics, which are in line with sustainability objectives (Yadav & Saini, 2022). Moreover, the increasing use of recycled paper-derived cellulose insulation in environmentally friendly constructions is attributed to its remarkable capacity for thermal efficiency (Teng et al., 2023).

2.8 Insulation Techniques in Buildings

Optimization of the building envelope design is a crucial component of thermal insulation. The proper distribution of insulation across an envelope reduces thermal bridging and improves overall energy efficiency (Guo et al., 2023).

In conventional construction, thermal performance can be maximized by utilizing a variety of insulating techniques. These insulating techniques include the use of spray foam insulation, rigid foam board insulation, loose-fill insulation, reflective insulation, insulated concrete forms (ICFs), structural insulated panels (SIPs), low-E windows, double glazing, insulating paints or coatings, and adding thermal mass. The selection of insulating techniques would be contingent upon several aspects. This includes but is not limited to building design, climate, budget, and the intended degree of thermal efficiency and comfort (Tamimi et al., 2023).

Nonetheless, the demand for increased energy efficiency and sustainability has prompted innovations in conventional insulation methods, such as the use of radiant barriers and reflective foils with multiple uses inside the building envelope (Lee et al.,

2016). The literature also shows developments in building envelope design, which goes beyond material advancements. Jelle et al. (2015) studied the potential of decreasing heat transfer through high-performance windows with low-emissivity coatings and multiple glazing layers.

Additionally, the utilization of continuous insulation systems and the incorporation of sophisticated frame techniques are also recommended (Fawaier & Bokor, 2022). They are reported to reduce thermal bridging and improve the overall performance of the building envelope. These recent advances highlight an inclination toward methods and materials that solve sustainability issues and provide better insulating qualities.

2.9 Heat Transfer Mechanisms

Heat transfer is an important phenomenon in science, especially in thermal energy studies. There are three mechanisms of heat transfer: conduction, convection, and radiation. A review of the fundamental heat transfer mechanisms as well as analytical and numerical methods of heat transfer is provided here:

2.9.1 Conduction

Conduction is the flow of thermal energy within a substance or between materials in direct physical contact. It happens due to kinetic energy being transferred from higher-temperature regions to lower-temperature regions by molecular vibrations and collisions. Heat conduction occurs through molecular vibrations in solids and collisions in gaseous mediums (Rajput, 2015). The thermal conductivity of a material, its dimensions, and the temperature gradient all affect the rate at which heat conduction occurs within it.

In the early 1800s, Joseph Fourier established the mathematical theory of heat conduction. By experimentation on a rectangular solid, the researcher discovered that the rate at which thermal energy is transferred from the hot side to the cold side is proportional to the cross-sectional area across which the heat flows, the temperature

difference, and inversely proportional to the material's thickness (Rajagopal, 2007). The law takes the following differential form to express one-dimensional steady-state heat conduction.

$$Q = -kA\frac{dT}{dx} \tag{2.1}$$

Where:

- Q is the heat transfer rate,
- k is the thermal conductivity of the material,
- A is the cross-sectional area through which heat is transferred,
- $\frac{dT}{dx}$ is the temperature gradient in the material.

The negative sign means that heat flows in the direction of decreasing temperature (Çengel & Ghajar, 2015).

2.9.2 Convection

Convection is the process of heat transfer between a surface and a moving fluid (liquid or gas). Convection comes from fluid motion. There are two types of convection, i.e., natural and forced convection. Natural convection occurs as a result of buoyancy and buoyant forces exerted on a fluid. It requires a temperature differential between the fluids. Natural convection can be seen in the form of sea wind or land breeze. Forced convection is created by external sources such as fans or pumps (Çengel & Ghajar, 2015).

Convective heat transfer is defined by Newton's Law of Cooling, which connects the rate of heat transfer to the temperature gradient between the fluid at the surface and its surrounding medium as well as the convective heat transfer coefficient. According to Bejan (2013), the law specifies the rate at which heat is lost from a body to its environment as a result of temperature differences. The law can be expressed as follows:

$$Q = hA(T - T_{ambient}) \quad (2.2)$$

Where:

- Q is the heat transfer rate,
- *h* is the convective heat transfer coefficient (in watts per square meter-kelvin, $W/(m^2 \cdot K)$),
- A is the surface area of the body in contact with the surrounding medium (in square meters, m^2),
- T is the temperature of the body (in kelvin, K),
- $T_{ambient}$ is the ambient temperature of the surroundings (in kelvin, K).

2.9.3 Radiation

The transfer of thermal energy via electromagnetic waves that don't require a medium to propagate is known as radiation (Rajput, 2015). Any object that has a temperature higher than zero produces radiant heat. The total energy radiated by a black body, or perfect emitter, is proportional to the fourth power of its absolute temperature, according to the Stefan-Boltzmann Law. This law relates an object's absolute temperature to the total radiant energy it emits (Modest, 2013). The Stefan-Boltzmann Law can be expressed mathematically as given below:

$$E = \sigma A T^4 \quad (2.3)$$

Where:

- E is the total radiated energy (emissive power) per unit surface area (in watts per square meter, W/m^2)
- σ is the Stefan-Boltzmann constant ($\sigma = 5.67 \times 10^{-8} W/(m^2K^4)$),
- A is the surface area of the object (in square meters, m^2),
- T is the absolute temperature of the object (in Kelvin, K).

Radiation studies are crucial to many applications. Examples of applications include space heating, solar energy consumption, and thermal analysis of engineering

systems. They become significant, particularly in applications where high temperatures are involved (AlZahrani et al., 2022).

2.10 Heat transfer in 3DPC walls

Lattice structures are characterized by a complex network of webs and face shells thereby forming a building envelope. These can be closed cells, like foams, or open cells, like a honeycomb structure. There are four main mechanisms of heat transfer in 3DPC building envelopes. These are thermal conduction through the solid and gas, radiation across the cells, and natural convection inside the cells (Briels et al., 2023). Figure 2.7 shows the four main phenomena of heat transfer through 3DPC wall panels.

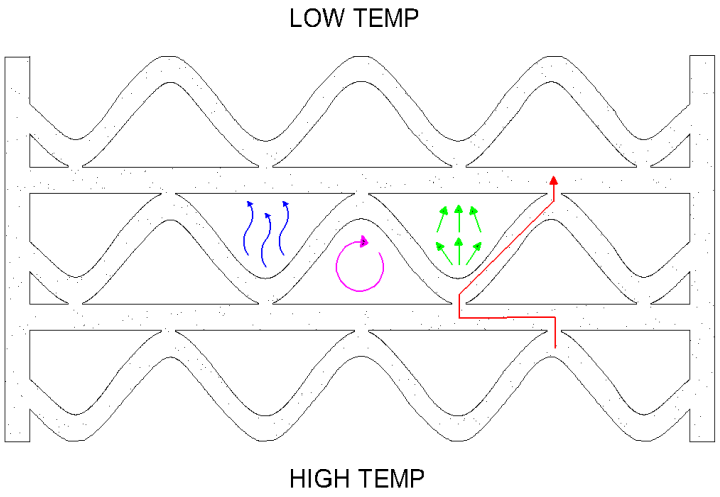


Figure 2. 7 Four main phenomena of heat transfer through 3DPC wall panels: conductive heat transfer through the gas (blue) and solid (red), convective (pink) heat transfer within the cells, and radiative (green) (Inspired by Briels et al., 2023)

2.11 Analytical Methods of Heat Transfer

For accurate thermal behavior and energy efficiency predictions to be made during the design phase of a building envelope, accurate thermal performance characterization is essential. The most crucial parameter for establishing the thermal performance of a building envelope is thermal transmittance (U-value). The

following section discusses the common analytical and numerical methods used to determine the U-value of a building envelope.

It can be challenging to calculate a building element's thermal performance, particularly when non-homogeneous parts are incorporated. The thermal behavior of building envelopes can be ascertained using a variety of analytical techniques. The type of construction and thermal insulation determine which option is the most appropriate (Martins, 2020). The methods provided below are the most commonly used to determine the thermal transmittance (U-values) and thermal resistance (R-values) of building envelopes under steady-state conditions.

2.11.1 Multilayer plane walls

For one-dimensional heat transfer analysis through homogeneous multilayer planar walls, this is one of the most popular methods. The principle of thermal resistance (R_T) is applied in determining the rate of heat transfer in these composite wall assemblies. The R-value is the ability of a material to resist heat from passing through it (Rajput, 2015). The rate of heat conduction, through a wall multilayer plane is directly proportional to the temperature differential, the wall area, and the average thermal conductivity but inversely proportional to the wall thickness (Çengel & Ghajar, 2015). This relationship is shown in Equation. 2.4, where T_1 and T_2 are the ambient temperatures on the two faces of the wall.

$$Q = \frac{T_1 - T_2}{R_T} \tag{2.4}$$

In heat flow calculations, the thermal resistance of every material layer must considered. The geometry of the system and its thermal characteristics, such as the surrounding fluid's thermal conductivity, affect the R-value (Advanced Architectural Products (AAP), 2023). The thermal resistance or R-value is the ratio of the thickness (d) of a specimen divided by the apparent thermal conductivity (k) (Kośny & Yarbrough, 2022). Çengel & Ghajar (2015) define thermal conductivity as a material's capacity to transfer heat. Equation 2.5 quantifies this interaction. High heat

flow correlates with high U-values. The total thermal resistance (R_T) of a building envelope, which is the sum of the thermal resistances of the outer layer, inner layer, and cavity insulation, is inversely proportional to its U-value (Equation 2.6).

Greater thermal resistance is indicated by lower U-values. Equation 2.7's direct proportionality illustrates how this leads to lower heat flux (Q), highlighting reduced heat flow across a system or assembly. Heat flux is a measure of heat energy that moves through a unit area in a unit of time (Welty et al., 2020). It is a dynamic illustration of the intensity of heat transfer. Because of this, the relationship between heat flux and R-value resembles that between electric current flow and electrical resistance (Figure 2.8). The R-value can be calculated by dividing the temperature difference (potential difference) between two surfaces by an established heat flux.

$$R_T = \frac{L}{kA} \tag{2.5}$$

$$U = \frac{1}{R_T} \tag{2.6}$$

$$Q = U\Delta T \tag{2.7}$$

For example, for a two-layer composite wall, illustrated in Figure 2.9, the total thermal resistance can be given by:

$$R_T = R_{conv,1} + R_{wall,1} + R_{wall,2} + R_{conv,2} \tag{2.8}$$

Where $R_{wall,1}$ and $R_{wall,2}$ are the thermal resistances of the wall layers. $R_{conv,1}$ and $R_{conv,2}$ are the thermal resistances of the surfaces (faces) against heat convection, or simply the convection resistance of the surfaces (Newton's law of cooling).

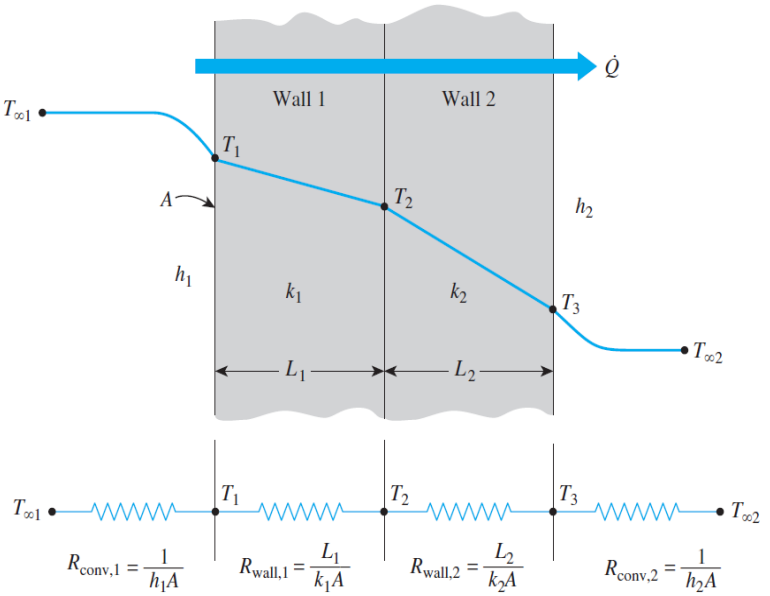


Figure 2. 8 The thermal resistance network for heat transfer through a two-layer plane wall subjected to convection on both sides (Çengel & Ghajar, 2015).

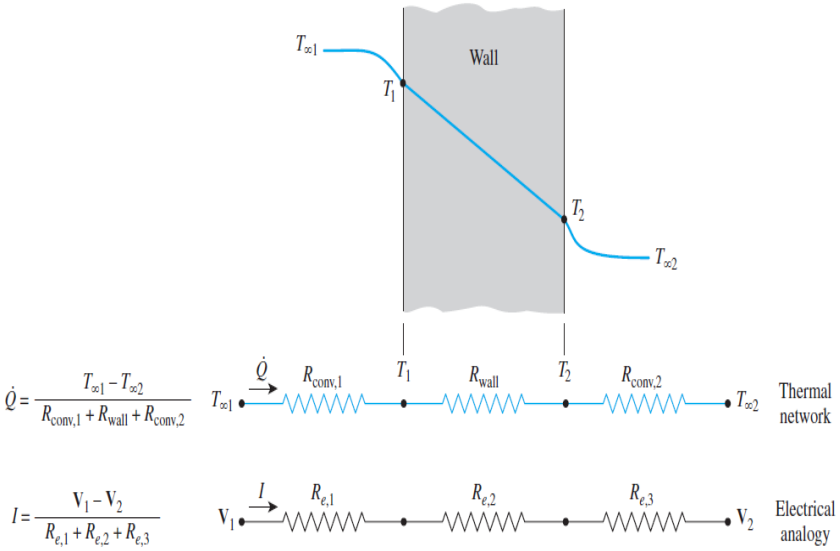


Figure 2. 9 The thermal resistance network for heat transfer through a plane wall subjected to convection on both sides and the electrical analogy (Çengel & Ghajar, 2015).

2.11.2 Parallel Path Method

This method assumes that heat moves along parallel pathways, or zones, as shown in Figure 2.10, with little to no heat exchange taking place in between. For one-dimensional heat transfer, this approach produces fairly precise results. On the other

hand, it is difficult to produce satisfactory results when applied to highly conductive structural elements. For conventional sandwich units or wood-frame assemblies, the parallel-path computation is useful (Kośny & Yarbrough, 2022).

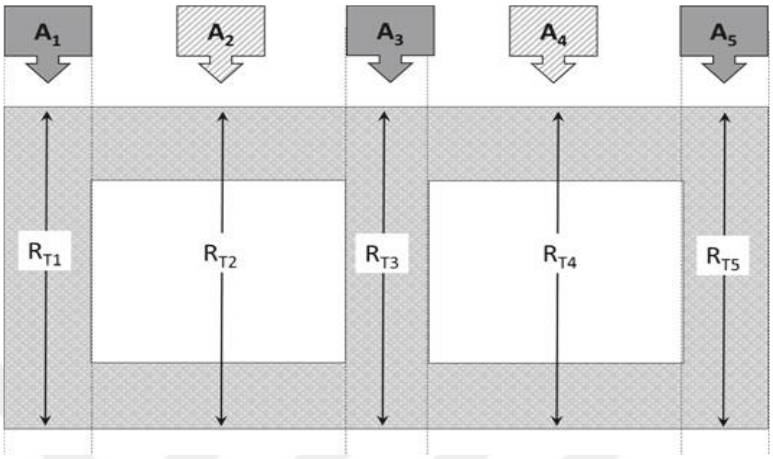


Figure 2. 10 Calculation schematic for the parallel path method (Kośny & Yarbrough, 2022).

Therefore, the heat flow (Q) through a unit containing multiple assemblies of defined areas can be expressed in terms of the R-value or U-value, as given below (Martins, 2020).

$$Q = \Delta T\left(\frac{A_1}{R_{T1}} + \frac{A_2}{R_{T2}} + \frac{A_3}{R_{T3}} + \frac{A_4}{R_{T4}} + \cdots\right) = \Delta T\sum_{i=1}^{n}\frac{A_i}{R_{Ti}} \tag{2.9}$$

$$Q = \Delta T\left(\frac{U_1}{A_1} + \frac{U_2}{A_2} + \frac{U_3}{A_3} + \frac{U_4}{A_4} + \cdots\right) = \Delta T\sum_{i=1}^{n}\frac{U_i}{A_i} \tag{2.10}$$

Since $U = \frac{1}{R_T}$ (Equation 2.6), the effective R-value (R_T) can be computed as:

$$R_T = \frac{1}{\sum A_i}\sum_{i=1}^{n}\frac{A_i}{R_{Ti}} \tag{2.11}$$

Where:

- R_{Ti} is the thermal resistance heat path (zone) "i". This is obtained by summing the resistance of all heat paths, including inner and outer convective air films.
- U_i is the heat transmission coefficient in BTU/(h·ft^2 ^{o}F) for assembly "i," including the effect of the interior and exterior surface films.
- A_i is the area of the heat path (zone) “i”, in ft2.
- ΔT is the temperature difference between the indoor and outdoor air.

2.11.3 Isothermal Planes (Series–Parallel Path) Method

The series-parallel method has been thought to be more realistic in portraying such systems in buildings with structural components consisting of different materials, such as steel, concrete, etc., or with high thermal conductivity (Kośny & Yarbrough, 2022). This approach makes the assumption that an isothermal (uniform temperature) is used to distinguish the less-conductive layers from the more-conductive ones.

It is not without limitations, though. For example, this analysis does not account for the effects of mass, moisture, air penetration orientation, building techniques, and other elements influencing overall performance, such as dynamic effects (Perlite Institute, 2013). Besides, for structures with widely spaced metal members of substantial cross-sectional area, this method can give thermal resistance values too low (Martins, 2020). The assembly's thermal resistive components play a major role in determining the thermal performance in this case. The Perlite Institute (2014) has provided realistic design information through comparison using this approach. For example, heat flow through wood-framed assemblies or masonry walls is analyzed using this approach.

In the case of a two-core concrete block, the U-value of the assembly can be calculated, provided that the thermal conductivities of the system components are known. In order to do this, just add the thermal resistances in parallel and series with the corresponding percent areas. The mathematics involved are presented here, together with a schematic of a typical two-core concrete block with perlite loose fill

insulation material (Figure 2.11). The block is taken to have square corners, no radii, and no ears for simplicity's sake (Perlite Institute, 2014).

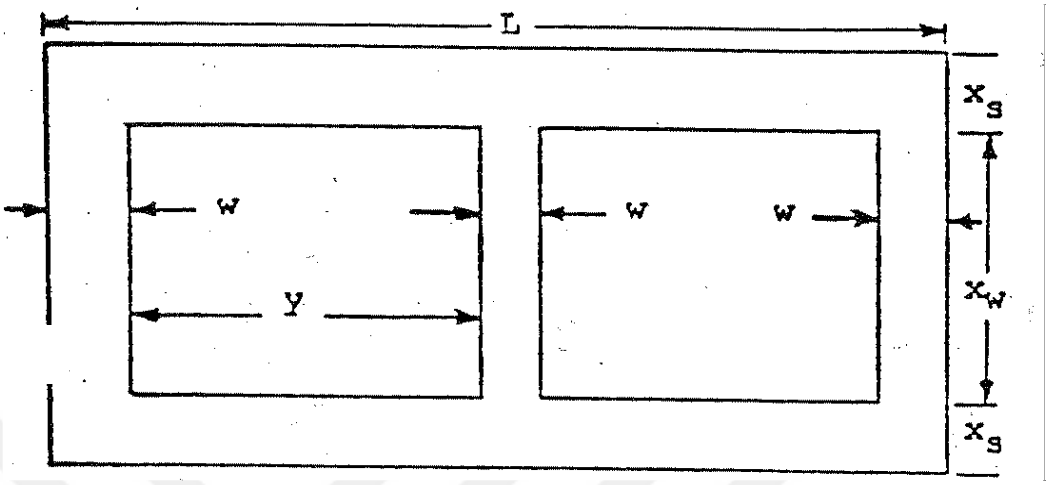


Figure 2. 11 Typical two-core concrete block (Perlite Institute, 2013)

The block is separated into multiple layers in this method. The face shells—which are less conductive together with cores (loose fill insulation) —are joined by the webs, which are more conductive and solid. Heat flows laterally through the face shells (Martins, 2020). A schematic presentation of thermal resistance for a two-core concrete block is given in Figure 2.12.

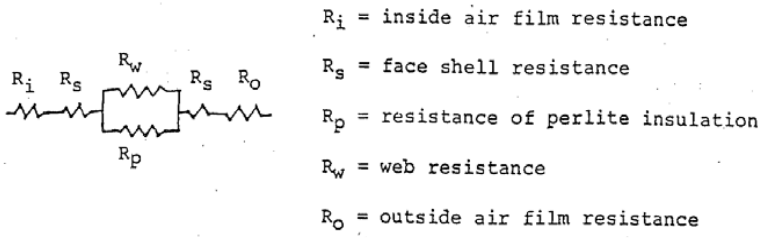


Figure 2. 12 A schematic presentation of thermal resistance for a two-core concrete block (Perlite Institute, 2013)

The overall thermal resistance of the block can therefore be determined using equation 2.12 below:

$$R_T = R_I + R_S + \left(\frac{A_c}{R_P} + \frac{A_W}{R_W}\right) + R_S + R_O \qquad (2.12)$$

Where

- R_I = inside air film resistance (literature value)
- R_S = face shell resistance $\left(\frac{X_S}{\lambda_C}\right)$
- R_P = Resistance of air/cavity insulation $\left(\frac{X_W}{\lambda_P}\right)$
- R_W = web resistance $\left(\frac{X_W}{\lambda_C}\right)$
- R_O = outside air film resistance (literature value)
- A_c = percentage of cross-sectional area not taken by webs, expressed as a decimal number, $\frac{2y}{L}$
- A_w = percentage of web cross-sectional area expressed as a decimal number, $1 - \frac{2y}{L}$
- X_s = thickness of face shell
- λ_C = apparent thermal conductivity of concrete
- X_W = thickness of the core web
- λ_P = apparent thermal conductivity of air/insulation

Other analytical methods used to determine the thermal performance of building envelopes not discussed include the zone method, modified zone method, linear thermal transmittance method, ISO 6946 method, and the simplified method of calculating U-values in light steel framing (Kośny & Yarbrough, 2022; Martins, 2020). Besides, the hot box method guarded, hot plate method, and heat flow meter method are among the experimental methods used to estimate the U-value of walls (Tamimi et al., 2023).

2.12 Numerical Methods of Heat Transfer

There are many sophisticated numerical computational techniques. These include computational fluid dynamics (CFD) and finite element analysis (FEA). By utilizing these sophisticated numerical techniques, it is possible to create incredibly complex models of building elements. The models are capable of depicting more accurate and

dependable thermal behavior (Lee, 2018). These numerical methods allow for the optimization of the constructive aspects and the rationalization of resources by developing complex numerical models that, if validated, have the benefit of being less costly in terms of both time and money.

Nevertheless, these complex numerical algorithms' accuracy needs to be verified. Hence, ISO 10211 contains standards that must be adhered to when thermal modeling building assemblies through test cases. Thus, the computation of the heat fluxes and surface temperatures is verified by using these specifications to assess the accuracy of the numerical algorithms and validate the calculation process. ANSYS, ABAQUS, COMSOL Multiphysics, THERM, Nastran, SolidWorks Simulation, MATLAB (with Simulink), OpenSees, and DIANA FEA are among the commercially available software for FEA (Kośny & Yarbrough, 2022). The finite element method (FEM) (software) for two- and three-dimensional (3D) analysis, as well as its dependability, are discussed in the following subsections.

2.13 Finite Element Method (FEM)

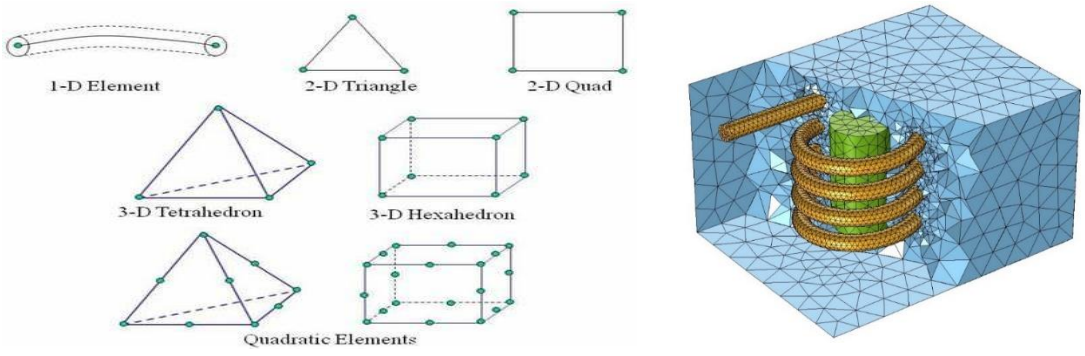
For the computation of differential and integral equations that emerge in many applied science and engineering domains, the Finite Element Method is a potent computing tool. Since most real-life problems are based on geometrically complicated domains, they frequently have various boundary conditions on distinct sections. Therefore, developing the approximation functions needed by the conventional variational methods and coming up with an analytical solution is typically challenging or impossible. For this reason, approximation techniques are required, and the finite-element method provides a solution to these challenges (Zieli, 1992).

This method breaks down complicated problems into smaller, more manageable components to approximate their answers. According to Thompson & Thompson (2017), each element is defined by a system of equations that connect the unknowns to particular locations inside the element called nodes. Unknowns in this respect include temperature and heat flux. Each element also makes use of shape functions to

describe the variations in the unknowns within it. A system of algebraic equations representing the whole problem domain is generated through the amalgamation of the equations of all the constituents. Direct methods, or iterative techniques, are used to solve the unknowns at the nodes. Consequently, FEM is adaptable and flexible when managing intricate geometries (Bergheau & Fortunier, 2013). The subsequent sections discuss the steps taken by advanced numerical algorithms embedded in FE software to approximate solutions.

2.13.1 Discretization of the Domain

Discretization of the domain, breaking down a complicated continuous geometry or physical domain into smaller, more manageable elements forms an essential step within the finite element analysis (FEA) process. The elements that can be in the form of triangles, quadrilaterals in 2D, and tetrahedra and hexahedra in 3D are used in order to provide an approximation of the intensities on the nature of a material or the structure will have, located in different regions (Frunză & Luca, 2010). The problem is divided into smaller parts, where meshing makes the numerical solution feasible. The mesh structure is provided as well as its connectivity by the geometry and node placement while holding specific elements exactly, and this brings about an accurate presentation of geometry and material properties (Lee, 2018). Figure 2.13 shows the common types of elements used in FEA as well as the discretization (meshing) of a sample model.



(a) (b)

Figure 2. 13 Element Types (Frunză & Luca, 2010) (b) The default free tetrahedral mesh feature in Ansys is applied to the entire model (Walter Frei, 2015).

The precision of the results is dependent on the accuracy and quality of the mesh. To ensure a well-distributed mesh that corresponds to the geometry's properties, mesh quality is measured based on element shape, aspect ratio, skewness, and other criteria. Furthermore, the simulation is guided by the assignment of boundary conditions (e.g., fixed nodes, prescribed temperatures) and material properties (e.g., thermal conductivity) to elements. Mesh refinement can be used to improve accuracy in crucial areas by adjusting mesh density based on simulation needs (Walter Frei, 2015).

As stated earlier, discretization via meshing is a key stage in FEA, allowing for the numerical approximation of physical behaviors by breaking down complicated geometry into discrete parts. Its dependability is ensured by a well-structured mesh. Using refinement to balance mesh density guarantees an efficient computational process while collecting crucial information for precise simulations (Thompson & Thompson, 2017).

2.13.2 Formulation of Governing Equations

The fundamental laws governing heat transfer are transformed into a set of equations in this step. These mathematical equations describe the behavior of the system under consideration and are based on heat transfer laws and modes discussed in the previous sections. These equations are converted into a set of partial differential equations (PDEs) that define the phenomenon of heat transfer within the elements (Manual, 2009). These equations are essential for the creation of FE models, thus determining temperature distribution, heat fluxes, air velocity contour maps, and many other parameters. This provides vital insights into the thermal behavior of the system under study (Lee, 2018).

2.13.3 Assignment of Material Properties and Boundary Conditions

It is imperative to accurately represent material properties and adequate boundary conditions for accurate thermal analysis. Material properties govern the movement of heat through a material. Boundary conditions define how the system interacts with its

surroundings (Manual, 2009). Boundary conditions set limitations and influences at the system's boundaries. These conditions govern how heat is exchanged or restrained at the system's boundaries. Precise knowledge and representation of these parameters are essential to obtain more accurate thermal distribution profiles within a system under investigation. Thus, understanding and applying proper boundary conditions is critical for accurately representing the real-world environment. Prescribed temperatures, heat fluxes, convection coefficients, and radiation parameters are examples of boundary conditions (Lee, 2018). These parameters must obtained by material testing, empirical research, or the use of established databases or technical standards.

2.13.4 Assembly of System Equations

The differential equations are amalgamated into a global system of linear or nonlinear equations thus yielding an FE model. This assembly involves the merging of the elemental stiffness matrices, mass matrices, and load vectors. They become a comprehensive system that captures the behavior of the entire structure or system (Thompson & Thompson, 2017). The assembly method makes use of connectivity information to determine how the elemental equations are related and merged to generate the global system. The resulting system of equations is frequently expressed in matrix form as K· Ø = F, where K is the global stiffness matrix, Ø is the vector of unknown nodal temperatures, heat fluxes, or other variables, and F is the vector of known nodal loads (boundary conditions) (Lewis et al., 1996). The system of matrices given in Figure 2.14 below is an illustration of the assembly of system equations in the form K·Ø = F.

$$\begin{bmatrix} k_{11}^{(1)} & k_{12}^{(1)} & 0 \\ k_{21}^{(1)} & k_{22}^{(1)} + k_{11}^{(2)} & k_{12}^{(2)} \\ 0 & k_{21}^{(2)} & k_{22}^{(2)} \end{bmatrix} \begin{Bmatrix} \phi_1 \\ \phi_2 \\ \phi_3 \end{Bmatrix} = \begin{Bmatrix} f_1^{(1)} \\ f_2^{(1)} + f_1^{(2)} \\ f_2^{(2)} \end{Bmatrix}$$

Figure 2. 14 Assembly of a 3x3 matrix system in the form K·Ø = F (Rehman et al., 2017)

The assembly of the system equations must be efficient and accurate to produce reliable simulation results. To improve the assembly process, advanced numerical methods and algorithms are frequently used, particularly for complex systems with a significant number of elements and degrees of freedom. Careful attention to detail during the formation stage guarantees that the final system of equations appropriately reflects the physical behavior of the examined system. This serves as a foundation for generating relevant insights during later numerical solution procedures (Lee, 2018).

2.13.5 Application of Solver

FEA software, like Ansys, uses several numerical solvers to solve the system of matrices obtained in the previous step. The solver utilizes a variety of mathematical and computational techniques to determine the system unknowns. It acts on the global system of equations derived during the assembly phase. In this system of equations, the stiffness matrix and load vector are known.

Depending on the nature of the equations and the degree of complexity of the problem, multiple-solving approaches may be employed (Manual, 2009). Direct solvers get a precise solution for the system by employing algorithms such as Gaussian elimination or LU decomposition. Iterative solvers like the conjugate gradient approach or the Generalized Minimal Residual (GMRES) method, on the other hand, are typically more efficient and practical for large-scale problems, especially when working with sparse matrices (Bergheau & Fortunier, 2013). For heat transfer studies, the implicit difference method is commonly applied (Lee, 2018).

2.13.6 Convergence and Solution Accuracy

Convergence is the process by which a numerical solution approaches a stable and consistent result as the iterative solver refines it. The iterative procedure refines the solution by making consecutive approximations. Convergence occurs when the difference between subsequent iterations is less than a defined tolerance. It means that additional iterations have no meaningful effect on the results. Thus indicating

that the solution has reached a point of stability (Dadkhah & Zecher, 2009). When applying the solver, it is imperative to observe and enhance solver settings, select a suitable solution technique, and modify the convergence criterion. Convergence essentially guarantees that the obtained solution appropriately represents the physical behavior of the system under consideration. A well-converged solution increases trust in simulation results by capturing the true thermal properties of the system (Thompson & Thompson, 2017).

According to Manual (2009), solution accuracy is a metric that quantifies the degree to which the numerical solution agrees with the true or exact solution of the mathematical model that describes a physical phenomenon. In the realm of thermal analysis, accuracy is assessed by comparing the simulated temperature distributions, heat fluxes, and other thermal characteristics with the experimentally verified values. The mesh density, material properties, element types, boundary conditions, and solver settings are some of the factors that affect the accuracy of the solution (Bergheau & Fortunier, 2013). Enhancing the mesh density or refinement of the mesh in crucial areas while utilizing high-quality elements can improve the accuracy of the solution. Mesh refinement essentially captures more subtle details and temperature gradients.

Furthermore, a balance between the convergence and the accuracy of the solution is crucial. It is imperative to make iterative adjustments to the mesh, solver settings, and other simulation parameters to attain high solution accuracy and convergence (Lee, 2018). This results in dependable simulation, thereby offering insightful information on the thermal behavior of the system being studied.

2.13.7 Post-Processing and Visualization

Post-processing is the examination and interpretation of simulation results to acquire a deeper understanding of the behavior of the system under analysis. Post-processing tools are employed to retrieve appropriate information from the solution data. This information includes stress contours, temperature profiles, heat flux distributions, and other crucial mechanical or thermal properties. Post-processing

helps in understanding the thermal behavior of a system. Thus, pointing out problem areas, and helping designers make well-informed choices (Dadkhah & Zecher, 2009).

A key component of post-processing is visualization, which enables users to represent the simulation results visually and intuitively. Graphical tools such as color gradients, vector plots, and contour maps can be utilized. Besides, animations and 3D visualization tools are available (Lee, 2018). This way, engineers and researchers can effectively communicate complicated data and make well-informed decisions. Post-processing and visualization also make the evaluation and validation of simulation results against experimental data or theoretical expectations easier. Users can evaluate the accuracy of the simulation and dependability by superimposing experimental data over the findings of the simulation. Figure 2.15 is an example of the surface heat flux contour map of a lattice structure studied in this thesis work.

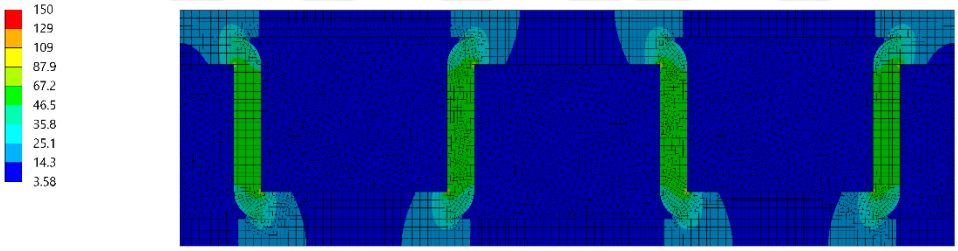


Figure 2. 15 Surface heat flux contour map of the a wall panel studied

2.14 Two-dimensional (2D) numerical models

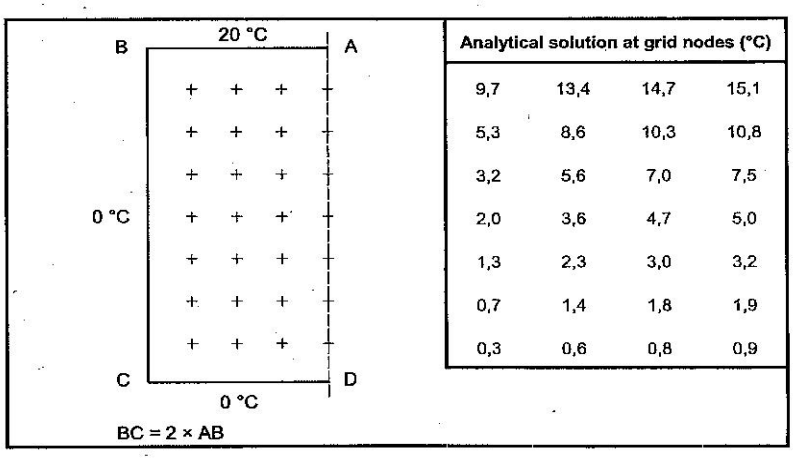
In ISO 10211:2007, specifications and two test cases were developed to validate 2D software. These consist of the temperature, the boundary conditions, the temperature distribution, and the geometric boundaries and subdivisions of the model. This standard stipulates that the results of the analysis of the computing software algorithm must match the test cases of references 1 and 2 for it to be categorized as a high-two-dimensional precision technique in steady-state.

For two-dimensional thermal analysis, practitioners have access to and employ a wide range of numerical tools, including PSI Therm, ANSYS Fluent, Heating3,

AnTherm, BISCO (for 2D) and TRISCO (for 3D), Comsol, and Heating3 (Kośny & Yarbrough, 2022). However, THERM, a free software program developed by Lawrence Berkeley National Laboratory (LBNL), is used in ISO 10211 for 2D analyses. The two test cases are discussed below.

2.14.1 Test Case 1

Figure 2.16 provides an analytical method for calculating the heat transfer through a half-square column with known surface temperatures. It also provides the analytical solution at 28 points on an equidistant grid. There must be a maximum of 0.1 °C variation between the temperatures indicated in the analytical solution and those determined by the procedure under validation (FEM). Test case 1, modeled in THERM, is shown in Figure 2.17. The program precisely produced the same results as the standard stipulates, indicating that the discrepancy between the software's and the standard's estimated temperatures was less than 0.1°C. The results are given in Table 2.1.



Analytical solution at grid nodes (°C)			
9,7	13,4	14,7	15,1
5,3	8,6	10,3	10,8
3,2	5,6	7,0	7,5
2,0	3,6	4,7	5,0
1,3	2,3	3,0	3,2
0,7	1,4	1,8	1,9
0,3	0,6	0,8	0,9

Figure 2. 16 The analytical solution of heat transfer through half a square column at 28 points of an equidistant grid (ISO 10211, 2007)

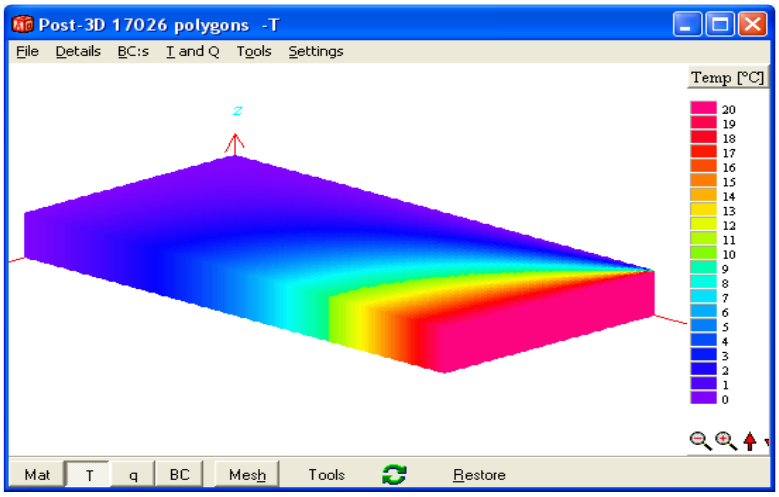


Figure 2. 17 Test case 1 performed in THERM (ISO 10211, 2007)

Table 2. 1 Test Case 1 surface temperature results obtained by THERM (ISO 10211, 2007)

Matrix of temperatures at marked points [C]			
9.66	13.38	14.73	15.09
5.25	8.64	10.32	10.81
3.19	5.61	7.01	7.47
2.01	3.64	4.66	5.00
1.26	2.31	2.99	3.22
0.74	1.36	1.77	1.91
0.34	0.63	0.82	0.89

2.14.2 Test Case 2

In the second case, a two-dimensional heat transfer scenario with related dimensions and boundary conditions is given in Figure 2.18 below, along with Table 2.2, which displays the boundary conditions and geometric and thermal properties.

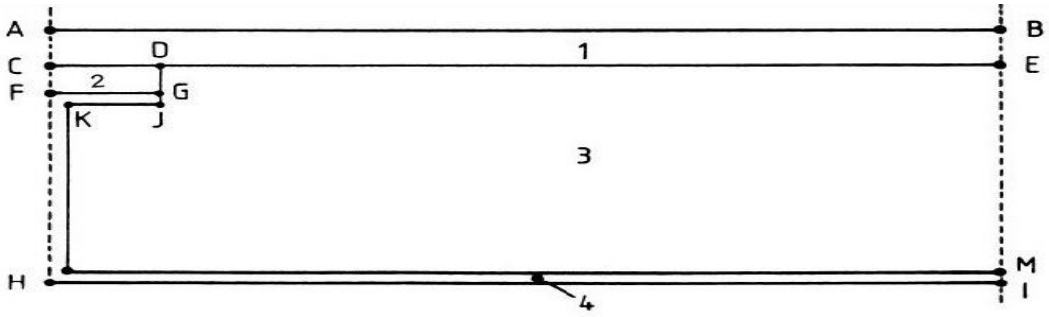


Figure 2. 18 Test case 2 for 2D heat transfer (ISO 10211, 2007)

Table 2. 2 Geometric and thermal properties and boundary conditions of Test Case 2 for 2D heat transfer (ISO 10211, 2007)

Dimensions (mm)	**Thermal Conductivity W/(m・K)**	**Boundary conditions**
AB = 500		AB: 0 °C with R_{se} = 0.06 m^2・K/W
AC = 6	1: 1.15	HI: 20 °C with R_{si} = 0.11 m^2・K/W
CD = 15	2: 0.12	
CF = 5	3: 0.029	
EM = 40	0.32639	
GJ = 1.5		
IM = 1.5		
FG - KJ = 1.5		

When modeled and run in THERM, the expected temperatures at the respective points are given in Table 2.3 below. The total heat flow rate should be 9.492 W/m.

Table 2. 3 Test Case 2 surface temperature results stipulated by ISO 10211 (2007)

Point	**A**	**B**	**C**	**D**	**E**	**F**	**G**	**H**	**I**
Temperature [˚C]	7.0643	0.7615	7.8951	16.33	0.8275	16.404	16.33	16.765	18.334
Total heat flow rate: 9.429 W/m									

Martins (2020) modeled test case 2 and fulfilled its requirements as depicted in Figure 2.19, with the same temperatures as indicated in Table 2.4. The total heat flow rate that was computed deviates from the standard by 0.0079 W/m, which is less than the necessary 0.1 W/m. There was precisely 9.492 W/m of total heat flow. After confirming that THERM is being used correctly, it can be concluded that the two-dimensional steady-state high-precision approach satisfies the requirements stated in ISO 10211.

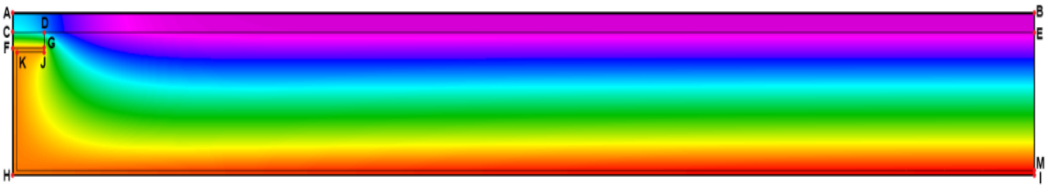


Figure 2. 19 Modeling of Test Case 2 in THERM by Martins (2020)

Table 2. 4 Test case 2 surface temperature results obtained by Martins (2020)

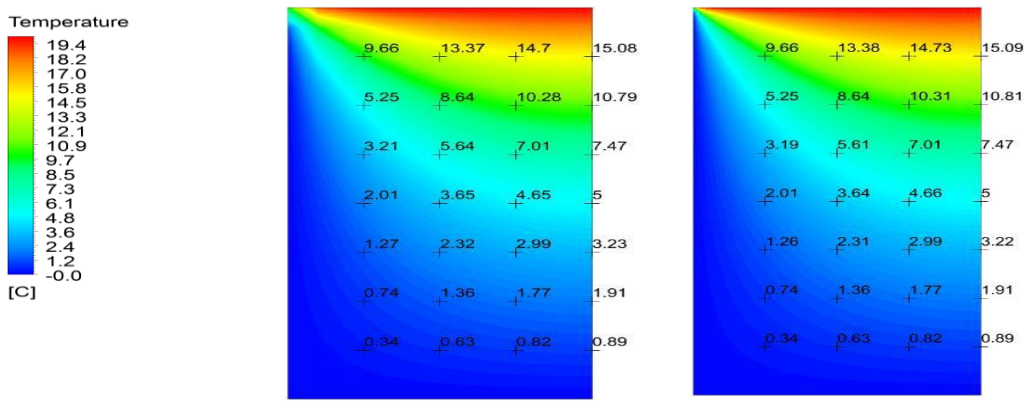
Point	**A**	**B**	**C**	**D**	**E**	**F**	**G**	**H**	**I**
Temperature [˚C]	7.0643	0.7615	7.8951	16.33	0.8275	16.404	16.33	16.765	18.334
Total heat flow rate: 9.429 W/m									

2.15 Three-dimensional (3D) numerical models

According to ISO 10211:2007, a software calculation algorithm must produce results that match reference test cases 1, 2, 3, and 4 in order to be categorized as a three-dimensional steady-state high-accuracy method.

2.15.1 Test Cases 1 and 2

The first two test cases are similar to those of the 2D FEM discussed earlier. Figure 2.20 presents Test Case 1 performed in Ansys, in which two analyses were made by varying the number of nodes. In the first model, Figure 2.20a, 924 nodes were used, whereas 72,114 nodes were used in the second (Figure 2.20b). A maximum difference of 0.05°C was seen when the two models' results were compared. It can be seen from Table 2.3 that there is less than 0.1°C variation between the values obtained in Ansys and the standard. Similarly, Figure 2.21 presents Test Case 2 performed in Ansys. From Table 2.4, it is concluded that Ansys fully passes this test.



(a) 924 nodes (b) 72,114 nodes

Figure 2. 20 Test case 1 results in Ansys by Martins (2020)

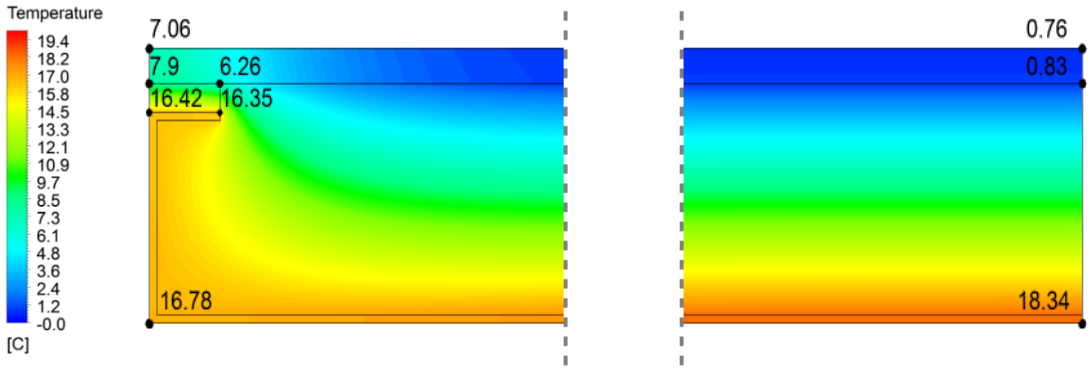


Figure 2. 21 Test case 2 results in Ansys by Martins (2020)

2.15.2 Test Case 3

In the third case, a scenario of 3D heat transfer is presented, where two walls meet in a corner and a floor element (Figure 2.22). The associated dimensions and boundary conditions are also provided in Table 2.5.

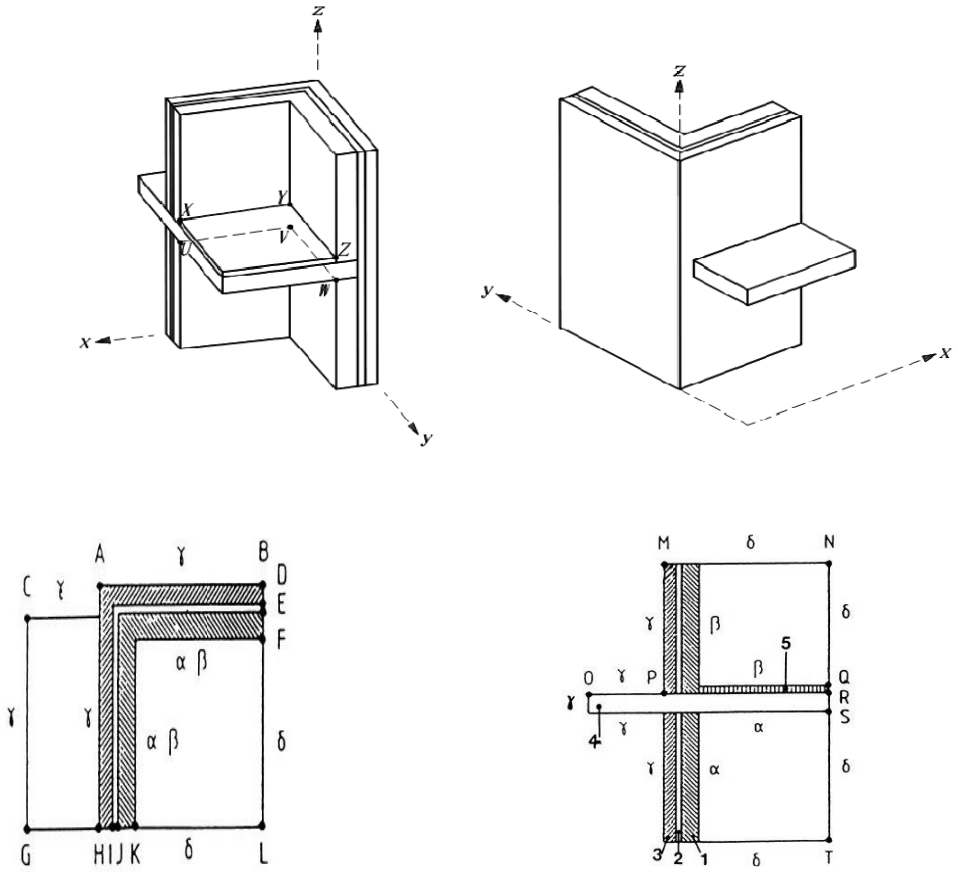


Figure 2. 22 Test Case 3 for 3D heat transfer (ISO 10211, 2007)

Table 2. 5 Boundary conditions of Test Case 2 for two-dimensional heat transfer (ISO 10211, 2007)

Label	**Boundary**
α	T=20˚C, R=0.2 m2K/W
β	T=15˚C, R=0.2 m2K/W
γ	T=0˚C, R=0.05 m2K/W
δ	Q=0 (adiabatic)

The modeling of Test Case 3 in Ansys by Martins (2020) is displayed in Figure 2.23. Table 2.6 compares the values defined in ISO 10211:2007 with those generated by the software Ansys. From the table, it can be concluded that the software meets the criteria of Test Case 3 with high precision.

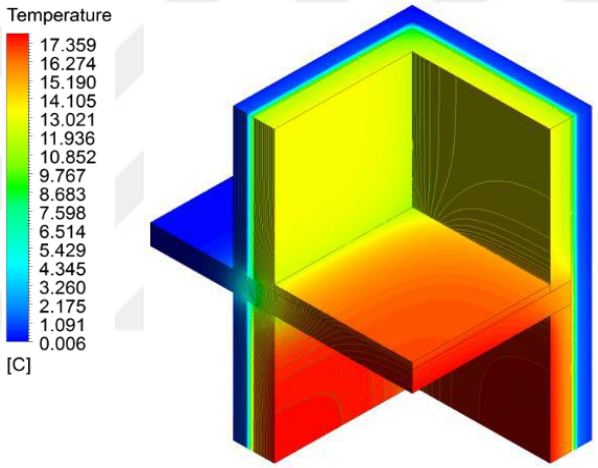


Figure 2. 23 Modelling of Test Case 3 in Ansys by Martins (2020)

Table 2. 6 Comparison between the values defined in ISO 10211 (2007) and software Ansys, for Test Case 3.

Measured Parameter	**Expected value**	**Ansys value**	**Difference**	**Difference Limit**
Minimum ambient temperature	11.32	11.276	0.044	0.1
Minimum ambient temperature	11.11	11.127	0.017	0.1
Heat flow	25.15	25.139	0.04	1
Heat flow	34.83	34.532	0.02	1

2.15.3 Test Case 4

Case 4 is a 3D thermal bridge consisting of an iron bar penetrating an insulation layer, as shown in Figure 2.24 below, together with the associated dimensions and boundary conditions.

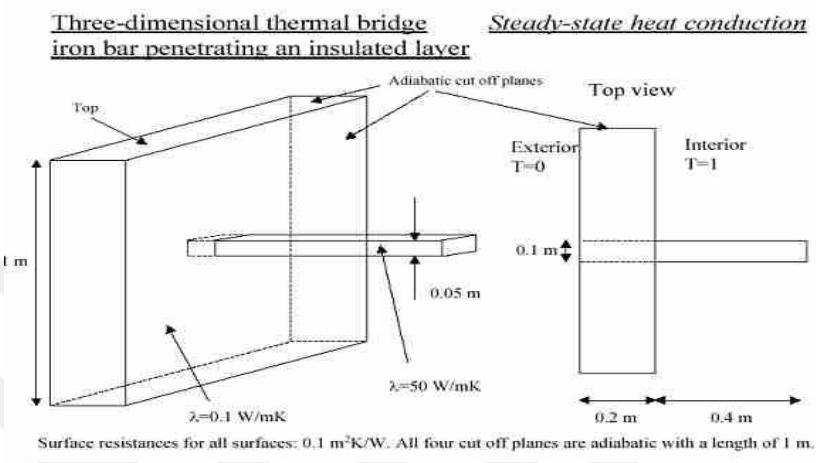


Figure 2. 24 Test case 4 for three-dimensional heat transfer (ISO 10211, 2007)

Martins (2020) modeled this test case (Figure 2.25) and made a comparison between the values defined in ISO 10211 and those obtained by the software Ansys, which are shown in Table 2.7. The software's high precision indicates that Ansys is being used correctly since it has confirmed that the three-dimensional steady-state high-precision numerical method satisfies the requirements set out in ISO 10211.

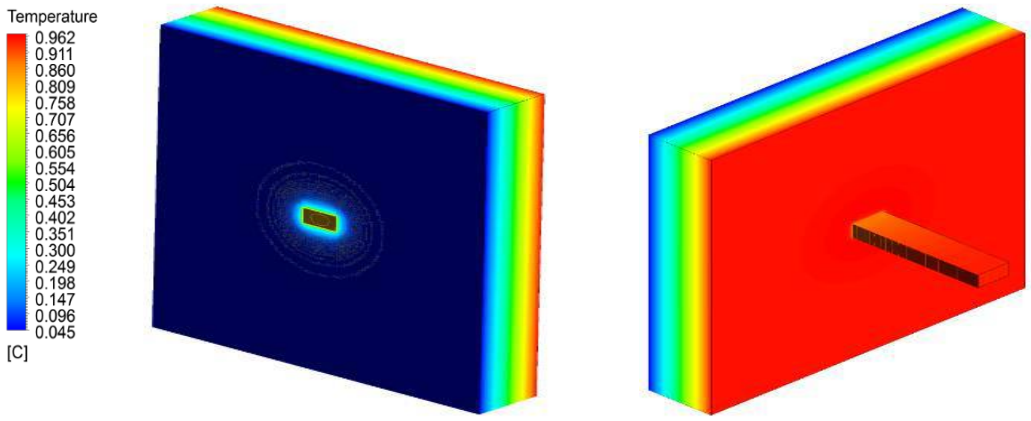


Figure 2. 25 Modeling of Test Case 4 in Ansys by Martins (2020)

Table 2. 7 Comparison between the values defined in ISO 10211 (2007) and software Ansys, for test case 4.

Measured Parameter	**Expected value**	**Ansys value**	**Difference**	**Difference Limit**
Maximum temperature on exterior surface	0.805 ˚C	0.809 ˚C	0.003 ˚C	<0.005 ˚C
Heat flow	0.540 W	0.537 W	0.61%	<1 %

CHAPTER THREE
NUMERICAL STUDIES

This section breaks down the organization of this thesis work. Three parametric (numerical) studies in Ansys are made and presented as separate chapters (chapters 4-6). Furthermore, the development of the FE model, mesh sensitivity, and validation of the constitutive model are also presented in this chapter.

3.1 Overview of Thesis

The scope and organization of this thesis work differs from the traditional master's thesis in that it is broken down into three parametric studies, produced in separate chapters. The three parametric studies are broken down under the following headings below.

1. The effects of the infill-geometry
2. The effects of Lattice Type, Filament Width, and Granular Filling Material.
3. Thermal Bridging effects in 3D Printed Foam Concrete

Each chapter shows advancements in understanding the infill structure's influence on thermal performance and dependent factors. This work is then successfully combined into a major conclusion, highlighting all important findings.

The dissertation is divided into seven chapters. Chapter 1 provides background information for the study. The research aims and objectives have been outlined. Chapter 2 goes into the current literature and provides a brief review of the mechanisms and methods of heat transfer, materials and properties of 3DPC, additive manufacturing techniques, insulation materials, and techniques in construction. Chapter 3 provides an overview of the thesis work, its organization, and the development and validation of the FE model. The next three chapters delve into individual parametric studies.

The effects of the infill geometry on the thermal behavior of 3DPC envelopes are studied in Chapter 4. Six infill structures with and without cavity insulation are studied. In Chapter 5, the effects of lattice type, filament width, and granular filling material are investigated. Three different lattice structures were modelled to have the same thickness and nearly equal contour lengths, voids, and insulation percentages. Additionally, the effects of filament width and the application of granular insulating materials (expanded polystyrene beads and loose-fill perlite) were also studied, along with the efficacy of insulation. In Chapter 6, the thermal bridging effects in 3D printed foam concrete (3DPFC) envelopes are examined. The effects of the contact (intersection) area of webs with the interior face shell, webs, and infill rows on the thermal performance of granularly insulated 3DPFC envelopes were analyzed. Six lattice structures were modeled to have the same thickness, height, length, and similar areas of insulation. Finally, Chapter 7 provides the overall summary and major conclusions of this master's research. Figure 3.1 is a flowchart for the organization of this thesis work.

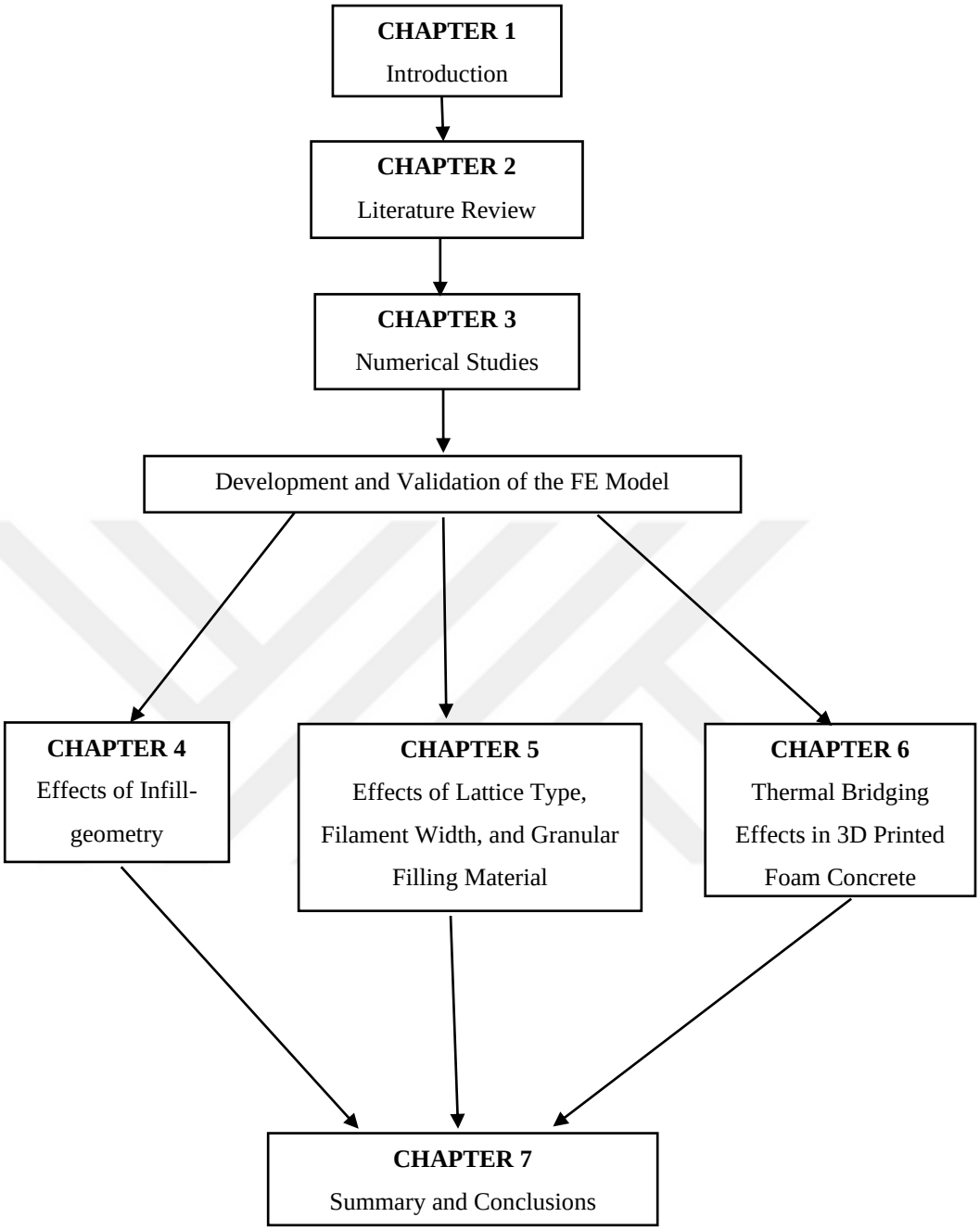


Figure 3. 1 Flowchart for the organization of the thesis work.

3.2 Development of the Finite Element Model

3.2.1 Heat Transfer Analysis

In the realm of heat transfer across 3DPC walls, there is a delicate interplay between conduction, convection, and radiation. Notably, conduction plays a dominant role in this process, which can be attributed to the thermal behavior of the

still air entrapped within the infill and the comparatively low temperatures at the external surfaces. The stagnant air acts as an insulator, impeding heat transfer via convective and radiative means. Because air movement is restricted, conduction becomes the primary mechanism for heat movement inside this region of the walls (AlZahrani et al., 2022).

Due to the unconfined nature of the surroundings, convective and radiative processes are prominent heat exchange mechanisms between ambient air and the interior and external wall surfaces. This enables greater fluid mobility and radiant energy exchange. However, the insulative properties of air cavities often decrease as the cavity size increases. Tamimi et al. (2023) found that heat transfer studies using still air are unreliable for cavities larger than 200 mm. Large cavities suffer from the development of convection currents, reducing their insulating efficacy. In contrast, smaller cavities, with still air forming a stagnant layer, function as effective insulators (Ouedraogo et al., 2018).

For one-dimensional heat transfer analysis through a building component consisting of homogeneous layers, EN ISO 6946 (International Organisation of Standardization (ISO) (2017) provides a simplified calculation method to determine thermal transmittance. In the simplified calculation method, the principle of thermal resistance is applied, and the thermal transmittance (U) is given by:

$$U = \frac{1}{R_T} \tag{3.1}$$

To determine the total thermal resistance through homogeneous layers, every material layer must be considered. The design thermal values of the layers can be provided as either design thermal conductivity or design thermal resistance. For a given thermal conductivity (λ), the thermal resistance (R) of a layer with a thickness (L) is obtained by:

$$R = \frac{L}{\lambda} \tag{3.2}$$

As a result, the total thermal resistance (R_T) of a plane-building component made up of thermally homogenous layers perpendicular to the heat flow is computed using the following expression:

$$R_T = R_{conv,i} + R_{layer,1} + R_{layer,2} + \cdots + R_{layer,n} + R_{conv,e} \quad (3.3)$$

$R_{conv,i}$ and $R_{conv,e}$ are the convectional resistances of the internal and external surfaces, respectively. The heat flow (Q) through an assembly of homogeneous layers is directly proportional to the thermal transmittance (U) and is given by:

$$Q = U\Delta T \quad (3.4)$$

The 3DPC walls are a homogeneous medium with constant thermal conductivity. Equation (3.5) describes three-dimensional heat conduction via a 3DPC envelope, which considers temperature variations in all three spatial directions: x, y, and z.

Since granular insulating materials are used for cavity insulation, these materials have interconnected voids between the individual grains, forming a tortuous but continuous air path through them. The heat transfer mechanisms within voids include solid and gas conduction, gas convection, and long-wave radiation (Simpson & Stuckest, 1990). EPS cell sizes, for instance, may typically be in the range of 50–350 µm, and the air convection component is negligible. The heat transfer through granular materials in this study is therefore determined using conductive contributions only, as radiation is also negligible due to low-temperature conditions (Ju¨ et al., 2010; Simpson et al., 2020).

$$\frac{\partial T}{\partial t} = \alpha\left(\frac{\partial^2 T}{\partial x^2} + \frac{\partial^2 T}{\partial y^2} + \frac{\partial^2 T}{\partial z^2}\right) \quad (3.5)$$

Where:

- T is the temperature as a function of x, y, z, and time t.

- α is the thermal diffusivity of the material.

When examining the correlation between structural loading and the thermal performance of masonry walls, the primary focus often lies in subjecting these walls to extremely high temperatures, such as in the case of a fire. The intense heat causes the masonry to bend towards the source of the fire, leading to potential issues with vertical loading after extended exposure. This is because the elements within the masonry become unstable laterally due to the significant stresses caused by moments from lateral displacement (De Mestrado & Rigão, 2012; Ismaiel et al., 2022; Ono, 2008). However, the small temperature differences applied in this study are not significant enough to produce thermal strains and, under certain conditions, generate stresses within the 3DPC walls. Therefore, unloaded 3DPC wall configurations were investigated in this study through an uncoupled heat-transfer analysis (structural analysis is not integrated).

The isotropic material model present in Ansys was employed throughout this study. In this model, heat conduction is considered to be homogenous throughout the lattice structures, and the thermal properties do not vary significantly with direction. This means that the lattice structures' response to temperature changes is consistent across its entire volume. Within the lattice structures, it is assumed that all material properties, including specific heat capacity and thermal conductivity, are uniform in all directions (Famà et al., 2021). The material properties are fed directly into the constitutive model.

In this heat transfer investigation, two parallel surfaces were identified as isothermal with varying temperatures. As a result, a perpendicular heat flow between these surfaces was established while disregarding any heat flux in the other direction since the other boundaries are considered insulated (adiabatic). The convective surface heat-transfer coefficients for the external and internal environments were set according to the provisions of EN ISO 6946: 25 $W/m^2.K$ and 7.69 $W/m^2.K$, respectively (ISO, 2017). The exterior and interior sink temperatures were determined to be 302.5 K and 297.5 K, respectively. To achieve a design temperature

difference of 5 K, the ambient temperature was maintained at a constant 295.15 K. Surface average weighted heat flux results were derived from simulations, and U-values were calculated by dividing the surface average weighted heat flux with the design temperature difference. The empty cavities were modeled as air layers. The thermal conductivity of still air was determined by dividing the thickness of the air layer with unventilated air layer thermal transmittance values interpolated from the relevant table given in EN ISO 6946. Figure 3.2 shows the application of boundary conditions to the FE models.

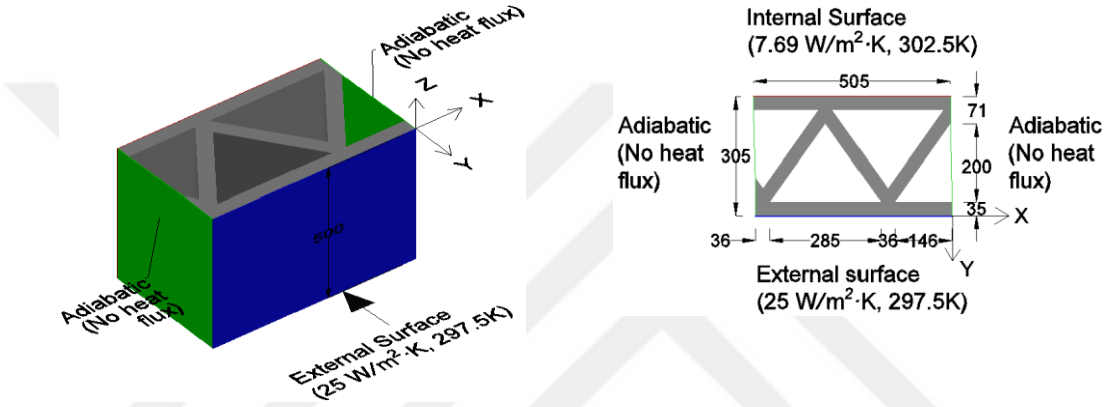


Figure 3. 2 The application of boundary conditions to the FE models (dimensions in mm).

3.2.2 Mesh Sensitivity Analysis

Mesh sensitivity analysis was performed to find the ideal element size that produces the more accurate results while consuming the least amount of computational time and resources. To do so, seven various mesh size combinations of global and edge seedings were investigated in five cavity layouts of hollow concrete bricks selected from the work of Henrique Dos Santos et al. (2017). They thermally characterized several cavity layouts of hollow concrete bricks. The cavity layouts selected for sensitivity analysis were B1, B3, B5, B7, and B9, and are provided in Figure 3.3. Edge seeding was used to selectively refine the mesh along edges or boundaries where higher mesh resolution is needed to improve the overall mesh quality. This sensitivity analysis's global/edge seeding combinations ranged from a very coarse combination of 20/2 mm to a finer 3/2 mm. Figure 3.4 depicts the mesh sensitivity analysis.

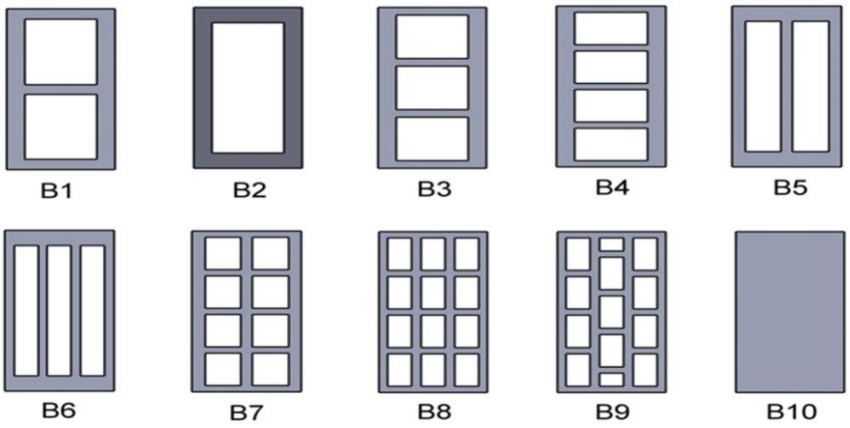


Figure 3. 3 Hollow concrete block layouts studied. Source: Henrique dos Santos, G., Fogiatto, M. A., and Mendes, N, numerical analysis of thermal transmittance of hollow concrete blocks. Journal of Building Physics, 41(1), 7–24, copyright © 2017 by SAGE Journals. Reprinted by Permission of SAGE Publications.

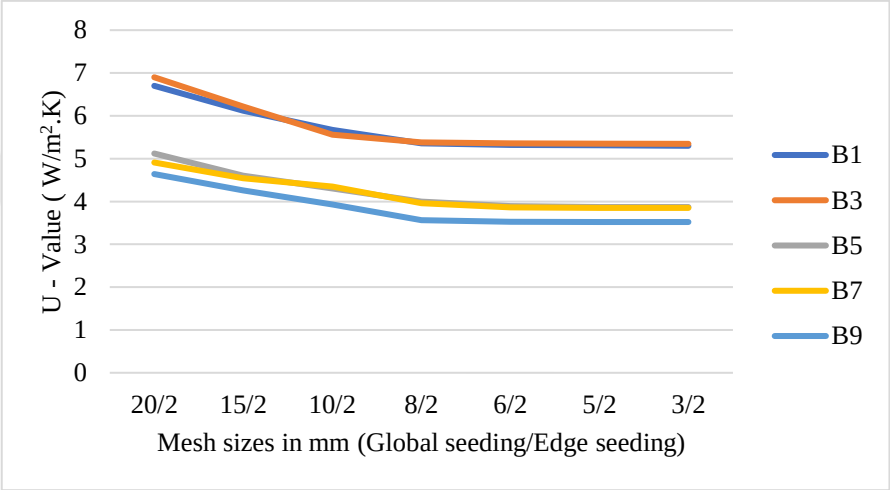


Figure 3. 4 Mesh sensitivity analysis.

Overall, the U-values decreased as the mesh sizes decreased. When the mesh combinations had global seedings greater than 8 mm, the decrease was significant; when the global seedings were less than 8 mm, the decrease was very minor and almost insignificant. In contrast, as the mesh sizes were reduced, the computing time increased. At 8/2 mm, there was a satisfactory balance between computational time and accuracy. The increase in computational time was large for 3/2 mm as the lowest mesh size studied. Therefore, the 5/2 mm combination was chosen to balance

computing efficiency and accuracy, as well as to obtain clearer heat flux contour maps.

3.2.3 Validation of Finite Element Model

Validating finite element models is critical since it provides accuracy assessment, model implementation verification, and confidence building in the model's predictive capabilities. As a result, the simulation models developed were tested against previously published literature. The validation was performed against the work of Henrique dos Santos et al. (2017). They performed the thermal characterization of several cavity layouts of hollow concrete bricks. This was completed by comparing the thermal transmittances obtained from FE simulations to those calculated using the analytical methodology presented in international regulation (EN ISO 6946). Therefore, 10 cavity layouts of hollow concrete blocks, provided in Figure 3.3, were modeled and validated. The thermal properties of the concrete blocks are provided in Table 5.1.

Figure 3.5 shows the U-value results obtained from the FE models developed by the authors and those calculated by Henrique dos Santos et al. for each block using EN ISO 6946. The simulation results are in good agreement with the standard values. The absolute average error is 2.88%, which is less than Henrique dos Santos et al.'s absolute average error of 3.81% when compared with their FEM (finite element modeling) results. Hence, the models are accurate and reliable and could be used for detailed parametric analysis of the energy performance of 3DPC building envelopes.

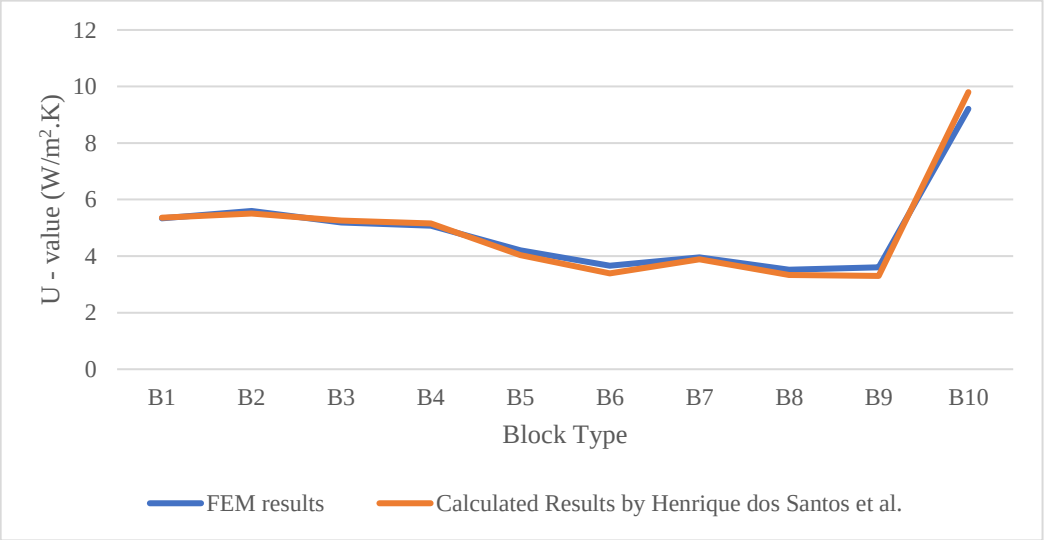


Figure 3. 5 U-value results were obtained from the FE models developed by the author and those determined by Henrique dos Santos et al. (2017).

The constitutive model used was also validated against the work of Tamimi et al. (2023). They studied the thermal performance of 3DPC walls both experimentally and numerically. They established the thermal transmittance values of the printed structures using heat flux meters and thermocouples. Figure 3.6 shows the wall geometry of Structure 1 adopted for validation.

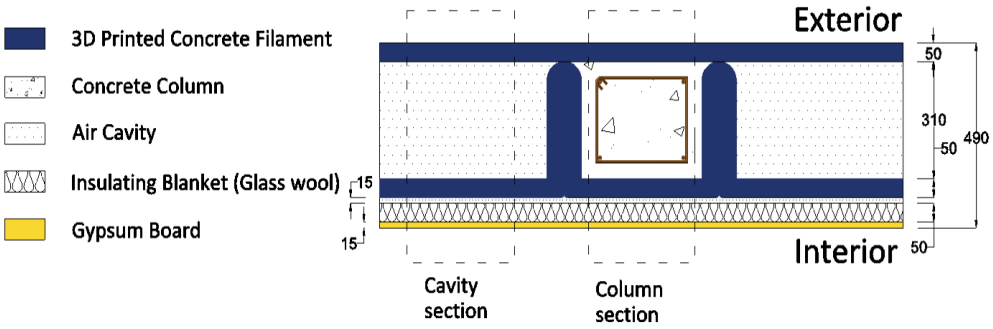


Figure 3. 6 Plan view of Structure 1 (dimensions in mm). Source: redrawn based on data from Tamini et al. (2023).

For the in situ measurement of the U-value, tests were conducted for both the column and cavity locations of Structure 1. Therefore, two models were developed, and the U-values were determined with the application of the same boundary conditions. The thermal conductivities of 3DPC filament, concrete, gypsum board,

glass wool, and steel are 0.781, 0.8, 0.159, 0.031, and 60.5 W/m.K, respectively (Tamimi et al., 2023).

The U-values from the FE simulations were 0.455 W/m^2 .K and 0.410 W/m^2 .K for the cavity and column locations, while those from in situ measurements were 0.440 W/m^2 .K and 0.395 W/m^2 .K, respectively (Tamimi et al., 2023). Despite the respective errors of 3.41% and 3.80% in the simulated results, the results show very good agreement. These errors may be attributed to the nature of the construction of this 3DPC technology. Sun et al. (2021) conducted an experimental study on the thermal performance of a 3DPC prototype building. They discovered that some 3D printing characteristics, such as the number of layers per printing, rest time during the printing process, and layer-by-layer appearance, can have adverse effects on 3DPC thermal performance and generate thermal defects. However, simplifications were made in the FE models such as assuming the wall panels to be straight-faced instead of the actual layer-by-layer appearance. Moreover, air may be entrapped between layers during the printing process, creating voids that may be insulative. All these phenomena have the potential to affect the overall thermal performance of 3DPC envelopes. It may be expected for FE models to have slightly higher U-values.

Assumptions on the size and spacing of the rebar were also made in the case of the column section due to a lack of clear information in the literature. For the longitudinal bars and lateral ties, 12 mm and 8 mm diameter bars at spacings of 50 mm (from faces of 3PDC) and 300 mm (center-to-center) were applied, respectively. Despite being minor by volume fraction of the concrete column, all these discrepancies may potentially affect the thermal resistance of the section. Therefore, the results of this validation can be relied on, as the errors are minimal and justifiable. The validation results also align with similar studies on heat conduction, such as that of Lu et al. (2024). They conducted numerical modeling and experimental verification for the anisotropic heat conduction process in the velocity probe of the thermal mass flowmeter. Their results showed that the average relative error between the simulated results and experimental data was 2.92%, and the maximum relative error was 10.91%.

CHAPTER FOUR
EFFECTS OF THE INFILL-GEOMETRY

4.1 Introduction

3D-printed concrete is becoming a promising solution as the construction industry evolves to achieve sustainability and environmental responsibility goals. This innovative construction method is transforming conventional practices (Zhang & Lepech, 2016). 3D-concrete printing has the potential to reduce the environmental impact of material transportation. The nature of the technology allows moving production directly to the construction site (Sprecher et al., 2017; Fitzgerald & Lautan, 2019). It offers enhanced material and energy efficiency (Sakin & Kiroglu, 2017). As a result, with increased knowledge of environmental protection legislation, the perception of sustainable growth in the construction industry is gaining traction. These days, the primary goal is to create a built environment that uses as little energy as possible (Suntharalingam, 2021).

One of the principal functions of walls is to maintain the internal climate of a building. These walls must not only be strong and durable, but they must also prevent heat loss, overheating in the summer, noise, and a rise in humidity. The construction industry is increasingly recognizing the need for energy sustainability in building designs. Thus, 3D-printed concrete buildings have the potential to play a vital role in this (Sakin and Kiroglu, 2017).

Thermal transmittance (U-value) is an important parameter during thermal studies. This value expresses the rate at which heat flows through a material or assembly. Jones and Pargeter (2019) underline the importance of U-values in assessing building energy efficiency and thermal performance.

It is important to correctly establish the U-value for various components of buildings such as walls, roofs, and windows. These metrics aid in forecasting a building's energy usage and thermal comfort (Rijal et al., 2017). However, determining the U-value of a building envelope can be a difficult task in real life.

The complexity stems from the fact that the various layers of materials, junctions, and interfaces all have a substantial impact on heat transfer. As highlighted by Roels et al. (2016), advanced modeling techniques such as finite element analysis (FEA) and computational fluid dynamics (CFD) provide more accurate forecasts of U-values for complex systems.

The world is divided into five major climate zones according to the Koppen-Geiger climate classification (M. Kottek, 2006). The thermal transmittance values (U-values) of building walls must conform with standard thermal transmittance values according to national legislation (Table 4.1). According to research investigating the usage of 3D-printed walls with integrated insulation, this could be a potential solution to increase thermal performance (Bos et al., 2016).

Table 4. 1 Standard thermal transmittance values as per national regulations for climatic zones of the Koppen-Geiger climate classification (M. Kottek, 2006)

Type	**Description**	**Criterion**	**Representative Country**	**Thermal transmittance (W/m^2.K)**			
				Walls	**Roof**	**Floors**	**Windows**
A	Equatorial climates	Tmin ≥ +18 °C	Jakarta (Indonesia)	0.529	0.557	0.557	4.54
B	Arid climates	Pann < 10 Pth	Amman (Jordan)	0.57	0.55	0.8	3.4
C	Warm temperate climates	-3 < Tmin < +18 °C	London (UK)	0.18	0.13	0.13	1.4
D	Snow climate	Tmin ≤ -3 °C	Ottawa (Canada)	0.21	0.162	0.162	2.2
E	Polar climate	Tmax < +10 °C	Nuuk (Greenland)	0.2	0.15	0.2	1.8

*Pann is the accumulated annual precipitation in mm/year, and Pth is a dryness threshold in mm.

Optimization of thermal performance in 3D-printed concrete walls can be influenced by a variety of factors. These include cavity size, geometry changes, and insulation. Several researchers have investigated the thermal performance of 3DPC envelopes. Alkhalidi & Hatuqay (2020) focussed on designing affordable, energy-efficient housing units. Suntharalingam et al. (2021) showed that intricate designs of infill structures that trap air, like lattice structures or double-rowed honeycombs, improve insulation. Nemova et al. (2022) were successful in developing a novel, and energy-efficient 3DPC envelope that adheres to climatic zones. Mansouri et al. (2022) demonstrated that subdividing big cavities into smaller ones can greatly lower heat

flux. AlZahrani et al., 2022) studied the energy efficiency of infill structures with the same void-to-concrete ratios.

Most of these studies use repeated cavity configurations, as opposed to a broader library of proposed configurations available in published literature by Mansouri et al. (2022), who estimated the convective heat transport in the huge air cavities of the 3D-printed concrete walls. Besides, the most widely applied insulation materials for cavity filling in these studies are rock wool and expanded polylactic acid (E-PLA). E-PLA is a bio-based foam material with potential as an insulation material. It has eco-friendly properties. However, it still has relatively limited usage compared to traditional materials. E-PLA, while occupying a niche market, sees its adoption impacted by factors including budget limitations, particular project needs, and the presence of alternative options. More studies are needed to investigate a broader library of wall cavity layouts and the use of other insulating materials, such as expanded polystyrene (EPS) beads. The selection of these materials is driven not only by the demands of sustainability and environmental responsibility in the building sector but also by their ease and versatility of application, conformity to irregular shapes, and cost-effectiveness. This current work aims to investigate the effect of the infill geometry on the thermal performance. It not only aims to fill a knowledge gap in the thermal performance of unstudied wall configurations but also to understand the effects of using different materials for cavity insulation.

4.2 Parametric Study

Following the wall configurations presented by Mansouri et al. (2022), who modeled the convective heat transfer in the large air cavities of the 3D-printed concrete walls, three cavity wall configurations were chosen to investigate the effect of wall cross-sectional configurations and thermal insulation on energy performance. These three distinct 3D-printed wall configurations were chosen as a starting point for the research. The lattice structures used in the numerical study had a constant filament width of 35 mm and a 220mm wall thickness. The infill structures also have a constant external volume of 1000 mm × 220 mm × 500 mm. DC3D4 cubic elements were used for meshing in all walls except for the sinusoidal wall panel

(WV). The WV walls used tetrahedral elements due to the sinusoidal nature of this infill type. A 3DPC mix that is suitable for load-bearing applications and has a thermal conductivity of 1.33 W/m.K. was used in this study (Pessoa et al., 2023). Figure 4.1 shows the infill structures chosen for the numerical study. A total of six models, with and without cavity insulation were investigated. A detailed description of the parametric study is given in Table 4.2.

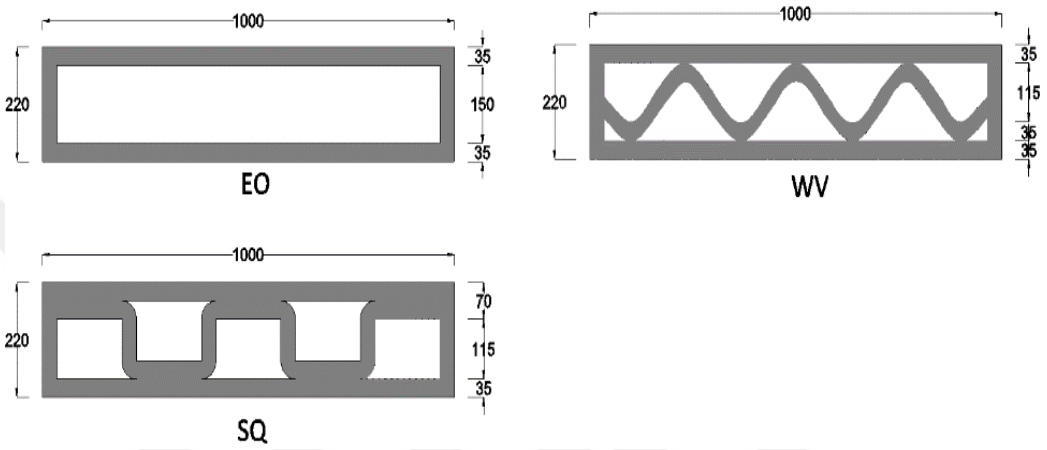


Figure 4. 1 Wall configurations chosen for the study Only exterior (EO) (No infill structure); Square Zigzag (SQ); Wavy Zigzag (WV)

Table 4. 2 Detailed description of the parametric study

Wall Configuration	**Insulation materials**	**Number of Models**
EO	Air and EPS	2
SQ	Air and EPS	2
WV	Air and EPS	2
Total		6

4.3 Results and Discussion

This section discusses the numerical simulation results obtained for the 3DPC wall configurations. The thermal transmittance values of all the models are given in Table 4.2. The effects of infill shapes and void area insulation are further discussed extensively herein.

Table 4. 3 Thermal transmittance values of all models in the parametric study

Wall Configuration	**Cavity-fill material**	**U-value (W/m^2.K)**
EO1	Air	4.296
EO2	EPS granules	0.208
SQ1	Air	3.863
SQ2	EPS granules	0.571
WV1	Air	3.459
WV2	EPS granules	0.389

Cavity insulation dictates the heat flow path through the 3DPC building envelopes. Both air and other cavity-fill materials have the potential to significantly affect the thermal performance of these building assemblies. This is mainly due to the differences in thermal conductivities between 3DPC and air or other fill materials. The heat path through insulated lattice assemblies is predominantly through the concrete webbing of the lattice structures. This is because of the high differences in thermal conductivities between 3DPC and insulating materials. However, in the case of stagnant air-filled lattice envelopes, this is only true with small cavities. Large cavities usually suffer from the development of convection currents. This reduces their insulating efficacy. In contrast to smaller cavities, with still air forming a stagnant layer, they function as effective insulators (Ouedraogo et al., 2018; Tamimi et al., 2023). Therefore, the thermal conductivity of stagnant air is proportional to the thickness of the air layer (ISO 6946, 2017). Thus, gas conduction is high in thicker air layers with a potential build up of convective currents.

Overall, the U-values for SQ1 and WV1 are close to and lower than that of EO1 in stagnant air conditions. EO1 shows the poorest thermal performance of the three wall types with 4.295 W/m^2.K, while SQ1 and WV1 have 3.863 and 3.459 W/m^2.K, respectively (Table 4.3). EO1 has the highest thermal transmittance despite having no webs (no infill structure) because of its highly conductive air layer. The air layer in EO1, i.e., 150 mm, is larger than that of SQ1 and WV1, both at 115 mm (Figure 4.1). This implies that the area over which gas conduction occurs is greater. However, the presence of webs in SQ1 and WV1 reduces the U-values in stagnant air conditions. This is because of the reduced thickness of the air layers. This implies that these air layers are less conductive than that of EO1. However, the thermal

transmittance of SQ1 is slightly higher than that of WV1 due to higher thermal bridging effects, which are discussed later in this section.

Granular expanded polystyrene (EPS) was introduced in the cavities to reduce the U-values and improve thermal performance. EPS has advantages including superior thermal insulation, lightweight characteristics, cost-effectiveness, and ease of application. It presents a viable option for improving insulation in 3D-printed walls because of its ability to efficiently minimize thermal conductivity (Muhieldeen et al., 2021; Ijjada & Nayaka, 2022).

Figure 4.3 shows the reductions in U-values due to cavity insulation. Overall, the incorporation of cavity insulation reduced the U-values and thus increased the thermal performance of the wall panels in all configurations. The EO2 (without infill structure) walls show the highest reduction in U-value compared to the other wall configurations. The percentage reduction in U-values was 95.16%. This is due to the absence of webs directly connecting the external and internal face shells. Since the thermal conductivity of 3DPC is higher than that of the surrounding insulation materials, the presence of webs in SQ2 and WV2 facilitates thermal bridging effects.

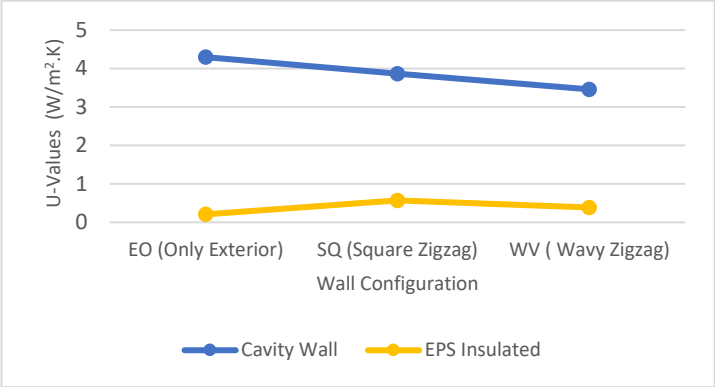


Figure 4. 2 Reductions in U-values due to cavity insulation

Of the two walls with webs, SQ walls had the relatively lowest percentage reductions at 85.22%. However, the overall percentage reductions between the square zigzag (SQ) and wavy zigzag (WV) wall panels are very close. This is suggestive of the relationship between U-values and the area of the void (cavity

insulation). This scenario will be further investigated in later stages of the research once there is more data from the inclusion of more wall configurations in the study. Tables 4.4 and 4.5 show the percentage reductions in U-values due to insulation and the void-concrete ratios of the 3DPC wall panels, respectively.

Figure 4. 3 Percentage reductions due to cavity insulation

Wall Configuration	EPS Insulated (%)
EO	95.16
SQ	85.22
WV	88.75

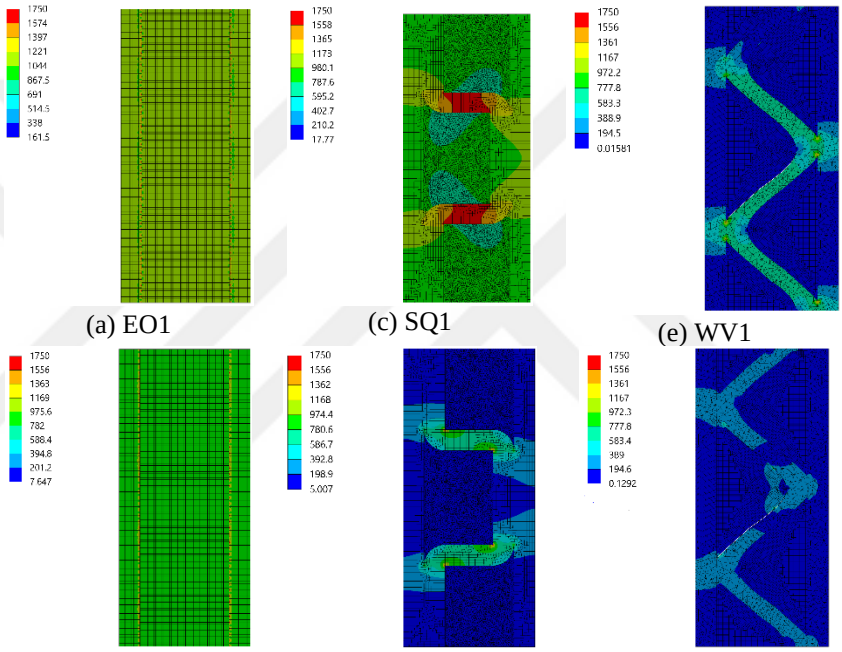
Figure 4. 4 Void-concrete ratios

Wall Configuration	Cavity Area (mm^2)	Concrete Area (mm^2)	Void-Concrete area ratio
EO	139500	80500	1.73
SQ	91638.9	128361.3	0.71
WV	104107.7	115892.3	0.9

From the results above (Table 4.3), the EO2 wall panel had the lowest U-value, i.e., 0.198 W/m2.K, exhibiting the best thermal performance. However, thermal bridges are evident between the external and interior faces of all walls except those of EO in Figure 5.1. This is because, under both stagnant air conditions and EPS cavity insulation, the thermal conductivity of 3DPC is significantly higher than that of both cavity-fill materials. However, the difference between the U-values of SQ2 and WV2 may be because of the differences in the contact (intersection) area of the webs with the interior face shells, as well as the presence of webs and their orientation. SQ2 has a large contact area and many straight and shorter webs than WV2. These geometric features in SQ2 have the potential to facilitate more heat transfer across the envelopes.

Similar observations were made by Pierzchlewicz (1996), who found that multicore blocks with staggered holes lengthen the heat flow path through walls in comparison to those with aligned holes. Moreover, the National Concrete Masonry Association (NCMA) (2012) found a 30% reduction in the thermal resistance of concrete blocks with two webs over the typical three-web concrete blocks. Therefore, the effects of contact areas and webs will also be studied in future stages of this work.

From the transmittance values, EO2 is suitable for all climatic zones except for the warm temperate climate (Table 4.1). The WV2 panel is only suitable for equatorial and arid climates, while the SQ2 panel is only suitable for arid climates. In this study so far, none of the wall panels had a U-value lower than the least transmittance value in Table 4.1, i.e., 0.18 W/m^2.K. In the later stages of the research, more infill structure variations will be studied, along with the use of other cavity insulation materials. Figure 4.6 displays the surface heat fluxes of the half models of the 3DPC wall panels.



(a) EO1 (c) SQ1 (e) WV1

(b) EO2 (d) SQ2 (f) WV2

Figure 4. 5 Surface heat fluxes of the half models of the 3DPC wall panels

4.4 Conclusions

Six lattice structures were modeled and studied. This was done to determine the effects of the infill structure on their thermal performance. A suitable constitutive model was applied and validated against published literature. Based on the findings of the analysis, the following conclusions were made:

1. The presence of webs reduces the U-values in stagnant air conditions because of the reduced thickness of the air layers.

2. The introduction of cavity insulation significantly reduces the U-values, thus increasing the thermal performance of the wall panels.
3. Thermal bridging effects occur due to thermal conductivity differences between 3DPC and cavity-fill materials.
4. The difference in contact (intersection) area of the webs with the interior face shells as well as the orientation of the webs have the potential to affect the thermal performance and will be investigated in future stages of the study.
5. There seems to be a relationship between U-values and the area of void (cavity insulation), which will be further investigated in the later stages of the research.
6. None of the wall panels had a U-value lower than the least transmittance value in Table 1, i.e., 0.18 $W/m^2.K$. This necessitates the need to study more infill structures in later stages of research, with the possibility of optimizing the thermal performance with the use of other cavity insulation materials. However, the EO2 wall panel had the lowest U-value, i.e., 0.198 $W/m^2.K$, exhibiting the best thermal performance of all the wall panels.

These results provide designers with insights to consider when planning buildings' energy needs. This study broadens understanding and gives better insight into the energy performance of building systems and cost-effective options during the adoption of additive manufacturing in the construction industry.

CHAPTER FIVE
EFFECTS OF LATTICE TYPE, FILAMENT WIDTH, AND GRANULAR FILLING MATERIAL

5.1 Introduction

The construction industry consumes more than half of all raw materials globally, emits the most carbon, and accounts for 40% of total energy consumed globally (Foggia, 2018). This has a significant environmental impact because of its energy consumption. Three-dimensional printed concrete (3DPC) has emerged as a potential answer as the building sector changes to meet the demands of sustainability and environmental responsibility. This revolutionary technique is altering traditional construction practices by promising increased material and energy efficiency (Apis Cor, 2023a; Sakin & Kiroglu, 2017). Three-dimensional concrete printing (3DCP) can reduce the environmental impact of material transportation by moving production directly to the construction site (Zhao et al., 2023). Furthermore, recent research into the incorporation of recycled elements implies that 3DCP can help reduce waste (Heng et al., 2019). As a result, with increased knowledge of environmental protection legislation, the perception of sustainable growth in the construction industry is gaining traction. These days, the primary goal is to create a built environment that uses as little energy as possible (Voskresenskaya et al., 2018).

Additive manufacturing presents a multitude of promising commercial prospects, with one of its key strengths lying in the capacity for product personalization (Jipa & Dillenburger, 2022). Largely attributed to its rapid prototyping, customizable features, and just-in-time production capabilities, this technology has unlocked many profitable avenues across various industries (Berman & Zarb, 2012). Businesses are strategically leveraging the perks of 3D printing by leveraging diverse printing processes and approaches. Notably, two techniques, the Material Deposition Method (MDM) and binder jetting stand out as optimal for large-scale construction and small-scale architectural components, respectively (Alkhalidi & Hatuqay, 2020).

The innovative MDM utilizes a nozzle to deposit construction material in a layered fashion, often as extruded concrete or mortar to construct 3D-printed structures (Alkhalidi & Hatuqay, 2020). In their study, Mechtcherine et al. (2020) investigated the application of MDM in construction, with a focus on creating building components using a robotic extrusion system. This cutting-edge technology has also been adopted by companies like Apis Cor, a pioneering construction startup, for on-site 3D printing of buildings. Their approach involves utilizing on-site robotic extrusion of construction materials to fabricate walls and structural elements (Apis Cor, 2023b).

Walls serve a crucial purpose in maintaining a stable internal microclimate within a building. Beyond just being resilient and long-lasting, these walls must also effectively block heat loss, excessive heat in the summer, noise pollution, and an increase in humidity. In response to the growing emphasis on energy sustainability in construction, 3DPC structures have emerged as a promising solution for achieving this objective (Hugo Hens, 2016; Sakin & Kiroglu, 2017). A key factor to consider in the assessment of a building's heat transfer capabilities is its thermal transmittance, also known as the U-value. This value expresses the rate at which heat flows through a material or assembly. Accurate U-value predictions are crucial in assessing various building components such as walls, roofs, and windows. These metrics are instrumental in projecting a building's energy consumption and ensuring thermal comfort. However, determining U-values is no easy task, as the intricate process is influenced by multiple factors such as the materials used, junctions, and interfaces, all of which play a critical role in heat transfer. Sophisticated modeling methods, such as finite element (FE) analysis and computational fluid dynamics (CFD), offer more accurate predictions of U-values for intricate systems.

A variety of factors, including cavity size, geometry changes, and the addition of insulation in cavities can influence the optimization of thermal performance in 3DPC walls. Researchers like Mansouri et al. (2022) showed that subdividing large cavities into smaller ones can significantly reduce heat flux. Nemova et al. (2022) experimentally studied the thermal performance of 3DPC-enclosing structures. They

were able to develop an innovative energy-efficient ventilated 3DPC envelope with a low thermal conductivity coefficient following the climatic zone. Alkhalidi and Hatuqay (2020) focused on designing energy-efficient and low-cost dwelling units by balancing cavities and 3D-printed material. Similarly, Suntharalingam et al. (2021) demonstrated that complex geometries, such as double-rowed honeycomb or lattice structures, enhance insulation by trapping air.

The cavity-insulating material used in previous studies (Alkhalidi & Hatuqay, 2020; Suntharalingam et al., 2021), expanded polylactic acid (E-PLA), a bio-based foam material, still has limited applications. While E-PLA has a niche market due to its green characteristics when compared to traditional materials, it still has a higher cost, lower thermal resistance (R-value), high sensitivity to moisture, relatively poor fire resistance, limited availability in some regions, and lack of extensive long-term performance data (Faruk et al., 2012; Parker et al., 2011; Stark & Matuana, 2007). Similarly, AlZahrani et al. (2022) investigated the energy efficiency of infill structures while maintaining equal void-to-concrete ratios. They found that modifying the infill structure of 3DPC walls affects their thermal conductivity. However, their study lacks clear information on the geometric parameters of all the walls and the structural considerations made.

Due to the lack of technical design standards in the additive manufacturing of concrete walls, studies on the evaluation of thermal performance can easily overlook the structural aspects of these walls. In almost all the studies delving into the thermal performance optimization of 3DPC walls, the premises of the selection of infill structures are not clearly addressed. Therefore, this study aims to examine the impact of the infill geometry on the energy performance of large-scale, commercially applied 3DPC walls using infill structures of sufficient structural integrity. The selection of infill structures used in this study is supported by experimental literature and industrial trends.

This work studies the effects of void area, filament width, and insulation on the thermal performance of 3DPC envelopes for the same thickness, contour lengths, and

void and insulation percentages. Because they are widely available, granular insulating materials, namely expanded polystyrene (EPS) beads and loose-fill perlite, are used in this study. The choice of these materials is also motivated by many other factors, such as ease and versatility of application, conformity to irregular shapes, recyclability, sustainability, and cost. Moreover, this study also aims to assert the extent to which thermal bridges affect the effective usage of granular insulating materials.

5.2 Methodology and Analysis

Three types of walls were chosen, and a thorough parametric analysis was carried out to investigate how the internal structure (infill structure) impacts energy performance. The study established the impact of void area effects, filament width, and insulation on the thermal behavior of these lattice envelopes. A detailed explanation of the parametric study can be found in Section 5.2.1. In selecting the three infill structures used in this study, a comprehensive approach was adopted to ensure that the lattice structures not only possess adequate structural integrity but also aligned with current industrial trends. The heat transfer analysis utilized Ansys Workbench for modeling. Appropriate numerical heat transfer models were created and verified using published data.

EPS beads and loose-fill perlite were applied for cavity insulation. Table 5.1 shows the thermal properties of the 3DPC and cavity-insulating materials (Abidi et al., 2014; Ochs & Müller-Steinhagen, 2005; QOROX, 2023). Lastly, an assessment of the thermal efficiency of insulation is made to assert the extent to which thermal bridges can produce significant heat losses, resulting in ineffective usage of the insulation material. This research contributes to the development of energy-efficient and sustainable 3DPC building envelopes. The sections that follow contain detailed information on the research's methodology.

Table 5. 1 Thermal properties of materials.

Material	Density (kg/m^3)	Thermal Conductivity (W/m.K)	Specific Heat (J/g.K)	Source
Concrete Block	2300	1.75	1	Henrique Dos Santos et al. (2017)
3DPC	1950	0.979	0.972	Pessoa et al. (2021); QOROX (2023)
Air	Ideal gas	0.0242	1.00643	Suntharalingam et al. (2021)
EPS	40	0.03	1.25	Ochs & Müller-Steinhagen (2005); Schiavoni et al. (2016)
Perlite	400	0.045	0.837	Abidi et al. (2014); Schiavoni et al. (2016)

5.2.1 Parametric Study

A holistic selection approach was taken in the selection of the three infill structures used for the parametric study. This is to ensure that the lattice structures studied not only have sufficient structural integrity obtained from experimentation literature but are also consistent with additive manufacturing industrial trends. Despite several novel structures for in-fill materials proposed in the literature, the selection of the lattice structures was limited to three. This is because of the limited structural performance data, especially under axial compression, which is the main loading direction for wall systems. Most of the literature on the mechanical performance properties of 3DPC infill structures focuses on their flexural performance as beams, with loadings in the vertical (layer deposition direction) and transverse (layer translation direction) loading directions. Moreover, some of the proposed infill structures still do not have commercial applications among companies in the 3DPC business.

The first lattice structure (T) is a truss topology (zigzag) obtained from the work of Daungwilailuk et al. (2021). They experimentally studied the large-scale 3DPC walls under unconfined axial compression to determine the effect of different infill patterns on mechanical behavior. Their study indicated that the inner truss inside 3DPC plays a role in the wall bracing. It can mitigate the wall bowing and prevent the buckling failure of the wall. Joh et al. (2020) note that when the wall and lateral supports are connected in parallel, there is a tendency for higher resistance to

buckling. Companies like Black Buffalo and QOROX commonly use this wall type (Bello & Memari, 2022).

The second wall type (A) used in this study is a square zig-zag configuration obtained from Apis Cor, a Guinness Book World Record holder for the world's largest 3D-printed building on Earth. The company affirms that its 12" lattice structure is of the same structural integrity as a 12" concrete block wall (Apis Cor, 2023b).

Lastly, the third wall structure (P) is an innovative cob design adopted from the literature of Bello and Memari (2022), who conducted an extensive review of the current state of 3D printing in the concrete industry. They looked at several companies currently in the additive manufacturing space and their approaches to the creation of 3DPC walls, including wall design. This cob design (the inside cavity is separated by a weave-like pattern) is unique to WASP, another leading company in the 3DPC industry based in Italy. In this wall design, no steel reinforcement is added to the wall, as the shape of the wall itself is designed to provide all the necessary strength (Alhumayani et al., 2020; WASP, 2022). Figure 5.1 shows the three wall types considered in the parametric analysis. The first, second, and third wall types are denoted by T, A, and P, respectively.

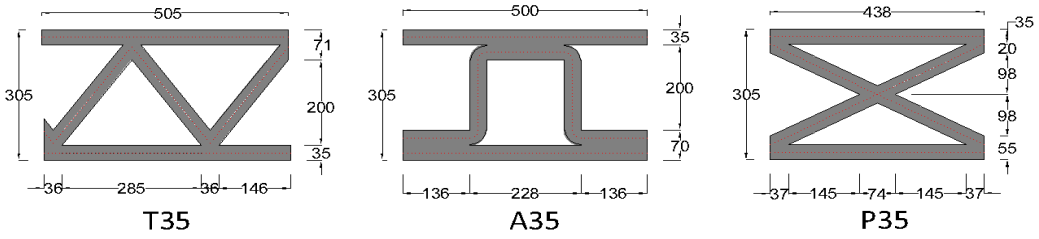


Figure 5. 1 Wall types (35 mm filament width) for the parametric analysis (dimensions in mm).

To study the effects of void area, filament width, and insulation on the thermal performance of 3DPC envelopes, all the lattice structures under this study were modeled to have the same thickness, height, nearly equal contour lengths, and void, and insulation percentages. All contour lengths were measured along the center lines of the respective filaments as shown by red-dotted lines in Figure 5.1. By keeping the

void area constant, the concrete area was increased by varying the filament width. This was completed using three nozzle sizes, i.e., 35 mm, 40 mm, and 50 mm, established from common industrial practice (Table 5.2). In the large-scale 3D printing of buildings, many companies, like Black Buffalo 3D, the first company to receive a building code compliance, at material, machine, and structural wall levels, use nozzle sizes of 1.38″–1.97″ (35–50 mm) (Black Buffalo 3D, 2021). For the 35 and 40 mm nozzles, the contour lengths, void, and insulation percentages are almost identical, while minor differences can be seen with the 50 mm nozzle size. Additionally, the T and A walls have very close void areas, while the P walls have a slightly lower void area. All walls are modeled to have an initial thickness of 12 in (304.8 mm) but increased slightly due to an increase in filament width. Furthermore, a constant wall height of 500 mm is maintained in all cases. A detailed description of the parametric study is given in Table 5.2, where T35 means wall type one with a 35 mm nozzle size. The same analogy applies to naming all the subsequent walls.

Table 5. 2 Detailed description of the parametric study.

Wall	**Nozzle Size (mm)**	**Contour Path Length (mm)**	**Concrete Area (mm^2)**	**Void Area (mm^2)**	**Void Percentage**	**Cavity Fill Material**	**No. of Models**
T35	35	1870	63,872.03	89,680.70	58.4	Air, EPS and Perlite	3
T40	40	1897.66	73,951.28	89,680.70	54.8	Air, EPS and Perlite	3
T50	50	2038	89,682	89,680.70	50	Air, EPS and Perlite	3
A35	35	1869.6	65,434.40	86,965.55	57.1	Air, EPS and Perlite	3
A40	40	1882.98	74,771.50	86,965.55	53.8	Air, EPS and Perlite	3
A50	50	1919.38	94,047.20	86,965.55	48	Air, EPS and Perlite	3
P35	35	1870	62,505.79	70,996.60	53.2	Air, EPS and Perlite	3
P40	40	1915.1	90,217.24	70,996.60	44	Air, EPS and Perlite	3
P50	50	2005.5	94,269.93	70,996.60	43	Air, EPS and Perlite	3

The thermal performance of building envelopes is significantly impacted by the design of their insulation. This design is heavily influenced by a financial trade-off between the initial investment in improving the envelope and the long-term cost of energy for maintaining the space, taking into account factors such as durability and maintenance expenses (Schumacher, 2013). An important aspect of this study is the incorporation of granular insulating materials, i.e., loose-fill EPS beads and perlite, for cavity filling of the hollow 3DPC building envelopes. The choice of these materials is not only motivated by the demands of sustainability and environmental responsibility in the construction industry but also by the ease and versatility of application, conformity to irregular shapes, and cost-effectiveness offered by these materials. EPS insulation is a highly efficient and environmentally friendly option, known for its lightweight and sturdy composition. As stated by the Insulation Company of America, it has always been free of harmful substances such as CFCs and HCFCs (Insulation Company of America, 2023). Its impressive characteristics, including its low thermal conductivity and lightweight structure, significantly reduce heat transfer in 3DPC structures (Yucel et al., 2020). Similarly, perlite, a naturally occurring inorganic mineral, is a long-lasting insulation material that can support its weight without settling or bridging. It boasts excellent thermal properties due to its amorphous volcanic glass structure and offers added protection against fires at a reasonable cost. Not only is perlite lightweight and easily poured, but it also does not require any special equipment or skills. This versatile material is mined and processed with minimal impact on the environment, making it a preferred choice for green communities that recognize its high-performance qualities (Davraz et al., 2020; Perlite Institute, 2014).

Granular insulating materials, as stated earlier, have interconnected voids between the individual grains, forming a tortuous but continuous air path through them. Tests conducted by Simpson et al. (2020) indicated that the thermal conductivity of loose EPS beads can be up to 5% higher than that of EPS boards of a similar density. Therefore, the thermal conductivity of the granular materials in this study was increased by 5%. A total of 27 wall models, with and without cavity insulation, are

considered in the parametric study (Table 5.2). It is worth noting that in real-life construction, in all the wall systems, a portion of the wall cavities are filled with concrete and rebar, while others are reserved for services such as electrical and plumbing. To maintain consistency, the analysis was conducted without the presence of concrete and reinforcement, as well as service lines in the cavities.

5.2.2 Thermal Insulation of Efficiency

Although insulation materials are mostly cheaper than concrete materials, they considerably increase the overall cost of construction. Thus, the effective use of these materials for insulation is important. By studying the relative thermal efficiency (T_{Eff}) of insulation materials, the effectiveness of these materials in preventing the flow of thermal energy in building assemblies can be quantified and cost-optimized. Thermal insulation efficiency is used as a measure of the extent to which unintended thermal bridges can produce significant heat losses, resulting in ineffective usage of the insulation material. It is often quantified in terms of the R-value (thermal resistance) (Kosny et al., 2007). The higher the thermal resistance, the more efficient the insulation is at increasing the thermal inertia. Since thermal resistance and U-value are reciprocals, the higher the U-value, the less efficient the insulation is.

The method of estimating the T_{Eff} value in this study is based on an R-value comparison of insulated (R_{in}) and uninsulated (R_{un}) envelopes, each having the same face area (A_{fa}). The equivalent R-value (R_{eq}) of the insulation material alone is the R-value of insulation inserts into the cavities collectively per wall. It is calculated as an equivalent transformed layer of the total insulation material used for cavity filling, having the same face surface area (A_{fa}) as the wall under consideration and containing the same volume of insulation (V_{Tins}). The equivalent thickness of the insulation layer is the quotient of the total volume of insulation (V_{Tins}) divided by the face surface area (A_{fa}), while R_{eq} is the product of the equivalent thickness and the thermal resistivity of the insulation material (Urban et al., 2011). T_{Eff} may be expressed by the following equation:

$$T_{Eff} = \frac{R_{in} - R_{un}}{R_{eq}} \times 100 \quad (5.1)$$

Where

- R_{in} is the R-value of the insulated wall panel,
- R_{un} is the R-value of the uninsulated wall panel, and
- R_{eq} is the equivalent resistance of insulation material alone, configured as a single uninterrupted layer.

5.3. Results and Discussion

This section discusses the numerical simulation results of the parametric study. The thermal transmittance values of all the models are given in Table 5.3. For nearly the same contour lengths, the effects of infill shapes, voids, and insulation areas, as well as filament width, are discussed herein.

Table 5. 3 Thermal transmittance values of all models in the parametric study.

Wall Configuration	U-Values (W/m^2.K)			Percentage Reduction (PR) (%)		Difference in PR (%)
	Air	Perlite	EPS	Perlite	EPS	
T35	3.485	0.509	0.445	85.39	87.23	1.84
T40	3.312	0.525	0.464	84.15	85.99	1.84
T50	3.093	0.593	0.534	80.83	82.74	1.91
A35	3.472	0.519	0.453	85.05	86.95	1.9
A40	3.296	0.559	0.496	83.04	84.95	1.91
A50	2.993	0.622	0.563	79.22	81.19	1.97
P35	2.77	0.489	0.417	82.35	84.95	2.6
P40	2.702	0.516	0.444	80.9	83.57	2.66
P50	2.459	0.558	0.49	77.31	80.07	2.77

5.3.1. Effect of Area of Stagnant Air

Overall, the U-values for T (truss-type) and A (zigzag-type) are very close, while those of P (weave-like pattern) are comparatively lower for nearly equal contour lengths (Table 5.3). In both the T and A walls, the thermal conductivities of the voids are the same due to identical air layer thicknesses (200 mm) (Figure 5.1). However, T walls have a slightly higher void area than A walls. T walls have a void area of 89,680.7 mm^2 while that of A walls is 86,965.55 mm^2 (Table 5.2). The difference in void area between the two wall types is 2715.15 mm^2. Despite the small difference,

the void percentages in both wall types are almost identical for the same filament width. For instance, for the same 35 mm nozzle, the void percentages for the T35 and A35 walls are 58.4% and 57.06%, respectively. The voids of the P walls, on the other hand, have two types of air layers based on the different thicknesses of the air layers. The larger voids are of the same thickness as those of the T and A walls, while the smaller ones have almost half the thickness (98 mm) (Figure 5.1). Additionally, the P walls have the lowest void area, 70,996.6 mm^2, comparatively (Table 5.2). The void area differences between P and A walls and P walls are 18,684.1 mm^2 and 15,968.95 mm^2, respectively. Consequently, the void percentages of the P walls are lower for the same filament width.

Figure 5.2 shows the heat flow paths in the surface heat flux contour maps of the walls. In T and A walls, heat transfer occurs predominately through voids via gas conduction (vibration and collision of gas particles). This is because the total thermal conduction of the stagnant air volume considered is slightly higher than that of the 3DPC in both wall types. It should be noted that the thermal conductivity of stagnant air is proportional to the thickness of the air layer (ISO, 2017). Thus, gas conduction is high in thick air layers. T35 has the highest U-value, 3.486 $W/m^2.K$, of all walls, indicating the poorest thermal performance (Table 3). P50 shows the best thermal performance under stagnant air conditions, with a U-value of 1.947 $W/m^2.K$. Furthermore, it is observed that for T and A walls of the same filament width (nozzle size), the U-values of the T walls are slightly higher than those of the A walls. For example, T40 has a U-value of 3.312 $W/m^2.K$ while that of A40 is 3.296 $W/m^2.K$. The thermal behavior may be because of the difference in void areas. Additionally, a notable decrease in the U-values is seen across all wall types with an increase in filament width (nozzle size). This may be because of the increase in concrete areas and subsequent decrease in void percentage. Since most of the heat transfer occurs via the more conductive voids, an increase in filament width more or less acts as an insulative reverse effect.

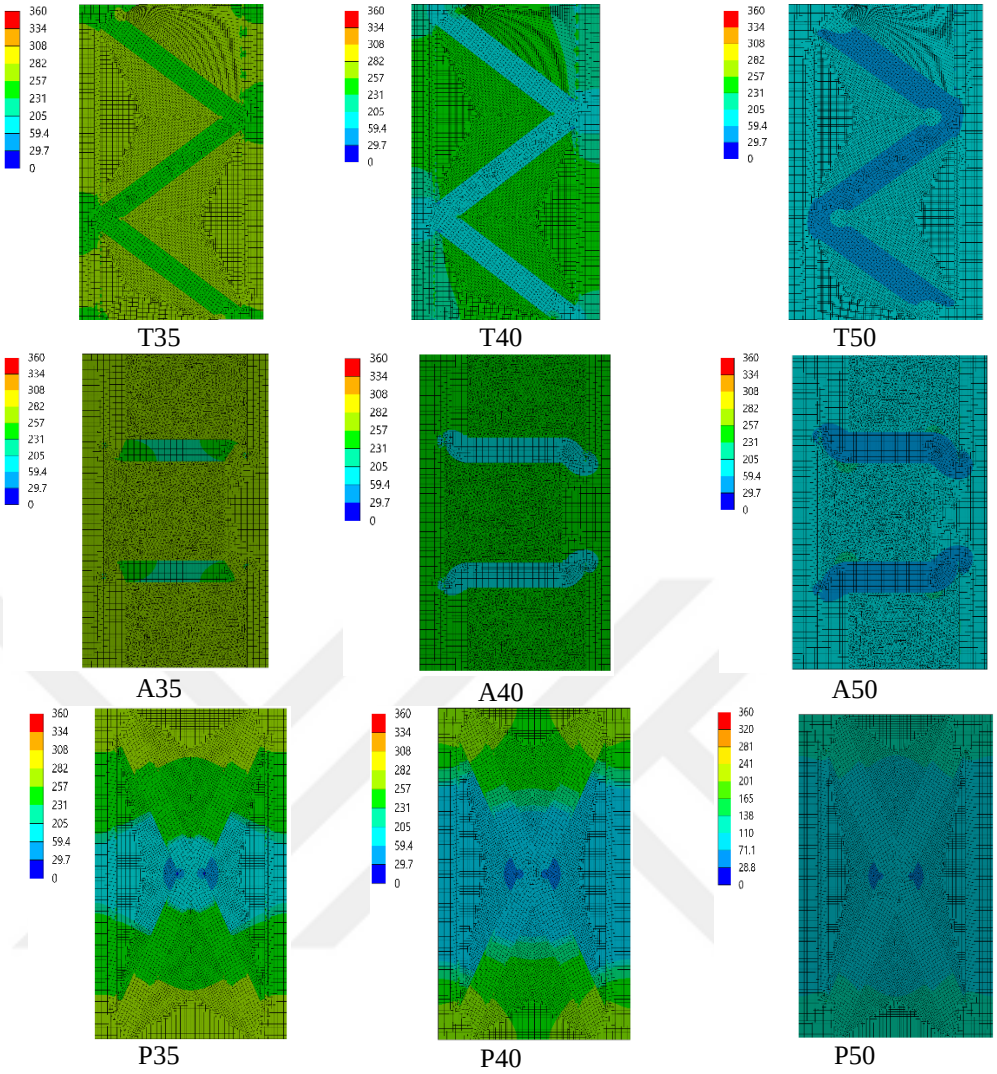


Figure 5. 2 Surface heat flux contour maps with stagnant air in cavities.

On the other hand, the heat path through P walls is different from the first two types. Since P walls have two types of air layers, the thermal conductivities of these layers are different. In the larger voids, the heat transfer mechanism is the same as that of T and A walls. However, smaller voids have lower thermal conduction than the 3DPC. They have an insulative effect, and heat transfer occurs predominantly via the webs in these regions. Due to the presence of insulative air layers in P walls and their low void area, these walls exhibit the best thermal behavior. P35 has a U-value of 2.77 W/m^2.K, while P50 has 1.947 W/m^2.K. Therefore, the thermal performance of 3DPC lattice envelopes under stagnant air conditions in voids is mainly affected by the void area. T walls with the largest void area have the worst performance,

while P walls with a smaller void area have the best thermal resistance. Figure 5.3 shows the thermal performance of the 3DPC envelopes with respect to their void area.

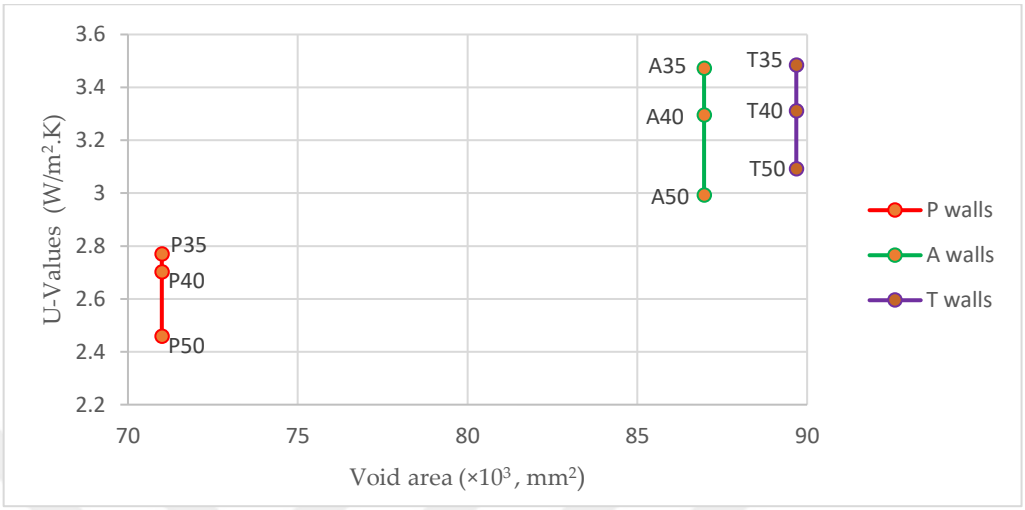


Figure 5. 3 Thermal transmittance variations with void area.

5.3.2. Effect of Cavity Insulation

To improve the thermal inertia, EPS beads, and loose fill perlite were applied in the cavities of the 3DPC lattice structures. The introduction of granular insulating materials significantly lowers the U-values for all wall types (Table 5.3). The thermal conductivity of the 3DPC is 32.6 and 21.8 times higher than that of EPS beads and loose-fill perlite, respectively (Table 5.1). Due to the high thermal conductivities between the 3DPC and the insulating materials, the heat path through all the insulated wall types is predominantly through the concrete webbing of the lattice structures. Thermal bridging is evident between the external and interior surfaces (Figures 5.4 and 5.5). Thermal bridges occur when highly conductive structural components penetrate the insulation plane (Canadian Concrete Masonry Producers Association (CCMP), 2013).

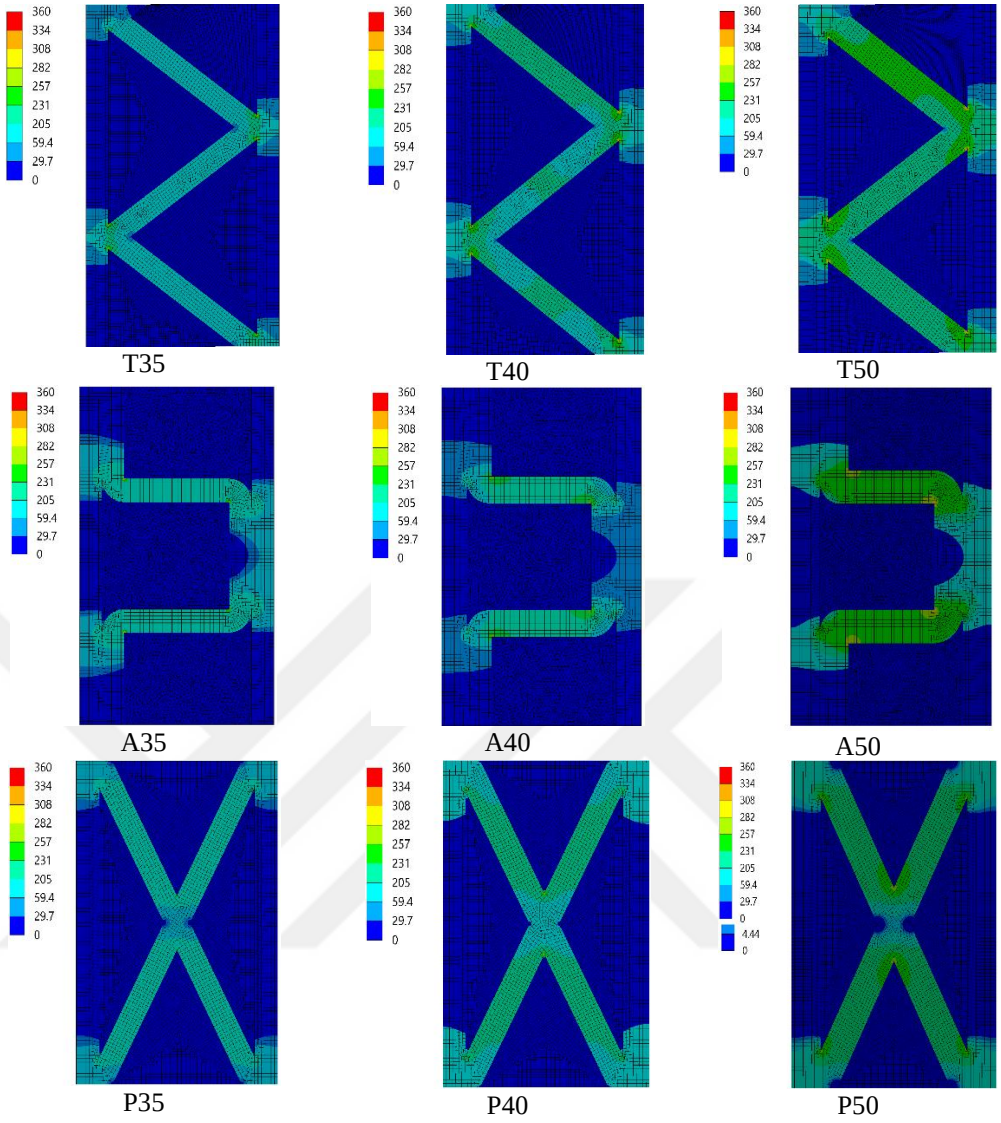


Figure 5. 4 Surface heat flux contour maps of loose fill perlite insulated walls.

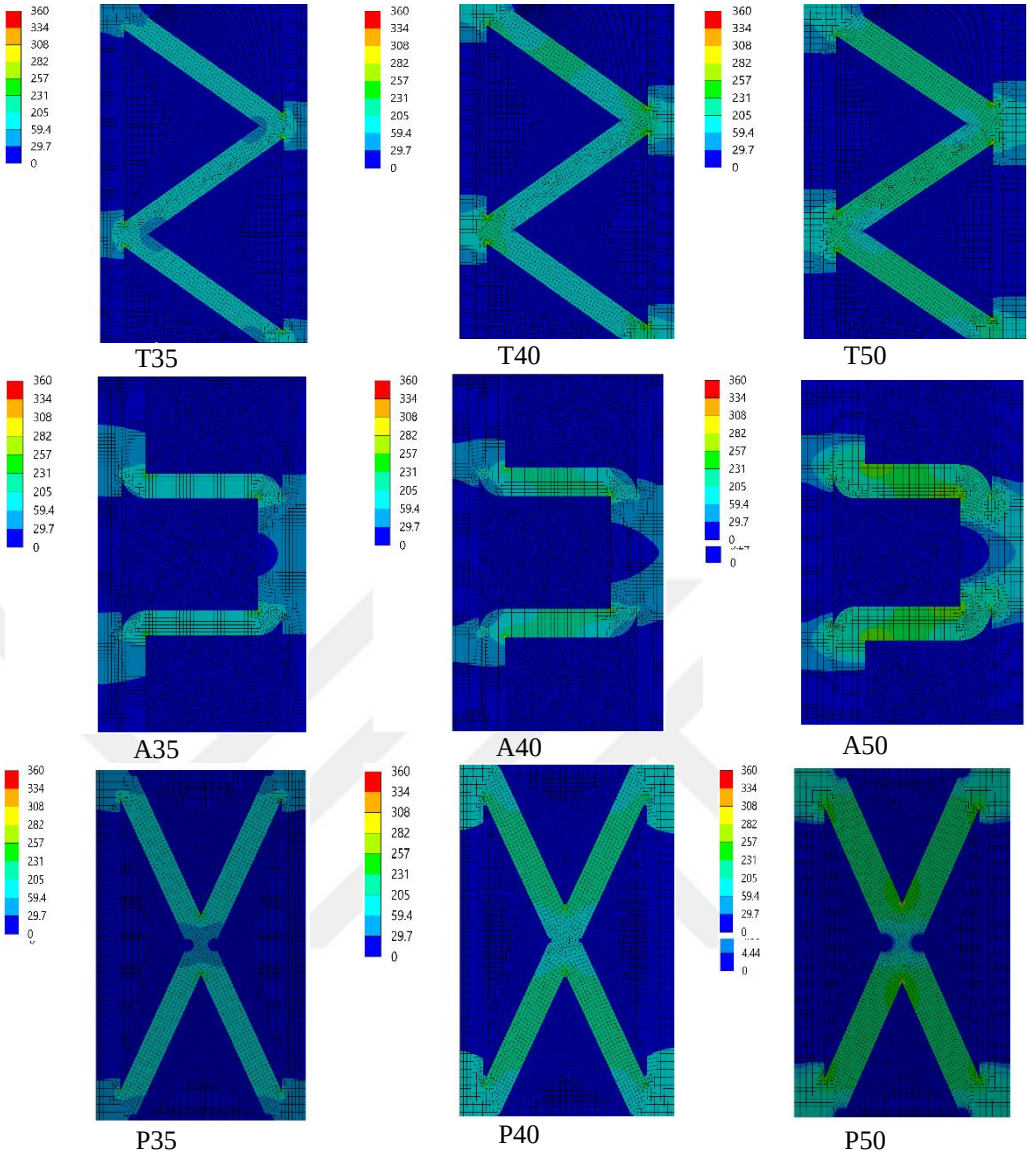


Figure 5. 5 Surface heat flux contour maps of EPS insulated walls.

The percentage reductions in U-values in all wall types for both insulating materials are close and vary between 77.3 and 87.2% (Figure 5.6). Even though the percentage reductions due to EPS are slightly higher than those of perlite, the average difference is very small, i.e., 2.16% (Table 5.3). For example, for the 35 mm filament width with EPS insulation, the percentage reductions in U-values for T35, A35, and P35 are 87.23%, 86.95%, and 84.95%, respectively. This shows that cavity insulation significantly improves the thermal performance of 3DPC envelopes, which complements the results presented by Alkhalidi and Hatuqay (2020). Overall, P-walls show the best thermal performance of all wall types. For example, P50 has 0.154 W/m^2.K has the lowest U-value, and A50 has 0.563 W/m^2.K has the highest U-

value of all EPS-insulated walls. This thermal behavior is contrary to the respective areas of insulation of the wall types. While cavity insulation significantly improves the thermal performance of 3DPC envelopes, there is a contradiction with the results presented by Suntharalingam et al. (2021). Their results showed that U-values decreased with an increase in void area with insulation due to larger amounts of insulation directing a reduction in material conductivities. However, the results of the current study say otherwise. T walls have the largest area of insulation of the three wall types in this study, while those of P walls are the smallest. Yet P-walls show the best thermal performance of all wall types. From the U-values of insulated lattice structures of the same thickness, contour lengths, and insulation percentage, it can be deduced that the individual differences in the thermal performance of 3DPC structures are not affected by the area of insulation but rather by thermal bridging resulting from the geometric properties of the structures. Figure 5.7 shows the thermal performance of the 3DPC envelopes with respect to their area of insulation.

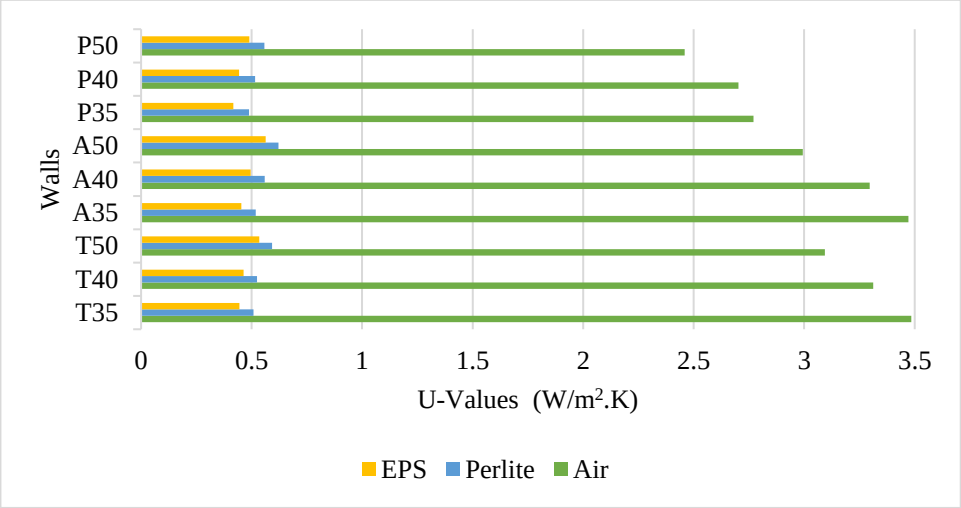


Figure 5. 6 Reductions in U-values due to cavity insulation.

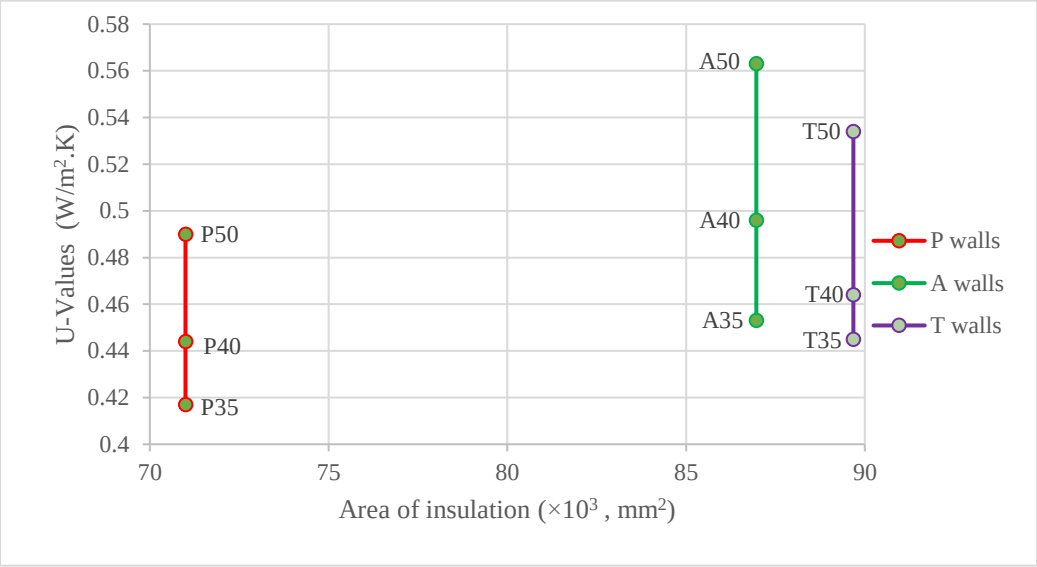


Figure 5. 7 Thermal transmittance variations with area of insulation.

5.3.3. Effect of Geometric Properties of Insulated Lattice Structures

Of the three wall types, the P walls have the longest webs due to their cob design. The webs in these walls cross each other at a small slant angle compared to those of the T walls, with webs subtending a larger angle of inclination (Figure 5.1). This makes the P walls have the longest web length (heat path), followed by the T walls. The webs of the A walls are the shortest since they are perpendicular to the exterior and interior surfaces of the lattice structures. It means that there is a short and more direct bridge between the two wall faces. For instance, for the 35 mm filament width, the web lengths for the P35, T35, and A35 are 479, 288, and 245 mm, respectively. Since heat transfer through these insulated lattice structures is predominantly by conduction through the webs, heat takes the longest distance to travel through the P walls and the shortest distance from the A walls. This partly explains why the P walls have the lowest U-values and the A walls the highest. Similar observations were made by Pierzchlewicz (1996), who compared the thermal performance of multicore and solid blocks. The researcher found that, when compared to multicore blocks with aligned holes, those with staggered holes elongate the heat flow path through walls. This improves the thermal resistance of the multicore blocks with staggered holes.

Furthermore, the contact or intersection area between the webs and face shells might also contribute to the thermal behavior of these insulated lattice envelopes. The A walls have the largest contact area of the three wall types. For instance, for the 35 mm filament width, the contact distance of A35 is 158 mm, whereas that of T35 and P35 is 36 mm and 37 mm, respectively. A large contact or intersection area means heat flow happens over a larger area. Similar observations were made by the National Concrete Masonry Association (NCMA) (2012), which studied heat transfer through concrete blocks with different numbers of webs. They found a 30% reduction in the thermal resistance of concrete blocks with two webs over the typical three-web concrete blocks.

Lastly, across all walls of the same type, the U-value increases with an increase in the filament width. For example, the U-values of the perlite-insulated T walls, T35, T40, and T50 are 0.509, 0.525, and 0.593 $W/m^2.K$. This is because an increase in filament width implies an increase in the cross-sectional area of the webs. Since thermal bridging is predominant, the area through which heat travels increases, thereby reducing the thermal performance. The thermal performance of insulated 3DPC envelopes of the same contour lengths and percentage of insulation is mainly affected by the web length, filament width, and the contact (intersection) area between the webs and face shells.

5.3.4. Thermal Efficiency of Insulation

The thermal efficiency (T_{Eff}) of the insulation was calculated to determine its effectiveness. Thermal bridges significantly affect the effectiveness of the insulation, as discussed in the previous sections. This is because of the large thermal conductivity differences between the 3DPC and the granular fill materials. The thermal efficiency of both insulating materials in all wall types varies between 26 and 44% (Table 5.4 and Figure 5.8). This shows that 56–74% of the applied insulation is not used and does not contribute to increasing the thermal resistance of the lattice structures. Therefore, to reduce the effect of thermal bridges that undermine the effective use of insulation, innovative wall designs such as combined double-row walls, which minimize or eliminate web connections, are a potential

solution. Other insulation techniques, such as internal wall insulation and the use of 3D-printed lightweight concretes, are other potential solutions. Higher-density concrete tends to have more compressive strength than lightweight concrete, but lightweight concrete has a lower thermal conductivity (Urban et al., 2011). The smaller the difference in thermal conductivities between the 3DPC and insulation fill material, the lower the effects of thermal bridging. This explains why perlite-insulated walls have slightly higher thermal efficiencies of insulation than EPS-insulated walls.

Table 5. 4 Thermal efficiency of insulation of perlite and EPS.

Wall Configuration	R_{un}	R_{in} (K·m/W)		R_{eq} (K·m/W)		T_{Eff} (%)	
		Perlite	EPS	Perlite	EPS	Perlite	EPS
T35	0.287	1.965	2.247	4.234	5.65	39.63	34.7
T40	0.302	1.905	2.155	4.167	5.556	38.47	33.36
T50	0.323	1.686	1.873	3.922	5.236	34.76	29.59
A35	0.288	1.927	2.208	4.132	5.525	39.66	34.74
A40	0.303	1.789	2.016	4.098	5.464	36.25	31.34
A50	0.334	1.608	1.776	4	5.348	31.84	26.97
P35	0.361	2.045	2.398	3.861	5.155	43.62	39.52
P40	0.37	1.938	2.252	3.774	5.025	41.55	37.45
P50	0.407	1.792	2.041	3.597	4.808	38.52	33.99

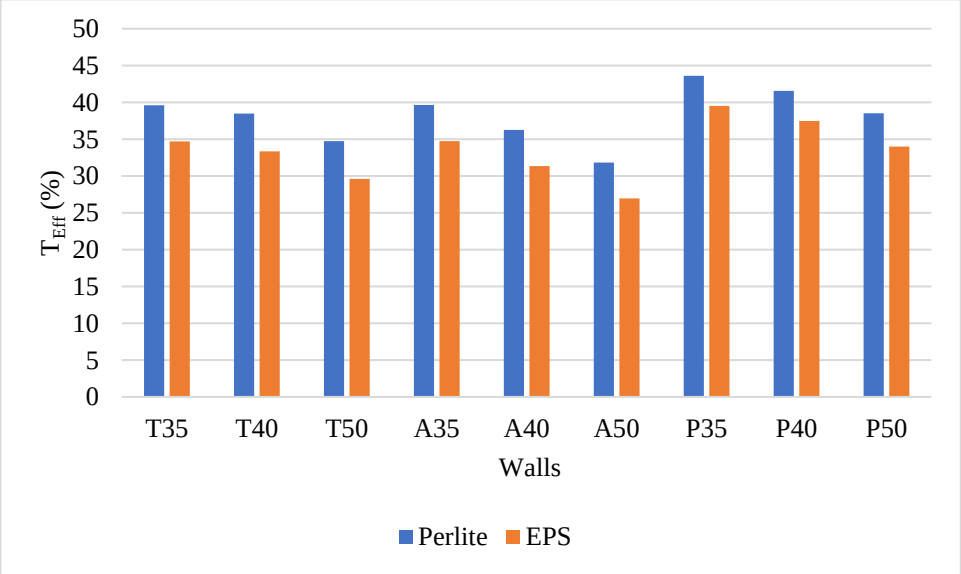


Figure 5. 8 Thermal Efficiency (T_{Eff}) of Insulation of Perlite and EPS.

When it comes to 3D-printed concrete, the generally traditional materials adopted are mainly cement and fine sand in most cases. It is worth noting that, despite the study focusing on 3DPC made of traditional materials, researchers have developed and applied various innovative materials. These range from different supplement cementitious materials (SCMs), phase change materials (PCM), admixtures, fibers, and different aggregate types (Hou et al., 2020; Zhang et al., 2021). When applied, all these materials have the potential to affect thermal performance based on their quantities and thermal conductivities.

By volume, aggregates, which occupy 60–70% of the volume of concrete, play an important role in the thermal performance of concrete (Hou et al., 2020). Lightweight aggregates are typically associated with low densities and low thermal conductivities. This is the case for recycled sand, which has growing applications in construction due to sustainability concerns. Mohammad et al. (2020) developed a high-performance lightweight concrete for 3D printing, while Pietras et al. (2023) developed a novel 3D printing cement-based composite material with granulated cork. The application of such materials improves the thermal performance of 3DPC envelopes.

Coarse aggregate application in 3DPC, however, is an unavoidable development for a variety of 3DPC applications in construction. Ji et al. (2019) introduced large-scale applications of coarse aggregates in 3DPC. Coarse aggregates have higher densities and thermal conductivities, thereby comprising thermal performance. SCMs, PCM, admixtures, and fibers also have the potential to influence the thermal properties of 3DPC. When compared to ordinary concrete, 3DPC tends to have a higher percentage of entrained air bubbles. This is due to the use of viscosity-modifying and enhancing admixtures to maintain the desired rheological properties. Furthermore, additional air is entrapped between 3PDC layers during the printing process because of the nature of layer-to-layer construction. Both entrained and entrapped air volumes may have the potential to enhance the thermal resistivity of 3DPC. Hao et al. (2022) studied the thermal conductivity of 3DPC made of recycled fine aggregate and PCM. Under the same size, density class, or mix design, they

noted that the thermal conductivity of the 3DPC can reach up to 31.04% lower than that of mold-cast concrete. The replacement ratios of cement with SCMs by volume fraction are relatively small, and in the case of fibers, with a typical volume fraction of 2%, their application could almost be insignificant (Soltan & Li, 2018). Other innovative materials that have found application in 3DPC are copper tailings, paraffin, and geopolymers, which have the potential to influence thermal properties (Al-Qutaifi et al., 2018; Ma et al., 2017). The composition of the mix designs of 3DPC presents opportunities for research into their effects on the thermal performance of 3DPC.

5.4 Conclusions

This work is a numerical study of 3DPC lattice envelopes to understand the influence of the geometry of the infill structure on their thermal performance. With emphasis on the buildability, scalability, and application of 3D concrete printing, the study was limited to lattice structures produced by the Material Deposition Method (extrusion). A holistic selection approach was taken in the selection of the three infill structures used in this study. This is to ensure that the lattice structures studied not only have sufficient structural integrity but are also consistent with additive manufacturing industrial trends. All the lattice structures were modeled to have nearly equal contour lengths and void and insulation percentages. Additionally, the effects of filament width and the application of granular insulating material (EPS beads and loose-fill perlite) were also studied. Lastly, the efficacy of insulation was also established to determine the extent to which unintended thermal bridges produce significant heat losses, resulting in the ineffective usage of the insulation material. Based on the findings of the analysis, the following conclusions were reached:

1. The thermal performance of 3DPC envelopes in stagnant air conditions is primarily influenced by the void area. T walls with the largest void area have the worst performance.
2. When the cavities are insulated, the individual differences in the thermal performance of 3DPC structures are not influenced by insulation area but by thermal bridging due to geometric properties. Despite having the smallest

insulation area, P-walls show the best thermal performance among all wall types.

3. The thermal performance of insulated 3DPC envelopes of the same contour lengths is mainly affected by the web length, filament width, and the contact (intersection) area between the webs and face shells.
4. Due to varying web lengths, heat travels the longest distance through the P walls and the shortest distance from the A walls via thermal bridging. Furthermore, a large contact or intersection area between the webs and face shells, as in the case of the A walls, reduces thermal performance.
5. The U-values of insulated lattice structures increase with an increase in the filament width. This is because of the increase in the cross-sectional area of the webs, through which thermal bridging is predominant.
6. The application of EPS beads shows better thermal performance than that of loose-fill perlite, owing to the lower thermal conductivity of EPS beads. To reduce thermal bridges and improve the effective use of insulation, the use of innovative wall designs, together with other insulation techniques and lightweight concrete, is recommended.

These results provide designers with insights to consider when planning buildings' energy needs. This study broadens our understanding and gives a better insight into the energy performance of building systems and cost-effective options during the adoption of additive manufacturing in the construction industry.

CHAPTER SIX
THERMAL BRIDGING EFFECTS IN 3D PRINTED FOAM CONCRETE

6.1 Introduction

Building quality has increased greatly in recent decades in response to increasing comfort needs as a result of technical advancement and rising societal living standards. Three-dimensional concrete printing (3DCP) is considered the most promising automated construction method for producing large load-bearing structures (Mechtcherine et al., 2020). This innovative technology offers numerous economic, social, and environmental benefits. Due to its rapid construction capabilities, it presents a potential solution to the global housing and accommodation crisis, particularly in developing countries (Khan et al., 2021).

Because of process optimization and automation, 3DCP increases production while compensating for a growing skilled personnel shortage. This automation in the construction process could significantly lower construction expenses. Shortening the construction period reduces costs. Some of these costs include facade scaffolding, construction management, and rental time for building site equipment (Adaloudis & Bonnin Roca, 2021; Otto et al., 2020). Furthermore, wall elements manufactured from 3DPC have excellent sound absorption and fire resistance capabilities (Raj et al., 2019). The recyclability of wall elements, which are primarily made of mineral materials, is easier and more cost-effective (Markin et al., 2021).

Buildings must meet modern requirements for comfort, considering aspects like lighting, acoustics, thermal climate, and interior air quality. Generally, air conditioning systems are used to provide thermal comfort. Heating and cooling loads account for a sizable portion of the energy used in residential and commercial buildings (Real et al., 2016; Wan et al., 2010). Heating, cooling, ventilation, and air conditioning (HVAC) costs are even higher in dilapidated buildings.

Reducing building energy usage is critical for both economic and environmental reasons. This can be accomplished by improving the thermal envelope, employing

more efficient systems, and implementing renewable energy technologies (Ji et al., 2019; Kossecka & Kosny, 2001). In Europe, the requirements for thermal insulation of the building envelope have increased over the past few decades and are predicted to continue to rise in the future as a crucial step towards minimizing thermal losses in the context of improving the energy performance of both new and existing buildings (Theodosiou et al., 2015).

The movement of heat by conduction through the building envelope includes both heat transfer through envelope elements and heat transfer through thermal bridges (Real et al., 2016). A thermal bridge occurs when materials with a different thermal conductivity completely or partially penetrate the building envelope, changing the fabric's thickness or creating a difference between internal and external areas, such as wall, floor, or ceiling junctions, all of which result in a significant reduction in the building envelope's thermal resistance (Alhawari & Mukhopadhyaya, 2018; Theodosiou et al., 2015; Viot et al., 2015). Heat flow rate and internal surface temperature are generally affected because of thermal bridges (Real et al., 2016). In Europe, thermal bridges can have a cumulative influence of up to 30% on a building's heating energy needs, according to Capozzoli et al. (2013).

Thermal performance in 3DPC building envelopes is affected by various factors. These factors include infill geometry, cavity size, and insulation. Several researchers have studied the thermal behavior of 3DPC envelopes. Nemova et al. (2022) developed an energy-efficient envelope that adheres to climatic zones. Mansouri et al. (2022) showed that subdividing big cavities into smaller ones can greatly lower heat flux. Alkhalidi & Hatuqay (2020) designed affordable, energy-efficient housing units by balancing voids and printed material. Suntharalingam et al. (2021) showed that intricate designs such as lattice structures or double-rowed honeycombs are capable of trapping air thereby improving insulation. AlZahrani et al., 2022) studied the energy efficiency of infill structures with the same void-to-concrete ratios. Similarly, Chamatete & Yalçınkaya (2024) examined how lattice type, filament width, and granular filling material affect the thermal performance of 3DPC building envelopes. They demonstrate that void area influences the thermal performance of 3DPC

envelopes under stagnant air conditions, whereas web length, filament width, and the contact (intersection) area between the webs and face shells influence thermal behavior when cavities are filled with insulating materials due to thermal bridging.

Webs in 3DPC infill structures serve as wall braces, reducing wall bowing and buckling failure (Joh et al., 2020), but because of their high thermal conductivity compared to the low thermal conductivity of the surrounding construction materials (Real et al., 2016), their presence within 3DPC building envelopes significantly contributes to the existence of thermal bridges. Three-dimensional printed foam concrete (3DPFC) can make a major contribution to reducing thermal bridging in this regard.

Foam concrete (FC) is a cellular-structured, lightweight cementitious material that is created by encasing a lot of air voids in a cement-based matrix. FC can be engineered to have any density between 200 and 1900 kg/m^3 (Fu et al., 2020). Interestingly, most of the research on cement-based materials for additive manufacturing (AM) is focused on using mortar or normal-weight concrete (NWC). Many researchers have long acknowledged the potential of FCs for traditional construction methods (Raj et al., 2019), but up until this point, very few studies have focused on the use of these materials in AM (Falliano et al., 2018; Henke et al., 2017; Markin et al., 2019).

In comparison to normal-weight concretes, utilizing FC allows for greater heat isolation across building envelopes while maintaining appropriate mechanical qualities for structural applications. Because of its decreased density, FC can reduce both the dead (permanent) load and the overall thermal conductivity of envelopes (Markin et al., 2021). The lower heat conductivity of the air trapped in the porous structure of the cement-based matrix is primarily responsible for the increased thermal insulation capacity (Raj et al., 2019).

Therefore, as an alternative to NWC, FC helps to reduce the thermal bridging effect in structural elements, allowing for less global heat loss through the building

envelope, fewer corrective insulation systems required to meet thermal comfort requirements, and more effective use of insulation. Moreover, the recyclability of wall elements, which are primarily made of mineral materials, as in the case of FC, is easier and more cost-effective than recycling or disposing of wall elements made of numerous materials with different qualities (Priyatham et al., 2023).

The building envelope is one of the most critical systems that influence a structure's energy performance (Real et al., 2016). A comprehensive analysis of thermal bridging through 3DPC building envelopes is compelling in this regard. In almost all the studies delving into the thermal performance optimization of 3DPC envelopes, only NWC is considered. Meanwhile, FC has tremendous potential as an innovative, cost-effective, and ecologically sound construction material, and its use in structural applications is expanding with enhanced research.

In all the previous studies, the potential of FC in enhancing the energy efficiency of 3DPC envelopes has still not been studied. Therefore, the purpose of this work is to study thermal bridging in 3DPFC envelopes due to infill geometry. The effects of the contact (intersection) area of webs with the interior face shell, webs, and infill rows on the thermal performance of granular cavity-filled 3DPFC envelopes are studied. Because of its wide availability, expanded polystyrene (EPS) is used in this study. Numerous additional considerations, including affordability, sustainability, recyclability, conformity to irregular shapes, and ease and variety of application, all played a role in the decision to choose this material. Furthermore, this study aims to establish the extent to which thermal bridges influence the effective use of insulation. By doing so, potential sources of poor thermal behavior attributed to the infill structure can be identified. This will facilitate informed design and construction decisions in additive manufacturing.

6.2 Methodology and Analysis

Six lattice structures were chosen, and a thorough parametric analysis was carried out to investigate how the internal structure (infill structure) impacts energy performance. The study established the effects of the contact (intersection) area of

webs with the interior face, webs, and infill rows on the thermal behavior of these lattice envelopes. A detailed explanation of the parametric study can be found in Section 6.2.1. The heat transfer analysis utilized Ansys Workbench for modeling. Appropriate numerical heat transfer models were created and verified using published data.

EPS beads were applied for cavity insulation. Table 6.1 shows the thermal properties of the 3DPFC and cavity-fill materials (Markin et al., 2021; Ochs & Müller-Steinhagen, 2005). Lastly, an assessment of the thermal efficiency of insulation is made to assert the extent to which thermal bridges can produce significant heat losses, resulting in ineffective usage of the insulation material. This research contributes to the development of energy-efficient and sustainable 3DPC building envelopes. The sections that follow contain detailed information on the research's methodology.

Table 6. 1 Thermal properties of materials.

Material	**Density (kg/m^3)**	**Thermal Conductivity (W/m.K)**	**Specific Heat (J/g.K)**	**Source**
Concrete Block	2300	1.75	1	Henrique Dos Santos et al. (2017)
3DPFC	1230	0.35	1.2	Markin et al. (2021); Wu et al. (2016)
Air	Ideal gas	0.0242	1.00643	Suntharalingam et al. (2021)
EPS	40	0.03	1.25	Ochs & Müller-Steinhagen (2005); Schiavoni et al. (2016)

6.2.1 Parametric Study

Based on industrial trends, four wall types were selected for the parametric study, and a total of six wall models were developed and studied. The first two walls (W1 and W2) used in this study are a square zig-zag configuration obtained from Apis Cor, a Guinness Book World Record holder for the world's largest 3D-printed building on Earth (Apis Cor, 2023a, 2023b). The only difference between these walls is the contact or intersection area of the webs with the interior face shell and the number of webs. The next two walls (W3 and W4) are adopted from CyBe Construction, another leading company in the three-dimensional concrete printing

(3DCP) business (CyBe Construction, 2023c). Similarly, these two walls only differ in the contact area. Finally, the last two walls (W5 and W6) are double-rowed, adopted from CyBe Construction and QOROX (CyBe Construction, 2023a, 2023b). Double-rowed wall systems produce large moments of inertia and have a growing application in 3DCP (Bello & Memari, 2022). Figure 6.1 shows the six walls considered in the parametric analysis. The interior and exterior face shells are denoted by Int and Ext respectively.

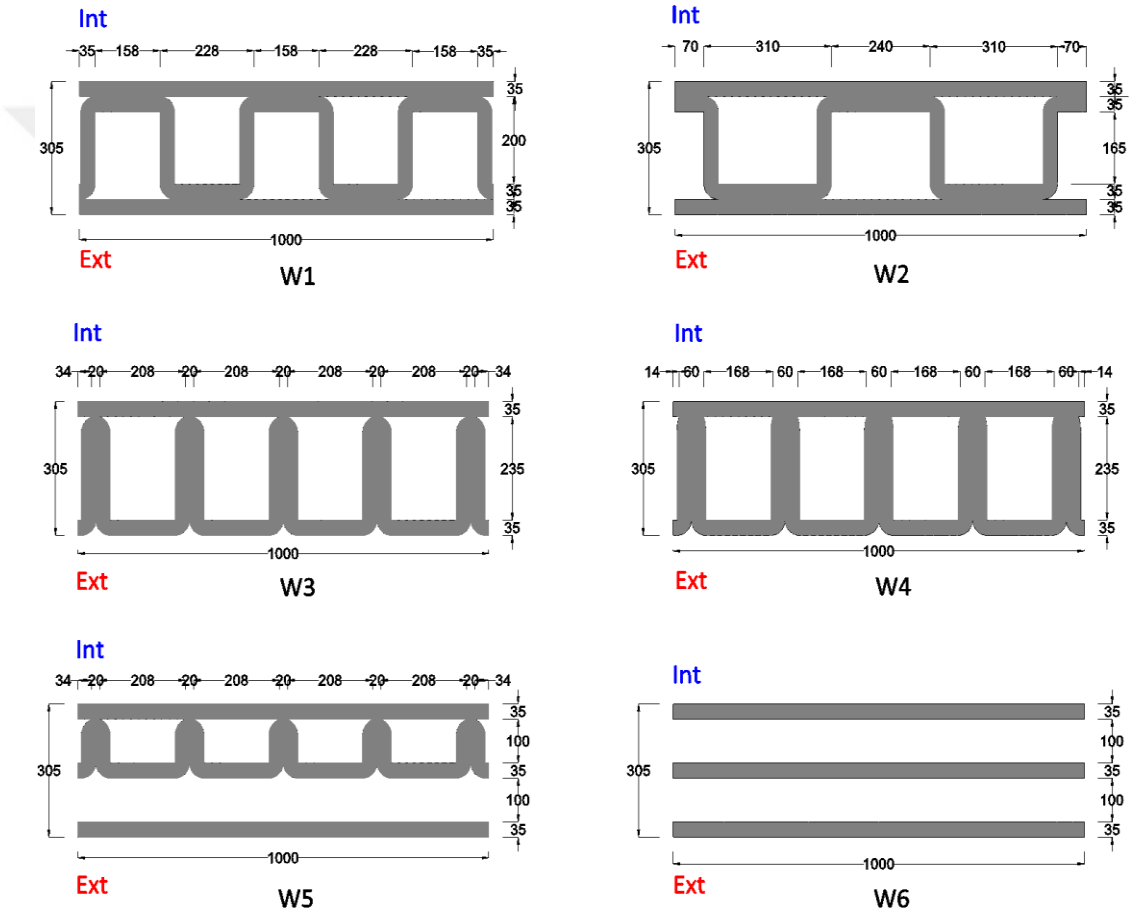


Figure 6. 1 Wall types (35 mm filament width) for the parametric analysis (dimensions in mm).

To study thermal bridging effects due to contact area and webs, as well as the effectiveness of insulation on the thermal performance of 3DPFC envelopes, all the lattice structures under this study were modeled to have the same thickness, height, length, and similar areas of insulation. The contact length of the webs with the interior face shell is measured per meter of the 3DPFC walls. W1 and W2 have the

same lattice structure. However, the contact length of the webs with the interior face is increased from 158 mm to 240 mm. Consequently, the number of webs between the exterior and interior face shells reduces to four in W2 as compared to six in W1.

Similarly, W3 and W4 are lattice structures with straight double webs which act as lateral supports. They both have the total same number of webs, i.e., 10. However, the contact length of each of the double webs is increased by 300% in W4. The contact length of the webs in W3 is 20 mm, while W4 has contact lengths of 60 mm. For the same geometric design, the contact length of webs can vary depending on the consistency of the 3DPC mix, the nozzle type, or the printing pattern. During the process of printing using more flowable mix designs, the contact length is likely to increase from the original geometric design when compared to less flowable mixes. Furthermore, rectangular nozzles tend to have better dimensional stability and control during the layering of filaments when compared to circular nozzles.

Lastly, W5 and W6 are double-rowed lattice structures. They show partial and complete isolation of the exterior and interior faces, respectively. This implies that the webs do not connect or partially connect the two outer surfaces. In real-life applications, however, the voids in infill structures are locations to install steel reinforcement, services, and insulation. In double-rowed lattice structures, the exterior row is mostly for insulation, while the interior row is left for services (Bello & Memari, 2022). All walls are modeled to a thickness of 12 in. (304.8 mm), length of 1000 mm, and height of 250 mm. Additionally, the insulation percentages of all the walls are within a similar range. A detailed description of the parametric study is given in Table 6.2.

Table 6. 2 Detailed description of the parametric study.

Wall	Number of Webs	Contact Length of webs (mm/m)	Concrete Area (mm^2)	Insulation Area (mm^2)	Insulation Percentage (%)	Cavity Fill Material	No. of Models
W1	6	474	142,708.78	162,195.45	53	EPS	1
W2	4	380	102,371.13	173,931.10	63	EPS	1
W3	10	100	142,357.04	155,093.07	52	EPS	1
W4	10	300	144,673.11	153,163.01	51	EPS	1
W5	10 (Not full length)	N/A	132,570.24	169,936.95	56	EPS	1
W6	Non	N/A	105,000.00	200,000.00	66	EPS	1
Total							6

The insulation design of building envelopes has a major effect on their thermal performance. This design considers several financial trade-offs, including durability and maintenance costs, between the initial investment in enhancing the envelope and the long-term energy costs for maintaining the area (Schumacher, 2013). Loose-fill EPS beads were used for cavity filling to enhance thermal performance. The selection of this material is not only driven by the demands of sustainability and environmental responsibility in the building sector, but also by their ease and versatility of application, conformity to irregular shapes, and cost-effectiveness. EPS insulation is a highly efficient and environmentally friendly choice known for its robust and lightweight structure. The Insulation Company of America asserts that it has always been free of harmful compounds like Chlorofluorocarbons (CFCs) and Hydrochlorofluorocarbons (HCFCs) (Insulation Company of America, 2023). Its remarkable characteristics, including its low thermal conductivity and lightweight structure, significantly reduce heat transfer in 3DPC structures (Insulation Company of America, 2023; Yucel et al., 2020).

Granular insulating materials, as stated earlier, have interconnected voids between the individual grains, forming a tortuous but continuous air path through them. Tests conducted by Simpson et al. (2020) indicated that the thermal conductivity of loose EPS beads can be up to 5% higher than that of EPS boards of a similar density. Therefore, the thermal conductivity of the granular materials in this study was increased by 5%. A total of 6 wall models, with cavity insulation, are considered in

the parametric study (Table 6.2). It is worth mentioning that in real-life construction, some of the wall cavities are filled with concrete and rebar, while others are designated for utilities such as electricity and plumbing. To ensure uniformity and simplicity, the analysis was performed in the absence of concrete, reinforcement, and service lines in the cavities.

6.2.2 Thermal Efficiency of Insulation

Thermal insulation efficiency (T_{Eff}) measures the effectiveness of insulation materials in preventing thermal energy flow in building assemblies, allowing for cost optimization and reducing unintended heat losses via thermal bridges (Urban et al., 2011). T_{Eff} may be expressed by the following equation:

$$T_{Eff} = \frac{R_{in} - R_{un}}{R_{eq}} \times 100 \quad (6.1)$$

Where R_{in} is the R-value of the insulated wall panel, R_{un} is the R-value of the uninsulated wall panel, and R_{eq} is the equivalent resistance of insulation material alone, configured as a single uninterrupted layer.

6.3 Results and Discussion

This section discusses the numerical simulation results of the parametric study. The thermal transmittance values of all the models are given in Table 6.3. For the same wall thickness, height, and similar percentages of insulation, the effects of the contact (intersection) area, presence of voids, and thermal efficiency of insulation, are discussed herein.

Table 6. 3 Thermal transmittance values of all models in the parametric study.

Wall Configuration	U-Values (W/m^2. K)	R-value (K.m /W)			T_{Eff} (%)
		Run	Rin	Req	
W1	0.652	0.58	1.534	5.155	18.5
W2	0.541	0.556	1.848	5.525	23.4
W3	0.484	0.429	2.066	4.926	33.2
W4	0.518	0.439	1.931	4.854	30.7
W5	0.235	0.633	4.255	5.405	67
W6	0.151	0.66	6.623	6.329	94.2

6.3.1. Effect of Contact Area

Cavity insulation dictates the heat flow path through the insulated 3DPFC walls. The thermal conductivity of the 3DPFC walls is 11.6 times higher than that of EPS beads (Table 6.1). Due to the high difference in thermal conductivity, the heat path through all the insulated wall types is predominantly through the concrete webbing of the lattice structures. In all walls except W6, thermal bridges occur due to the complete and partial penetration of webs through the building envelopes. This results in a significant reduction in the building envelope's thermal resistance and performance (Canadian Concrete Masonry Producers Association (CCMP), 2013; Real et al., 2016). Thermal bridges are evident between the external and interior faces in Figure 6.2.

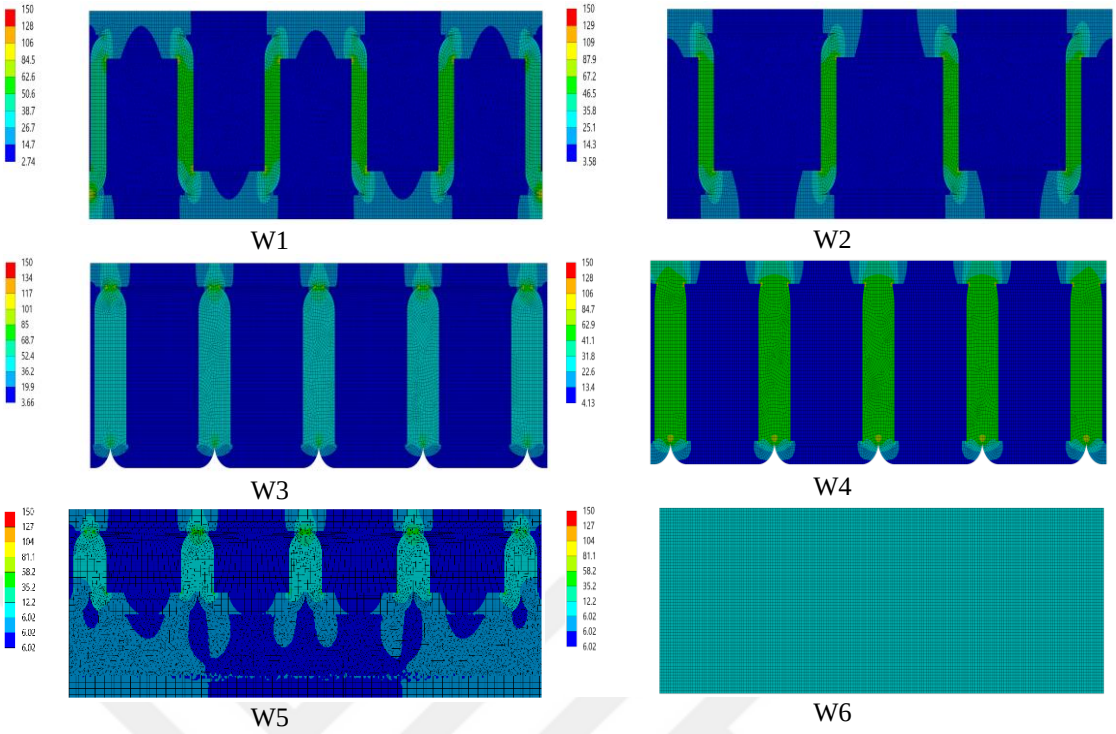


Figure 6. 2 Surface heat flux contour maps of EPS cavity-filled walls.

From the U-values, it is clear that the thermal performance of insulated 3DPC building envelopes is directly proportional to the contact area of the webs with the interior surface (Table 6.3). The larger the contact area of the webs with the interior face, the higher the thermal transmittance. Of all walls, the double-rowed walls show superior thermal performance. W6 has the lowest U-value, i.e., 0.151 W/m^2.K, indicating the best thermal performance, while W1 has the highest U-value, i.e., 0.652 W/m^2.K, hence showing the poorest performance (Table 6.3).

The U-value is directly proportional to the contact length. W1 has the longest web contact length, i.e., 474 mm/m, while in W6, the exterior and interior faces are entirely isolated, i.e., no webs (Table 6.2). However, W2 with 0.541 W/m^2.K shows slightly better thermal performance than W1 due to its reduced contact length, i.e., 380 mm/m. W4 has a 300% increase in contact length, i.e., 300 mm/m, when compared to W3 with 100 mm/m. The increase in contact length between these two walls shows a consequential increase in thermal transmittance. This is because more area is available through which heat conduction occurs. Thus, W3 has a U-value of 0.484 W/m^2.K while that of W4 is 0.518 W/m^2.K.

When it comes to the double-rowed lattice structures, the isolation of the exterior and interior face shells by a layer of insulation significantly improves thermal performance. There is partial isolation in W5, while W6 has complete isolation. For this reason, W5 with a U-value of 0.235 W/m^2.K shows a slightly higher thermal transmittance than W6. Similar findings were reported by Suntharalingam et al. (2021). They showed that double-rowed lattice structures have superior thermal performance due to enhanced insulation.

Based on the parametric study results, the thermal performance of insulated lattice structures does not depend on the area of insulation (Tables 6.2 and 6.3). W1 shows the poorest thermal performance (highest U-value) despite having an area of insulation higher than that of W3 and W4. Similar findings were made by Chamatete & Yalçınkaya (2024) in a previous study (Chapter 5), they investigated the effects of lattice type, filament width, and granular filling material on the thermal performance of 3DPC building envelopes. Figure 6.3 shows the thermal performance of the 3DPC envelopes with respect to their area of insulation.

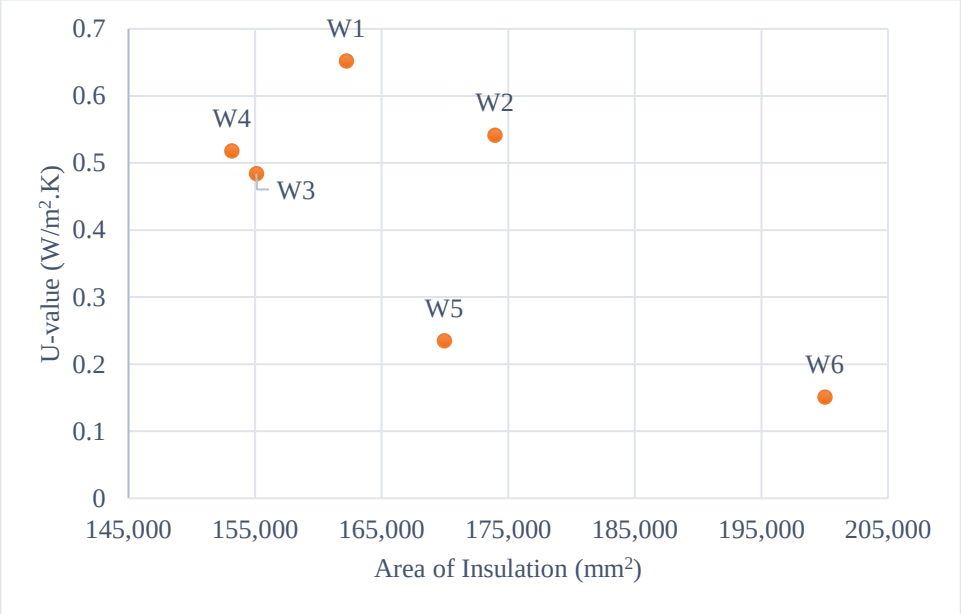


Figure 6. 3 Thermal transmittance variations with area of insulation.

6.3.2. Effect of Webs

From the results, the thermal performance of insulated 3DPC is directly affected by the presence of webs. This is due to thermal bridging effects. As stated earlier, walls W5 and W6 show superior thermal performance due to the absence of webs which directly connect the exterior and interior faces. The presence of webs in the interior row of W5 slightly deteriorates its thermal resistance when compared to W6 (Figure 6.1). However, when it comes to the number of webs completely connecting the two surfaces, walls W3 and W4 contain the highest number of webs. They consist of five double webs, i.e., 10 webs in total on each wall, compared to W1 and W2, which have 6 and 4 webs, respectively (Table 6.2).

Despite having comparatively many webs, walls W3 and W4 show better thermal performance than W1 and W2, mainly due to constricted contact points with the interior face. This indicates that the number of webs connecting the exterior and interior faces may have a lesser influence on the thermal performance than their contact areas. However, these findings are contrary to those made by the National Concrete Masonry Association (NCMA), (2012), which studied heat transfer through concrete blocks with different numbers of webs. They found a 30% reduction in the thermal resistance of concrete blocks with two webs over the typical three-web concrete blocks.

It is worth mentioning that the webs in walls W3 and W4 are slightly longer than those in W1 and W2. Since heat transfer is predominantly by conduction through the webs, heat takes a longer distance to travel through the webs of these walls than those of W1 and W2. This also potentially justifies why walls W1 and W2 have the highest thermal transmittance values. Similar observations were made by Pierzchlewicz (1996) in multicore and solid blocks. The researcher found that multicore blocks with staggered holes lengthen the heat flow path through walls in comparison to those with aligned holes. As a result, the multicore blocks with staggered holes have improved heat resistance.

Since thermal bridging effects are dominant in cavity-insulated 3DPC lattice structures, their thermal performance is mainly governed by the nature of the connection of the exterior and interior faces. The absence or lack of direct connection between the exterior and interior face shells produces superior thermal performance. However, when there is a direct connection between the two faces, the thermal performance of these envelopes is mainly affected by the contact (intersection) area of the webs rather than the number of webs.

Despite webs being a significant source of thermal bridges in 3DPC infill structures, from a structural point of view, they serve as wall braces, reducing wall bowing and buckling failure (Joh et al., 2020). Therefore, the presence of webs, the nature of their connection between the exterior and interior faces, as well as the contact area, can all affect the structural integrity of the 3DPC envelopes. While the absence or lack of direct connection between the exterior and interior face shells produces superior thermal performance, it potentially undermines its lateral stability. This is very crucial for load-bearing walls. Furthermore, an increase in the contact (intersection) area may also enhance the overall structural integrity of the envelopes. Therefore, a delicate balance between thermal performance and load bearing capacity is necessary in the application of 3DCP. In the case of double-rowed lattice structures, as stated earlier however, the exterior row is mostly for insulation, while the interior row is left for loading and services (Bello & Memari, 2022).

6.3.3. Thermal Efficiency of Insulation

The thermal efficiency (TE_{ff}) of the insulation was calculated to determine its effectiveness. Thermal bridges significantly affect the effective usage of the insulation, as discussed in the previous sections. Thermal bridges significantly affect the effectiveness of the insulation, as discussed in the previous sections. This is because of the large thermal conductivity differences between the 3DPC and cavity-fill materials. The thermal efficiency of insulation in all wall types varies between 18.5 and 94.2% (Table 6.3 and Figure 6.4). Walls W1 and W2 show the lowest T_{Eff} values at 18.5 and 23.4%, respectively. This implies that 81.5% and 76.6% of the applied insulation, respectively, is not used and does not contribute to increasing the

thermal resistance of the lattice structures. Walls W3 and W4 also show poor insulation efficiency, with 33.2 and 30.7%, respectively. All the single-row walls have T_{Eff} values less than 50%.

However, the double-rowed walls (W5 and W6) show the most effective use of insulation, with 67 and 94.2%, respectively. This is at least twice as much and even more effective insulation usage when compared to the single-rowed walls (W1-W4). This implies that only 33 and 5.8% of the applied insulation, respectively, is not used and does not contribute to increasing the thermal resistance of the lattice structures. Thus, the TE_{ff} values of the single-rowed walls show that thermal bridging effects due to webbing significantly undermine the effective use of insulation. On the other hand, the application of innovative wall designs such as combined double-row walls, which minimize or eliminate web connections, is a potential solution.

Additionally, lightweight concretes generally have low thermal conductivities (Urban et al., 2011). Therefore, the application of 3DPFC significantly improves the efficiency of insulation due to reduced thermal bridging effects. These findings on the T_{Eff} of lattice structures support the recommendations of Urban et al. (2011).

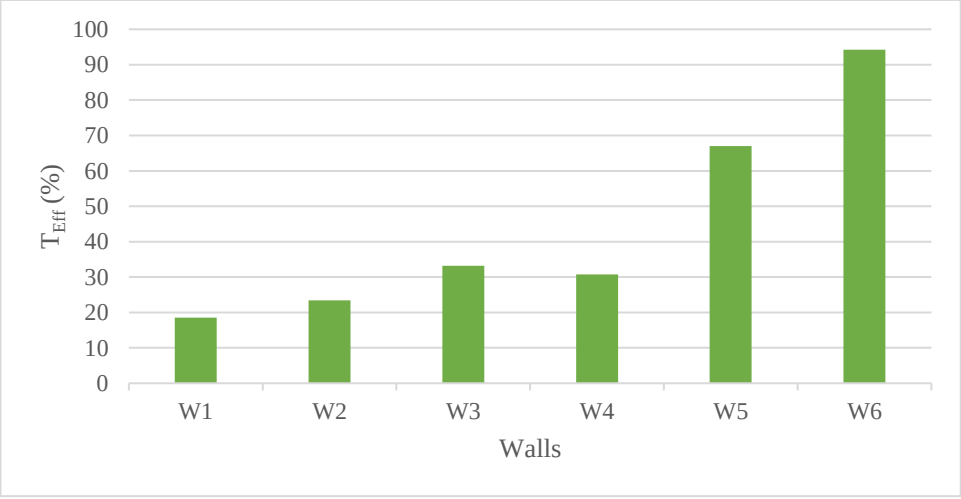


Figure 6. 4 Thermal Efficiency (T_{Eff}) of EPS Insulation.

When it comes to 3D-printed concrete, the generally traditional materials adopted are mainly cement and fine sand in most cases. It is worth noting that, despite the study focusing on 3DPC made of traditional materials, researchers have developed and applied various innovative materials. These range from different supplement cementitious materials (SCMs), phase change materials (PCM), admixtures, fibers, and different aggregate types (Hou et al., 2020; Zhang et al., 2021). When applied, all these materials have the potential to affect thermal performance based on their quantities and thermal conductivities.

6.4 Conclusions

This work is a numerical study of 3DPC lattice envelopes to understand the influence of the geometry of the infill structure on their thermal performance. The selection of the infill structures used in this study was done according to additive manufacturing industrial trends. All the lattice structures were modeled to have the same thickness, height, length, and similar areas of insulation. The effects of the contact (intersection) area of webs with the interior face, webs, and infill rows on the thermal performance of granularly insulated 3DPFC envelopes were studied. Lastly, the efficiency of insulation was established to determine the extent to which unintended thermal bridges produce significant thermal losses. Based on the findings of the analysis, the following conclusions were reached:

1. The U-value of a 3DPC building envelope is directly proportional to the contact area of webs with the interior face shell. The larger the contact area of the webs with the interior face, the higher the thermal transmittance.
2. The thermal performance of insulated lattice structures studied in this thesis work does not depend on the area of insulation.
3. The lack of direct connection between the exterior and interior surfaces produces superior thermal performance and yet potentially undermines the structural integrity. This necessitates a delicate balance between thermal and structural performance in real-life applications.

4. When there is a direct connection between the two face shells, the thermal performance of these envelopes is mainly affected by the contact (intersection) area of the webs rather than the number of webs.
5. Thermal bridging effects due to webbing significantly undermine the effective use of insulation. The application of innovative wall designs such as combined double-row walls, which minimize or eliminate web connections, is a potential solution.
6. The application of FC in 3DCP significantly improves the thermal efficiency of insulation due to the smaller difference in thermal conductivities between the 3DPFC and insulating materials when compared to normal concrete mixes.

These results provide designers with insights to consider when planning buildings' energy needs. Potential sources of poor thermal behavior attributed to the infill structure have been identified. This will facilitate informed design and construction decisions in additive manufacturing. Therefore, the study expands our understanding and provides a deeper insight into the energy performance of building systems as well as cost-effective possibilities for the construction industry's use of additive manufacturing.

CHAPTER SEVEN
SUMMARY AND CONCLUSIONS

The construction industry is considered a low-tech sector. This is because it is largely reliant on manual labor. This industry lacks innovation and is experiencing a slow adoption of digital advancements. Despite being largely un-green, the construction industry generates significant material waste and needs more skills. Meanwhile, the world population is projected to skyrocket by 2050 creating a huge crisis for accommodation. 3DCP has been identified as a potential answer to some of these challenges. The technology offers technical, social, economic, and environmental benefits. It allows for the production of formwork-free complex shapes at low costs. It also allows for the fast construction of custom-tailored buildings. It reduces material wastage and emissions, curbs energy consumption, and allows for optimized structural designs. 3DPC has the potential to disrupt the construction industry in the future.

The digital transformation of the building industry is just getting started, with less attention given to thermal insulation. The construction industry has a huge role to play in environmental responsibility and the energy optimization of 3DPC building envelopes is crucial. This thesis study focuses on the thermal performance and thermal bridging effects in 3DPC building envelopes, focusing on infill structure, cavity insulation, and thermal bridging. Three numerical studies are conducted on large-scale, commercially applied 3DPC walls using sufficient structural integrity infill structures.

Attention to structural performance is given to the selection of infill structures considered in this thesis work. This is because a delicate balance between thermal and structural performance is necessary in the application of 3DCP. Structural integrity guarantees the safety and stability of a building. Common building loads include the weight of the occupants and furniture, wind loads, seismic pressures, and dead loads such as the building's permanent weight. All these loads can be supported by a well-designed structure. The optimization of structural performance ensures that

building materials are used more effectively. This means that material wastage can be minimized without sacrificing strength. A well-designed structure guarantees longevity with reduced maintenance costs.

On the other hand, the HVAC systems in buildings consume a substantial amount of energy. Efficient interior temperature control lowers energy use when thermal design is done correctly. Occupant comfort can be ensured by temperature stability and reduced draft. Buildings with higher energy efficiency have a smaller carbon footprint and emit less greenhouse gases of this, structural and thermal factors need to be integrated by engineers and architects working together. The pursuit for thermal comfort can occasionally conflict with that of maximum structural performance. This trade-off must be balanced. Thicker walls, for example, use more materials. This may compromise the structural efficiency but provide better insulation.

A holistic selection approach was taken in the selection of infill structures used in this thesis work. This is to ensure that the lattice structures studied not only have sufficient structural integrity but are also consistent with additive manufacturing industrial trends. A constitutive model is developed, and validated against published literature and then applied to the selected lattice structures. The effects of filament width, web length, and configuration, contact area of webs with the interior face shell as well as granular filling materials are studied. The thermal efficiency of insulation is also determined.

Based on the studies, the following conclusions are made:

1. The void area primarily influences the thermal performance of 3DPC envelopes in stagnant air conditions. The presence of webs reduces the U-values in stagnant air conditions because of the reduced thickness of the air layers.
2. The introduction of cavity insulation significantly reduces the U-values, thus increasing the thermal performance of the wall panels.

3. The thermal performance of insulated lattice structures does not depend on the area of insulation but on the infill geometry due to thermal bridging.
4. The thermal performance of insulated 3DPC envelopes of the same contour lengths is mainly affected by the web length and configuration, filament width, and the contact (intersection) area between the webs and face shells.
5. For the same thermal properties, the longer the web length, the lower the U-value due to increased resistivity.
6. The absence or lack of direct connection between the exterior and interior surfaces produces superior thermal performance.
7. When there is a direct connection between the two face shells, the thermal performance of these envelopes is mainly affected by the contact (intersection) area of the webs rather than the number of webs.
8. The U-value of a 3DPC building envelope is directly proportional to the contact area of webs with the interior face shell. The larger the contact area of the webs with the interior face, the higher the thermal transmittance.
9. The U-values of insulated lattice structures increase with an increase in the filament width. This is because of the increase in the cross-sectional area of the webs, through which thermal bridging effects are dominant.
10. Thermal bridging effects due to webbing significantly undermine the effective use of insulation.
11. The application of EPS beads shows better thermal performance than that of loose-fill perlite, owing to the lower thermal conductivity of EPS beads.
12. The application of FC in 3DCP significantly improves the thermal efficiency of insulation due to the smaller difference in thermal conductivities between the 3DPFC and insulating materials when compared to normal concrete mixes.
13. The application of innovative wall designs such as combined double-row walls, which minimize or eliminate web connections, is a potential solution.

This thesis work expands our understanding of the thermal behavior of 3DPC building envelopes. It provides a deeper insight into the energy performance of

building systems as well as cost-effective possibilities as the construction industry adopts additive manufacturing.

REFERENCES

Abidi, S.; Nait-Ali, B.; Joliff, Y.; Favotto, C. Impact of perlite, vermiculite, and cement on the thermal conductivity of a plaster composite material: Experimental and numerical approaches. *Compos. Part B Eng.* 2014, *68*, 392–400. https://doi.org/10.1016/j.compositesb.2014.07.030.

Adaloudis, M., & Bonnin Roca, J. (2021). Sustainability tradeoffs in the adoption of 3D Concrete Printing in the construction industry. *Journal of Cleaner Production*, *307*, 127201. https://doi.org/10.1016/j.jclepro.2021.127201

Al Tamimi, A.; Hassan, H.; Rodriguez-Ubinas, E.; Alhaidary, H.; Mansouri, A. Thermal performance of 3D concrete printed walls: Calculated and in-situ measured U-values. *J. Asian Archit. Build. Eng.* 2023. https://doi.org/10.1080/13467581.2023.2278467.

Alhawari, A., & Mukhopadhyaya, P. (2018). Thermal bridges in building envelopes – An overview of impacts and solutions. *International Review of Applied Sciences and Engineering*, *9*(1), 31–40. https://doi.org/10.1556/1848.2018.9.1.5

Alhumayani, H.; Gomaa, M.; Soebarto, V.; Jabi, W. Environmental assessment of large-scale 3D printing in construction: A comparative study between cob and concrete. *J. Clean. Prod.* 2020, *270*, 122463. https://doi.org/10.1016/j.jclepro.2020.122463.

Alim Khan, S., Koç, M., & Al-Ghamdi, S. G. (2021). *Sustainability assessment, potentials and challenges of 3D printed concrete structures: A systematic review for built environmental applications*. https://doi.org/10.1016/j.jclepro.2021.127027

Alkhalidi, A.; Hatuqay, D. Energy efficient 3D printed buildings: Material and techniques selection worldwide study. *J. Build. Eng.* 2020, *30*, 101286. https://doi.org/10.1016/j.jobe.2020.101286.

Al-Qutaifi, S.; Nazari, A.; Bagheri, A. Mechanical properties of layered geopolymer structures applicable in concrete 3D-printing. *Constr. Build. Mater.* 2018, *176*, 690–699. https://doi.org/10.1016/j.conbuildmat.2018.04.195.

AlZahrani, A.A.; Alghamdi, A.A.; Basalah, A.A. Computational Optimization of 3D-Printed Concrete Walls for Improved Building Thermal Performance. *Buildings* 2022, *12*, 2267. https://doi.org/10.3390/BUILDINGS12122267.

Apis Cor. (2023a). *Construction with Robotic Precision*. Technologies. https://apis-cor.com/technologies/

Apis Cor. (2023b). *Progress on 3D printing*. https://www.linkedin.com/posts/apis-cor_3dprinted-wall-concrete-activity-7142975182201110528-_FrU?utm_source=share&utm_medium=member_android

Apis Cor. Construction with Robotic Precision. Technologies. Available online: https://apis-cor.com/technologies/ (accessed on 21 December 2023).

Apis Cor. Progress on 3D Prinitng. Available online: https://www.linkedin.com/posts/apis-cor_3dprinted-wall-concrete-activity-7142975182201110528-_FrU?utm_source=share&utm_medium=member_android (accessed on 22 December 2023).

ASTM F42, "Standard Terminology for Additive Manufacturing Technologies," *American Society for Testing and Materials,* 2015.

Bejan, A. (2013). Convection Heat Transfer. John Wiley and Sons.

Bello, N.D.; Memari, A.M. Comparative Review of the Technology and Case Studies of 3D Concrete Printing of Buildings by Several Companies. *Buildings* 2023, *13*, 106. https://doi.org/10.3390/BUILDINGS13010106.

Bergheau, J. M., and Fortunier, R. (2013). *Finite element simulation of heat transfer*. John Wiley and Sons.

Berman, B.; Zarb, F.G. 3-D printing: The new industrial revolution. *Bus. Horiz.* 2012, *55*, 155–162. https://doi.org/10.1016/j.bushor.2011.11.003.

Black Buffalo 3D. NEXCON Brochure. Available online: https://bb3d.io/nexcon-brochure/ (accessed on 24 December 2023).

Briels, D., Renz, M., Nouman, A., and Auer, T. (2023b). “Heat flux simulations for the AM facade demonstrator "Marriage of two Materials",” in Dataset (Munich, Germany: TUM). doi:10.14459/2023mp1716509

Caffrey, T., Wohlers, T., & Campbell, I. (2016). Executive summary of the Wohlers Report 2016.

Canadian Concrete Masonry Producers Association (CCMP). *Metric Technical Manual—Thermal Properties & Design Details (Section 6)*; CCMP: Toronto, ON, Canada, 2013. Available online: https://ccmpa.ca/download/metric-technical-manual/ (accessed on 16 December 2023).

Capozzoli, A., Gorrino, A., & Corrado, V. (2013). *A building thermal bridges sensitivity analysis*. https://doi.org/10.1016/j.apenergy.2013.02.045

Çengel, Y. A., and Ghajar, A. J. (2015). Heat and Mass Transfer: Fundamentals and Applications. McGraw-Hill Education.

Chamatete, K., & Yalçınkaya, Ç. (2024). Numerical Evaluation on Thermal Performance of 3D Printed Concrete Walls: The Effects of Lattice Type, Filament Width and Granular Filling Material. *Buildings 2024, Vol. 14, Page 926*, *14*(4), 926. https://doi.org/10.3390/BUILDINGS14040926

Craveiro, F., Duarte, J.P., Bartolo, H. (2019). Additive manufacturing as an enabling technology for digital construction: A perspective on Construction 4.0. Automation in Construction, 103, 251-267.

CyBe Construction. (2023a). *Prefabricated prefinished volumetric construction*. https://www.linkedin.com/posts/cybe-construction_we-revisit-memories-over-the-last-couple-activity-7128652555257040896-fNGo/?utm_source=share&utm_medium=member_android

CyBe Construction. (2023b). *Southern Hemisphere's Largest Fully 3D Printed Building Completed — CyBe Construction*. https://cybe.eu/largest-3d-printed-building/

CyBe Construction. (2023c). *The Smart Building Smart Construction Award*. https://www.linkedin.com/posts/cybe-construction_we-are-smart-construction-innovator-cybe-activity-7127565402221498368-XbZq/?utm_source=share&utm_medium=member_android

Dadkhah, F., and Zecher, J. (2009). *Ansys Workbench Software Tutorial with Multimedia CD: Release 12*. SDC publications.

Daungwilailuk, T.; Pheinsusom, P.; Pansuk, W. Uniaxial load testing of large-scale 3D-printed concrete wall and finite-element model analysis. *Constr. Build. Mater.* 2021, *275*, 122039. https://doi.org/10.1016/j.conbuildmat.2020.122039.

Davraz, M.; Koru, M.; Akdag, A.; Kılınçarslan, S.ß.; Delikanlı, Y.; Çabuk, M. Investigating the use of raw perlite to produce monolithic thermal insulation material. *Constr. Build. Mater.* 2020, *263*, 120674. https://doi.org/10.1016/j.conbuildmat.2020.120674.

De Mestrado, D., & Rigão, A. O. (2012). *Universidade Federal De Santa Maria Centro De Tecnologia Programa De Pós-Graduação Em Engenharia Civil E Ambiental Comportamento De Pequenas Paredes De Alvenaria Estrutural Frente A Altas Temperaturas*.

Di Foggia, G. Energy efficiency measures in buildings for achieving sustainable development goals. *Energy Procedia* 2018, *134*, 702–711. https://doi.org/10.1016/j.heliyon.2018.

Falliano, D., Di Torino, P., De Domenico, D., Ricciardi, G., & Gugliandolo, E. (2018). *Mechanical Characterization of Extrudable Foamed Concrete: An Experimental Study*. https://doi.org/10.1999/1307-6892/10008710

Famà, A.; Restuccia, L.; Ván, P. Generalized ballistic-conductive heat transport laws in three-dimensional isotropic materials. *Contin. Mech. Thermodyn.* 2021, *33*, 403–430. https://doi.org/10.1007/S00161-020-00909-W/METRICS.

Faruk, O.; Bledzki, A.K.; Fink, H.-P.; Sain, M. Biocomposites reinforced with natural fibers: 2000–2010. *Prog. Polym. Sci.* 2012, *37*, 1552–1596. https://doi.org/10.1016/j.progpolymsci.2012.04.003.

Fitzgerald, C., & Lautan, B. (2019). An investigation into the viability of PLA recycling for 3D printing to combat plastic waste. Journal of Cleaner Production, 226, 684-694.

Fu, Y., Wang, X., Wang, L., & Li, Y. (2020). Foam Concrete: A State-of-the-Art and State-of-the-Practice Review. *Advances in Materials Science and Engineering*, *2020*. https://doi.org/10.1155/2020/6153602

Hao, L.; Xiao, J.; Sun, J.; Xia, B.; Cao, W. Thermal conductivity of 3D printed concrete with recycled fine aggregate composite phase change materials. *J. Clean. Prod.* 2022, *364*, 132598. https://doi.org/10.1016/J.JCLEPRO.2022.132598.

Heng, G.; Ting, A.; Wei, Y.; Tay, D.; Qian, Y.; Tan, M.J. Utilization of recycled glass for 3D concrete printing: Rheological and mechanical properties. *J. Mater. Cycles Waste Manag.* 2019, *21*, 994–1003. https://doi.org/10.1007/s10163-019-00857-x.

Henke, K., Talke, D., & Winter, S. (2017). Multifunctional Concrete-Additive Manufacturing by the Use of Lightweight Concrete. *Interfaces: Architecture. Engineering. Science*. https://www.researchgate.net/publication/334318777

Henrique Dos Santos, G., Fogiatto, M. A., & Mendes, N. (2017). Numerical analysis of thermal transmittance of hollow concrete blocks. *Journal of Building Physics*, *41*(1), 7–24. https://doi.org/10.1177/1744259117698522/ASSET/IMAGES/LARGE/10.1177_1744259117698522-FIG11.JPEG

Hens, H. Ambient conditions, building performance and material properties. In *Applied Building Physics*; John Wiley & Sons.: Hoboken, NJ, USA, 2016. Available online: https://books.google.com/books/about/Applied_Building_Physics.html?id=fdo7CwAAQBAJ (accessed on 24 January 2024).

Hou, S.; Duan, Z.; Xiao, J.; Ye, J. A review of 3D printed concrete: Performance requirements, testing measurements and mix design. *Constr. Build. Mater.* 2020, *273*, 121745. https://doi.org/10.1016/j.conbuildmat.2020.121745.

Hwang D and B. Khoshnevis, "Concrete wall fabrication by contour crafting," in *21st International Symposium on Automation and Robotics in Construction (ISARC 2004), Jeju, South Korea*, 2004.

Insulation Company of America. What is Expanded Polystyrene (EPS) Foam? The Possibilities Are Endless! Available online: https://insulationcorp.com/eps/ (accessed on 20 December 2023).

Ismaiel, M.; Chen, Y.; Cruz-Noguez, C.; Hagel, M. Thermal resistance of masonry walls: A literature review on influence factors, evaluation, and improvement. *J. Build. Phys.* 2022, *45*, 528–567. https://doi.org/10.1177/17442591211009549/ASSET/IMAGES/LARGE/10.1177_17442591211009549-FIG8.JPEG.

ISO 6946: 2017; Building Components and Building Elements—Thermal Resistance and Thermal Transmittance—Calculation Methods. International Organisation of Standardization (ISO): Geneva, Switzerland, 2017. Available online: https://www.iso.org/standard/65708.html (accessed on 24 January 2024).

ISO 10211:2007. (2007). Test Case 1 (HEAT2). *Validation of HEAT2 7.0/HEAT3 5.0*.

Jan Kosny, P.; Yarbrough, P.D.; Childs, P.; Mohiuddin, P.S.A. How the Same Wall Can Have Several Different R-Values: Relations Between Amount of Framing and Overall Thermal Performance in Wood and Steel-Framed Walls. In Proceedings of the ASHRAE THERM X, Thermal Performance of the Exterior Envelopes of Buildings X, Clearwater, FL, USA, 2–5 December 2007.

Ji, G.; Ding, T.; Xiao, J.; Du, S.; Li, J.; Duan, Z. A 3D Printed Ready-Mixed Concrete Power Distribution Substation: Materials and Construction Technology. *Materials* 2019, *12*, 1540. https://doi.org/10.3390/MA12091540.

Jipa, A.; Dillenburger, B. 3D Printed Formwork for Concrete: State-of-the-Art, Opportunities, Challenges, and Applications. *3d Print. Addit. Manuf.* 2022, *9*, 84–107. https://doi.org/10.1089/3DP.2021.0024.

Joh, C.; Lee, J.; Bui, T.Q.; Park, J.; Yang, I.H. Buildability and Mechanical Properties of 3D Printed Concrete. *Materials* 2020, *13*, 4919. https://doi.org/10.3390/MA13214919.

Jones, D. R., & Pargeter, R. (2019). Heat Loss, Heat Gain, and U-values. Springer.

Ju, J.; Schellenberg, J.; Wallis, M. Dependence of Thermal Properties of Expandable Polystyrene Particle Foam on Cell Size and Density. *J. Cell. Plast.* 2010, *46*, 209–222. https://doi.org/10.1177/0021955X09350803.

Kahraman, R., & Avşar, Ö. (2015). An experimental study on thermal conductivity and mechanical properties of expanded polystyrene (EPS) lightweight concrete. Construction and Building Materials, 76, 399-405.

Kośny, J., and Yarbrough, D. W. (2022). Thermal Efficiency of Insulation in Building Structures—The Impact of Thermal Bridging. In Thermal Insulation and Radiation Control Technologies for Buildings (pp. 443-486). Cham: Springer International Publishing.

Kossecka, E., & Kosny, J. (2001). *Influence of insulation configuration on heating and cooling loads in a continuously used building*.

Kottek, M, J. G. (2006). World Map of the Köppen-Geiger climate classification updated. Meteorologische Zeitschrift - Vol. 15, 259-263.

Kumar, M. B., & Sathiya, P. (2021). Methods and materials for additive manufacturing: A critical review on advancements and challenges. Thin-Walled Structures, 159, 107228.

Le, T. T., Austin, S. A., Lim, S., Buswell, R. A., Gibb, A. G., & Thorpe, T. (2012). Mix design and fresh properties for high-performance printing concrete. Materials and structures, 45, 1221-1232.

Lee, H. H. (2018). *Finite element simulations with ANSYS Workbench 18*. SDC publications.

Lewis, R. W., Morgan, K., Thomas, H. R., and Seetharamu, K. N. (1996). *The finite element method in heat transfer analysis*. John Wiley and Sons.

Lu, G.; Liu, Y.; Kang, J.; Lyu, M.; Lai, Y.; Dong, Z. Numerical modeling and experimental verification for anisotropic heat conduction process in velocity probe of the thermal mass flowmeter. *Appl. Therm Eng.* 2024, *236*, 1359–4311. https://doi.org/10.1016/j.applthermaleng.2023.121845.

Ma, G.; Li, Z.; Wang, L. Printable properties of cementitious material containing copper tailings for extrusion based 3D printing. *Build. Mater.* 2018, *162*, 613–627. https://doi.org/10.1016/j.conbuildmat.2017.12.051.

Mansouri, A.; Binali, A.; Aljawi, A.; Alhammadi, A.; Almir, K.; Alnuaimi, E.; Alyousuf, H.; Rodriguez-Ubinas, E. Thermal modeling of the convective heat transfer in the large air cavities of the 3D concrete printed walls. *Cogent. Eng.* 2022, *9*, 2130203. https://doi.org/10.1080/23311916.2022.2130203.

Manual, U. D. F. (2009). Ansys Fluent 12.0. *Theory Guide*, 67.

Markin, V., Krause, M., Otto, J., Schröfl, C., & Mechtcherine, V. (2021). 3D-printing with foam concrete: From material design and testing to application and sustainability. *Journal of Building Engineering*, *43*, 102870. https://doi.org/10.1016/j.jobe.2021.102870

Markin, V., Sahmenko, G., Nerella, V. N., Näther, M., & Mechtcherine, V. (2019). *Investigations on the foam concrete production techniques suitable for 3D-printing with foam concrete*. https://doi.org/10.1088/1757-899X/660/1/012039

Martins, C. M. D. O. (2020). Hot Box Apparatus Design and Construction for the Determination of the Thermal Performance of Building Elements (Doctoral dissertation).

Mechtcherine, V., Bos, F. P., Perrot, A., Leal Da Silva, W. R., Nerella, V. N., Fataei, S., Wolfs, R. J. M., Sonebi, M., & Roussel, N. (2020). *Extrusion-based additive manufacturing with cement-based materials-Production steps, processes, and their underlying physics: A review*. https://doi.org/10.1016/j.cemconres.2020.106037

Mechtcherine, V.; Nerella, V.N.; Will, F.; Näther, M.; Otto, J.; Krause, M. Large-scale digital concrete construction-CONPrint3D concept for on-site, monolithic 3D-printing. *Autom. Constr.* 2019, *107*, 102933. https://doi.org/10.1016/j.autcon.2019.102933.

Modest, M. F. (2013). Radiative Heat Transfer. Academic Press.

Mohammad, M.; Masad, E.; Seers, T.; Al-Ghamdi, S.G. High-Performance Light-Weight Concrete for 3D Printing. *RILEM Bookseries* 2020, *28*, 459–467. https://doi.org/10.1007/978-3-030-49916-7_47/COVER.

Mohammed W. Muhieldeen, Lim Chong Lye, M.S.S. Kassim, Tey Wah Yen, & K.H Teng. (2021). Effect of Rockwool Insulation on Room Temperature Distribution. Journal of Advanced Research in Experimental Fluid Mechanics and Heat Transfer, 3(1), 9–15. Retrieved from https://www.akademiabaru.com/submit/index.php/arefmht/article/view/3751

National Concrete Masonry Association (NCMA). Thermal Catalog of Concrete Masonry Assemblies. Available online: https://ncma.org/resource/thermal-catalog-of-concrete-masonry-assemblies/ (accessed on 18 December 2023).

Nemova, D.; Kotov, E.; Andreeva, D.; Khorobrov, S.; Olshevskiy, V.; Vasileva, I.; Zaborova, D.; Musorina, T. Experimental Study on the Thermal Performance of 3D-Printed Enclosing Structures. *Energies* 2022, *15*, 4230. https://doi.org/10.3390/EN15124230.

Ochs, F.; Müller-Steinhagen, H. Temperature and Moisture Dependence of the Thermal Conductivity of Insulation Materials. 2005. Available online: www.itw.uni-stuttgart.de (accessed on 24 January 2024).

Ono, R. Parâmetros para garantia da qualidade do projeto de segurança contra incêndio em edifícios altos. *Ambiente Construído* 2008, *7*, 97–113. Available: https://seer.ufrgs.br/index.php/ambienteconstruido/article/view/3731 (accessed on 24 January 2024).

Otto, J., Kortmann, J., & Krause, M. (2020). Wirtschaftliche Perspektiven von Beton-3D-Druckverfahren. *Beton- Und Stahlbetonbau*, *115*(8), 586–597. https://doi.org/10.1002/BEST.201900087

Ouedraogo, E.; Ouédraogo, E.; Coulibaly, O.; Kaboré, B.; Imbga, K.B.; Ouédraogo, A. Optimization of the air gap thickness for the insulation of double-walled walls of a building. *Asian J. Sci. Technol.* 2018, *9*, 8786–8794. Available online: https://www.researchgate.net/publication/328743687 (accessed on 24 January 2024).

Parker, K.; Garancher, J.P.; Shah, S.; Fernyhough, A. Expanded polylactic acid—An eco-friendly alternative to polystyrene foam. *J. Cell. Plast.* 2011, *47*, 233–243. https://doi.org/10.1177/0021955X11404833.

Pearce, C. M. Blair, K. J. Laciak, R. Andrews, A. Nosrat, and I. Zelenika-Zovko, "3-D printing of open source appropriate technologies for self-directed sustainable development," *Journal of Sustainable Development*, vol. 3, no. 4, p. 17, 2010

Perlite Institute, Inc, https://www.perlite.org/wp-content/uploads/2018/03/thermal-performance-perlite-insulated-masonary.pdf

Perlite Institute. Perlite and the Environment. Available online: https://www.perlite.org/environmental/ (accessed on 24 December 2023).

Pessoa, S.; Jesus, M.; Guimarães, A.S.; Lucas, S.S.; Simões, N. Experimental characterisation of hygrothermal properties of a 3D printed cementitious mortar.

Case Stud. Constr. Mater. 2023, *19*, e02355. https://doi.org/10.1016/j.cscm.2023.e02355.

Pierzchlewicz, J. Modern Concrete Wall-Units with Improved Thermal Resistance for Housing in Hot Climate. *Sultan Qaboos Univ. J. Sci. [SQUJS]* 1996, *1*, 69–80. https://doi.org/10.24200/SQUJS.VOL1ISS1PP69-80.

Pietras, D.; Zbyszyński, W.; Sadowski, T. A 3D Printing Method of Cement-Based FGM Composites Containing Granulated Cork, Polypropylene Fibres, and a Polyethylene Net Interlayer. *Materials* 2023, *16*, 4235. https://doi.org/10.3390/MA16124235.

Priyatham, B. P. R. V. S., Lakshmayya, M. T. S., & Chaitanya, D. V. S. R. K. (2023). *Review on performance and sustainability of foam concrete*. https://doi.org/10.1016/j.matpr.2023.04.080

QOROX, "Leading printed structures Welcoming freeform design opportunities". 2023. https://qorox.co.nz/wp-content/uploads/2022/09/QOROX-Brochure-V7.pdf (Accessed on 20 December 2023)

Raj, A., Sathyan, D., & Mini, K. M. (2019). *Physical and functional characteristics of foam concrete: A review*. https://doi.org/10.1016/j.conbuildmat.2019.06.052

Rajput, R. K. (2015). *A textbook of heat and mass transfer*. S. Chand Publishing.

Real, S., Gomes, M. G., Rodrigues, A. M., & Bogas, J. A. (2016). *Contribution of structural lightweight aggregate concrete to the reduction of thermal bridging effect in buildings*. https://doi.org/10.1016/j.conbuildmat.2016.06.018

Rigão, A.O. Comportamento de Pequenas Paredes de Alvenaria Estrutural Frente a Altas Temperaturas. August 2012. Available online: http://repositorio.ufsm.br/handle/1/7809 (accessed on 24 January 2024).

Rijal, H. B., Tuohy, P., Nicol, F., Humphreys, M. A., & Samuel, A. (2017). A review of occupant behavior in bedrooms and assessment of control strategies for improved thermal comfort. Building and Environment, 112, 294-309.

Roels, S., Nicol, F., Laverge, J., Carmeliet, J., & de Dear, R. (2016). Integrated model for accurate evaluation of convective heat loss from a building zone. Building and Environment, 97, 64-79.

Sakin, M.; Kiroglu, Y.C. 3D Printing of Buildings: Construction of the Sustainable Houses of the Future by BIM. *Energy Procedia* 2017, *134*, 702–711. https://doi.org/10.1016/J.EGYPRO.2017.09.562.

Santos, G.H.D.; Fogiatto, M.A.; Mendes, N. Numerical analysis of thermal transmittance of hollow concrete blocks. *J. Build. Phys.* 2017, *41*, 7–24. https://doi.org/10.1177/1744259117698522/ASSET/IMAGES/LARGE/10.1177_1744259117698522-FIG11.JPEG.

Schiavoni, S.; D'alessandro, F.; Bianchi, F.; Asdrubali, F. Insulation materials for the building sector: A review and comparative analysis. *Renew. Sustain. Energy Rev.* 2016, *62*, 988–1011. https://doi.org/10.1016/j.rser.2016.05.045.

Schumacher C, S. J. O. D. (2013). Development of a new hot box apparatus to measure building enclosure thermal performance. *Thermal Performance of the Exterior Envelopes of Whole Buildings XII International Conference. ASHRAE.*

Simpson, A.; Rattigan, I.G.; Kalavsky, E.; Parr, G. Thermal conductivity and conditioning of grey expanded polystyrene foams. *Cell. Polym.* 2020, *39*, 238–262. https://doi.org/10.1177/0262489320934263/ASSET/IMAGES/LARGE/10.1177_0262489320934263-FIG14.JPEG.

Simpson, A.; Stuckest, A.D. Thermal conductivity of porous materials: II Theoretical treatment of radiative heat transfer. *Build. Serv. Eng. Res. Technol.* 1990, *11*, 13–19. https://doi.org/10.1177/014362449001100103.

Soltan, D.G.; Li, V.C. A self-reinforced cementitious composite for building-scale 3D printing. *Cem. Concr. Compos.* 2018, *90*, 1–13. 10.1016/j.cemconcomp.2018.03.017.

Sprecher, B., Pearce, J. M., & Hall, A. (2017). Economic Analysis of Greenhouse Gas Emissions of PV and CSP in 2050. Environmental Progress & Sustainable Energy, 36(5), 1393-1400.

Stark, N.M.; Matuana, L.M. Characterization of weathered woodeplastic composite surfaces using FTIR spectroscopy, contact angle, and XPS. *Polym. Degrad. Stab.* 2007, *92*, 1883–1890. https://doi.org/10.1016/j.polymdegradstab.2007.06.017.

Sun, J.; Xiao, J.; Li, Z.; Feng, X. Experimental study on the thermal performance of a 3D printed concrete prototype building. *Energy Build.* 2021, *241*, 110965. https://doi.org/10.1016/j.enbuild.2021.110965.

Suntharalingam, T.; Upasiri, I.; Gatheeshgar, P.; Poologanathan, K.; Nagaratnam, B.; Santos, P.; Rajanayagam, H. Energy Performance of 3D-Printed Concrete Walls: A Numerical Study. *Buildings* 2021, *11*, 432. https://doi.org/10.3390/BUILDINGS11100432.

Tamimi, A. Al, Hassan, H., Rodriguez-Ubinas, E., Alhaidary, H., & Mansouri, A. (2023). Thermal performance of 3D concrete printed walls: calculated and in-situ measured U-values. *Journal of Asian Architecture and Building Engineering*. https://doi.org/10.1080/13467581.2023.2278467

Theodosiou, T. G., Tsikaloudaki, A. G., Kontoleon, K. J., & Bikas, D. K. (2015). Thermal bridging analysis on cladding systems for building facades. *Energy and Buildings*, *109*, 377–384. https://doi.org/10.1016/j.enbuild.2015.10.037

Thompson, M. K., and Thompson, J. M. (2017). *ANSYS mechanical APDL for finite element analysis*. Butterworth-Heinemann.

Urban, B., Engelmann, P., Kossecka, E., & Kosny, J. (2011). Arranging Insulation for Better Thermal Resistance in Concrete and Masonry Wall Systems. *Proceedings of the 9th Nordic Symposium on Building Physics, Tampere, Finland*, *29*. https://www.researchgate.net/publication/266602609 (accessed on 24 January 2024).

Viot, H., Sempey, A., Pauly, M., & Mora, L. (2015). *Comparison of different methods for calculating thermal bridges: Application to wood-frame buildings*. https://doi.org/10.1016/j.buildenv.2015.07.017

Voskresenskaya, E.; Vorona-Slivinskaya, L.; Panov, S. Legal regulation of environmental protection, management of natural resources, and environmental safety in construction sector. *MATEC Web Conf.* 2018, *193*, 02025. doi:10.1051/matecconf/201819302025.

Wan, K. K. W., Li, D. H. W., Liu, D., & Lam, J. C. (2010). *Future trends of building heating and cooling loads and energy consumption in different climates*. https://doi.org/10.1016/j.buildenv.2010.07.016

WASP. 3D Printer House | Crane WASP. Available online: https://www.3dwasp.com/en/3d-printer-house-crane-wasp/ (accessed on 23 December 2023).

Welty, J., Rorrer, G. L., and Foster, D. G. (2020). *Fundamentals of momentum, heat, and mass transfer*. John Wiley and Sons.

Yang, Y., Dong, S., & Wang, Z. (2017). Study on lightweight concrete with expanded polystyrene (EPS) as aggregate. IOP Conference Series: Materials Science and Engineering, 191, 012034.

Yucel, K.T.; Basyigit, C.; Ozel, C. Thermal insulation properties of expanded polystyrene as construction AND insulating materials. *Constr. Build. Mater.* 2020, *263*, 120674. Available online: https://www.researchgate.net/publication/237669763 (accessed on 24 January 2024).

Zhang, C.; Nerella, V.N.; Krishna, A.; Wang, S.; Zhang, Y.; Mechtcherine, V.; Banthia, N. Mix design concepts for 3D printable concrete: A review. *Cem. Concr. Compos.* 2021, *122*, 104155. https://doi.org/10.1016/j.cemconcomp.2021.104155.

Zhang, M., Khoshnevis, B., and Zhang, J. (2020). Thermal conductivity of 3D-printed geopolymers: An experimental study. Materials and Design, 195, 109030.

Zhang, Y., & Lepech, M. D. (2016). Comparing the Environmental Impacts of Additive Manufacturing vs. Traditional Machining via Life-Cycle Assessment. Rapid Prototyping Journal, 22(1), 92-102

Zhao, Z.; Ji, C.; Xiao, J.; Yao, L.; Lin, C.; Ding, T.; Ye, T. A critical review on reducing the environmental impact of 3D printing concrete: Material preparation, construction process and structure level. *Constr. Build. Mater.* 2023, *409*, 133887. https://doi.org/10.1016/j.conbuildmat.2023.133887.

Zieli, T. G. (1992). *Introduction to the finite element method*. Poland: Institute of Fundamental Technological Research of the Polish Academy of Sciences.